

# PACIFIC EARTHQUAKE ENGINEERING RESEARCH CENTER

## **Nonlinear Site Response and Seismic Compression at Vertical Array Strongly Shaken by 2007 Niigata-ken Chuetsu-oki Earthquake**

**Eric Yee**

**Jonathan P. Stewart**

Department of Civil and Environmental Engineering  
University of California, Los Angeles

**Kohji Tokimatsu**

Center for Urban Earthquake Engineering  
Tokyo Institute of Technology

#### Disclaimer

The opinions, findings, and conclusions or recommendations expressed in this publication are those of the author(s) and do not necessarily reflect the views of the study sponsor(s) or the Pacific Earthquake Engineering Research Center.

# **Nonlinear Site Response and Seismic Compression at Vertical Array Strongly Shaken by 2007 Niigata-ken Chuetsu-oki Earthquake**

**Eric Yee**

**Jonathan P. Stewart**

Department of Civil and Environmental Engineering  
University of Los Angeles

**Kohji Tokimatsu**

Center for Urban Earthquake Engineering  
Tokyo Institute of Technology

PEER Report 2011/107  
Pacific Earthquake Engineering Research Center  
College of Engineering  
University of California, Berkeley

December 2011



## ABSTRACT

Strong ground motions from the  $M_w$  6.6 2007 Niigata-ken Chuetsu-oki earthquake were recorded by a free-field downhole array installed near the Service Hall at the Kashiwazaki-Kariwa nuclear power plant. Site conditions at the array consist of about 70 m of medium-dense sands overlying clayey bedrock, with ground water located at 45 m. Ground shaking at the bedrock level had geometric mean peak accelerations of 0.55g, which reduced to 0.4g at the ground surface, indicating nonlinear site response. Ground settlements of approximately  $15 \pm 5$  cm occurred at the site. A site investigation was performed to develop relevant soil properties for ground response and seismic compression analysis, including shear wave velocities, shear strength, relative density, and modulus reduction and damping curves.

Ground response analysis of relatively weak motion aftershock data provides good matches of the observed resonant site frequencies and amplification levels, suggesting that the velocity profile and assumption of one-dimensional response may be reasonable over the frequency range of interest. Initial analysis of the aftershock data was performed using equivalent-linear and nonlinear ground response procedures in which soil backbone curves were matched to test data for modest strain levels  $< \sim 0.5\%$ . These analyses over-predicted high-frequency ground response, suggesting that the laboratory-based small strain damping level is too low for field conditions. Increasing the small strain damping to about 2-5% in the sand layers provided improved results. Subsequent ground response analysis of strong-motion data produces a strain localization phenomenon where large strains developed at a depth having a velocity contrast. Accordingly, we introduced a procedure to modify the large-strain portion of backbone curves to asymptotically approach the shear strength. When implemented in nonlinear and equivalent linear ground response, the strain localization phenomenon is removed, strains in the upper portion of the soil profile are increased, and predicted ground motions match observations reasonably well.

Measured relative densities ( $D_R$ ) at the site ranged from approximately 40% (from tube samples) to 65% (from SPT correlations). A material specific volumetric strain material model for that range of  $D_R$  was developed, which when coupled with the shear strain demands from the ground response analysis, predicts ground settlements ranging from 8 to 12 cm for horizontal ground shaking and 12 to 18 cm when vertical ground motions are considered. Those settlement estimates are reasonably consistent with the observations from the site.



## **ACKNOWLEDGMENTS**

This work was supported primarily by the Pacific Earthquake Engineering Research Center (PEER) Lifelines program and by the U.S. Geological Survey External Research program under contract number G11AP20039. This support is gratefully acknowledged. We also wish to thank Akio Abe of Tokyo Soil Research Company for his efforts with the field work and RCTS laboratory testing and Pile Dynamics, Inc., for providing the equipment for SPT energy measurements. We also thank Veronica Tolnay De Hagymassy for her assistance with laboratory work at UCLA.

Any opinions, findings, and conclusions or recommendations expressed in this material are those of the authors and do not necessarily reflect those of the PEER center or the U.S. Geological Survey.



# CONTENTS

<b>ABSTRACT</b> .....	<b>iii</b>
<b>ACKNOWLEDGMENTS</b> .....	<b>v</b>
<b>TABLE OF CONTENTS</b> .....	<b>vii</b>
<b>LIST OF FIGURES</b> .....	<b>ix</b>
<b>LIST OF TABLES</b> .....	<b>xiii</b>
<b>1 INTRODUCTION</b> .....	<b>1</b>
<b>2 PREVIOUS STUDIES</b> .....	<b>7</b>
<b>2.1 Nonlinear Site Response</b> .....	<b>7</b>
<b>2.2 Seismic Compression Case Studies</b> .....	<b>10</b>
<b>3 SITE CHARACTERIZATION</b> .....	<b>17</b>
<b>3.1 Results of Geotechnical Exploration (Current and Prior Studies)</b> .....	<b>17</b>
<b>3.2 Laboratory Testing</b> .....	<b>20</b>
3.2.1 Index Tests .....	20
3.2.2 Relative Densities .....	20
3.2.3 Shear Strength and Modulus Reduction and Damping Relations.....	20
3.2.4 Cyclic Volume Change .....	22
<b>4 GROUND MOTION DATA FROM SERVICE HALL ARRAY</b> .....	<b>29</b>
<b>5 GROUND RESPONSE ANALYSIS</b> .....	<b>35</b>
<b>5.1 Dynamic Soil Properties for Analysis</b> .....	<b>35</b>
<b>5.2 Ground Response Analysis using Aftershock Data</b> .....	<b>41</b>
<b>5.3 Initial Ground Response Analysis using Main Shock Recordings</b> .....	<b>50</b>
<b>5.4 Revised Ground Response Analysis considering Strength Adjusted Backbone Curves and Increased Damping</b> .....	<b>54</b>
5.4.1 Modification of Backbone Curve to Capture Shear Strength .....	54
5.4.2 Effects of Modified Backbone Curves on Analysis Results.....	56
5.4.3 Damping Adjustment .....	60
<b>6 GROUND FAILURE ANALYSIS</b> .....	<b>65</b>
<b>6.1 Potential for Liquefaction at Depth</b> .....	<b>65</b>
<b>6.2 Seismic Compression</b> .....	<b>66</b>
<b>7 SUMMARY AND CONCLUSIONS</b> .....	<b>71</b>
<b>REFERENCES</b> .....	<b>75</b>

- APPENDIX A: DETAILED BORING LOG (ELECTRONIC SUPPLEMENT)**  
<[http://peer.berkeley.edu/publications/peer\\_reports/reports\\_2011/reports\\_2011.html](http://peer.berkeley.edu/publications/peer_reports/reports_2011/reports_2011.html)>
- APPENDIX B: ACCELERATION, VELOCITY, AND DISPLACEMENT HISTORY FOR MAIN SHOCK (ELECTRONIC SUPPLEMENT)**  
<[http://peer.berkeley.edu/publications/peer\\_reports/reports\\_2011/reports\\_2011.html](http://peer.berkeley.edu/publications/peer_reports/reports_2011/reports_2011.html)>
- APPENDIX C: ACCELERATION, VELOCITY, AND DISPLACEMENT HISTORY FOR AFTERSHOCK L (ELECTRONIC SUPPLEMENT)**  
<[http://peer.berkeley.edu/publications/peer\\_reports/reports\\_2011/reports\\_2011.html](http://peer.berkeley.edu/publications/peer_reports/reports_2011/reports_2011.html)>
- APPENDIX D: ACCELERATION, VELOCITY, AND DISPLACEMENT HISTORY FOR AFTERSHOCK S (ELECTRONIC SUPPLEMENT)**  
<[http://peer.berkeley.edu/publications/peer\\_reports/reports\\_2011/reports\\_2011.html](http://peer.berkeley.edu/publications/peer_reports/reports_2011/reports_2011.html)>

## LIST OF FIGURES

Figure 1.1	Map of Kashiwazaki area showing location of KKNPP site relative to fault rupture plane by Miyake et al. (2010). Shading on fault plane indicates slip in meters.....	1
Figure 1.2	Map of Kashiwazaki-Kariwa nuclear power plant showing locations of downhole arrays and geometric mean peak accelerations from 2007 Niigata-ken Chuetsu-oki earthquake. Peak accelerations are shown for surface ('sur') and bedrock ('br') conditions.....	3
Figure 1.3	Geologic log at SHA site including instrument locations and results of penetration and suspension logging geophysical testing.....	4
Figure 1.4	Photographs of (a) raised pile at vertical array, showing ground settlement; and (b) settlement around Service Hall building.....	5
Figure 2.1	Acceleration histories for data from the 2004 Parkfield earthquake and simulation results from site response program DeepSoil. Results are shown for two horizontal directions and two elevations (V1, ground surface; D2, 10 m depth) with the recorded input motions at elevation D3.....	8
Figure 2.2	Comparison of interpreted soil behavior by extracting soil parameters using two different methods, with curves from laboratory tests and those from system identification, Lotung array.....	9
Figure 2.3	Transfer functions at two stations, illustrating inter-event variability: (a) IWTH25 is characteristic of a site with a large degree of inter-event variability, and (b) IWTH05 is characteristic of a site with low inter-event variability. The median prediction of the transfer function is shown as a black line, and the 95% confidence band is shown in gray.....	10
Figure 2.4	Transfer functions at two stations, illustrating goodness-of-fit: (a) IWTH04 is characteristic of a site where the SH1D model accurately predicts the transfer functions, and (b) IWTH12 is characteristic of a site where the SH1D model poorly predicts a transfer function.....	10
Figure 2.5	Jensen Filtration Plant profile.....	11
Figure 2.6	Comparison of settlements under (a) components and combined random motions and (b) in three-dimensional shake table tests.....	12
Figure 2.7	Plan and settlement of Santa Clarita Site B.....	13
Figure 2.8	(a) Seismic compression and (b) variation of normalized vertical strain with number of cycles of soil from Site B.....	14
Figure 2.9	Vertical profiles of shear strain from site response analyses (top frame) and lateral profiles of observed and calculated settlement (bottom frame) along a cross section for site B.....	15
Figure 2.10	Schematic of observed ground deformation at a highway embankment site.....	16

Figure 3.1	Variation with depth of energy ratio in standard penetration tests. ....	19
Figure 3.2	Modulus reduction and damping curves from resonant column and torsional shear tests performed on specimens from four samples. ....	22
Figure 3.3	Results of simple shear tests showing cyclic volume change characteristics of sandy materials in upper 70 m of SHA site. ....	24
Figure 3.4	Comparison of parameter $a$ for KKNPP sand with slope parameter $b = 1.2$ against the clean sand model by Duku et al. ....	25
Figure 3.5	Simple shear results from applying ground motions at 8.2 m depth taken from site response analyses and the resultant settlement time history. FN and FP ground motions were also applied separately. ....	27
Figure 4.1	Main shock velocity histories from the upper three instruments at the SHA site rotated into the FN and FP directions. ....	31
Figure 4.2	Pseudo-acceleration response spectra for the three components of recorded main shock ground motions at SHA site. ....	32
Figure 4.3	Surface-to-rock (2.4 m/99.4 m) transfer functions and surface (2.4 m) H/V spectral ratios for main shock and aftershock recordings. ....	34
Figure 5.1	Variation of pseudo reference strain with mean confining pressure from RCTS tests (this study), previous RCTS tests (neighboring site), and model predictions. ....	37
Figure 5.2	Values of pseudo reference strain used for analysis as function of with confining pressure and depth through the soil column. ....	39
Figure 5.3	Comparison of the Darendeli and Menq models: (a) modulus reduction and (b) damping curve models to sample test data from 20 m deep. Resultant modulus reduction and damping curves are labeled as “Model” ....	40
Figure 5.5	Results of EQL and nonlinear ground response analyses for aftershock L. ....	43
Figure 5.6	Peak strain profiles from EQL and nonlinear analyses for aftershock L. ....	44
Figure 5.7	Peak accelerations from EQL and nonlinear analyses for aftershock L. ....	45
Figure 5.8	Results of EQL and nonlinear ground response analyses for aftershock S. ....	46
Figure 5.9	Peak strain profiles from EQL and nonlinear analyses for aftershock S. ....	47
Figure 5.10	Peak accelerations from EQL and nonlinear analyses for aftershock S. ....	48
Figure 5.11	Transfer function and coherence for the main shock and two aftershocks. ....	48
Figure 5.12	Response spectra at 5% damping for aftershock L and EQL analysis results for varying levels of small strain damping. ....	49
Figure 5.13	Response spectra at 5% damping for aftershock S and EQL analysis results for varying levels of small strain damping. ....	50

Figure 5.14	Results of EQL and nonlinear ground response analyses using increased damping ( $D_{min}=2\%$ ). .....	52
Figure 5.15	Peak strain profiles from EQL and nonlinear analyses with increased damping ( $D_{min}=2\%$ ). .....	53
Figure 5.16	Comparison of backbone curve from FN nonlinear site response analysis at 50.8 m depth and estimated drained shear strength. ....	53
Figure 5.17	Diagram for constructing shear strength adjusted modulus reduction curves. ....	55
Figure 5.18	Comparison of the original and strength adjusted (a) modulus reduction and (b) damping models for the layer of soil containing the first sensor, (c) modulus reduction and (d) damping models for a layer at 8.2 m depth, and (e) modulus reduction and (f) damping models for the layer of soil containing the second sensor. ....	57
Figure 5.19	Results of strength adjusted EQL and nonlinear ground response analyses. ....	58
Figure 5.20	Peak strain profiles from strength adjusted EQL and nonlinear analyses. ....	59
Figure 5.21	Peak accelerations from strength adjusted EQL and nonlinear analyses. ....	60
Figure 5.22	Response spectra at 5% damping for main shock and nonlinear analysis results using strength adjusted backbone curves and varying levels of small strain damping. ....	61
Figure 5.23	Peak accelerations from increased damping on strength adjusted nonlinear analyses. ....	62
Figure 5.24	Results of strength adjusted EQL and nonlinear ground response analyses with increased damping. ....	63
Figure 5.25	Peak strain profiles from strength adjusted EQL and nonlinear analyses with increased damping. ....	64
Figure 6.1	Relationship between shear strain amplitude, $\gamma_c$ , and number of cycles, $N$ , to cause selected amounts of vertical strain, $\varepsilon_v$ . ....	67
Figure 6.2	Number of cycles from strength-adjusted EQL analysis. ....	67
Figure 6.3	Sample effective strain demand profiles, vertical strain profiles, and resultant settlements from a site specific analysis for $D_R = 40\%$ and $65\%$ . ....	69



## LIST OF TABLES

Table 3.1	Summary of soil index tests, triaxial compression shear strength tests, and resonant column-torsional shear tests for dynamic soil properties .....	21
Table 3.2	Suites of cyclic simple shear tests and regressed parameters .....	25
Table 4.1	Ground motions used for this study .....	30
Table 4.2	Filter frequencies applied to vertical array data .....	30
Table 4.3	PGA and PGV from rotated motions .....	31



# 1 Introduction

The  $M_w$  6.6 Niigata-ken Chuetsu-oki earthquake occurred on July 16, 2007, off the west coast of Niigata Prefecture, Japan. An overview of the damage from this important earthquake is provided by Kayen et al. [2009] and references therein. As shown in Figure 1.1, the main shock ruptured a buried reverse-slip fault, rupturing up-dip from a focal depth of 9 km. Based on source inversions by Miyake et al. [2010], the focal mechanism for this event has conjugate fault planes with a strike of  $34^\circ$  and dips of  $54^\circ$  to the northwest and  $36^\circ$  to the southeast. The southeast-dipping plane is preferred (shown in Figure 1.1) based on asperities analysis, the aftershock pattern observed from ocean-bottom seismometers, and results of reflection surveys [Miyake et al. 2010].

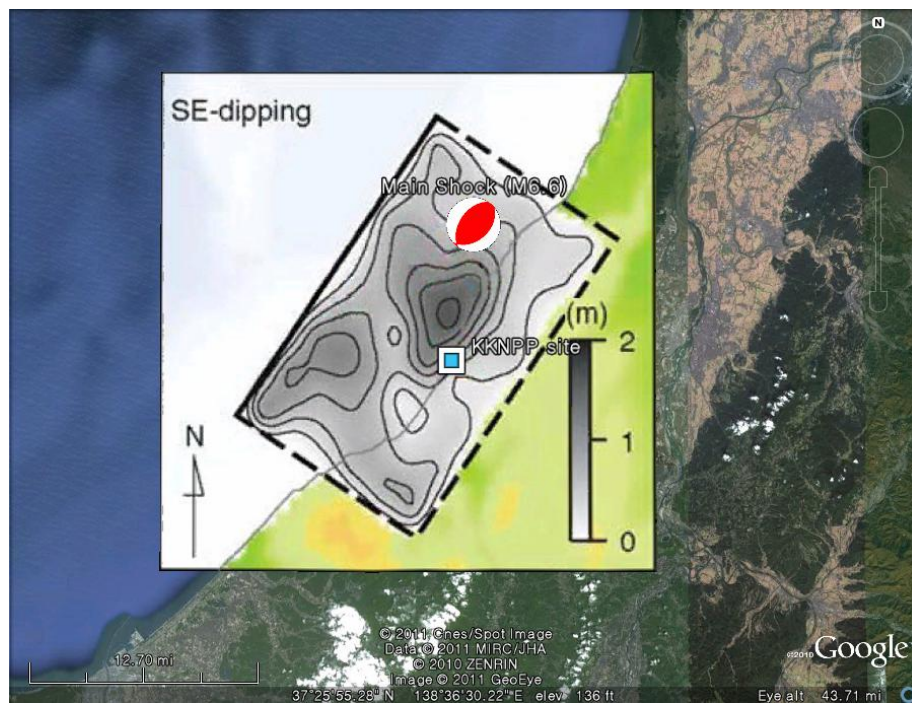
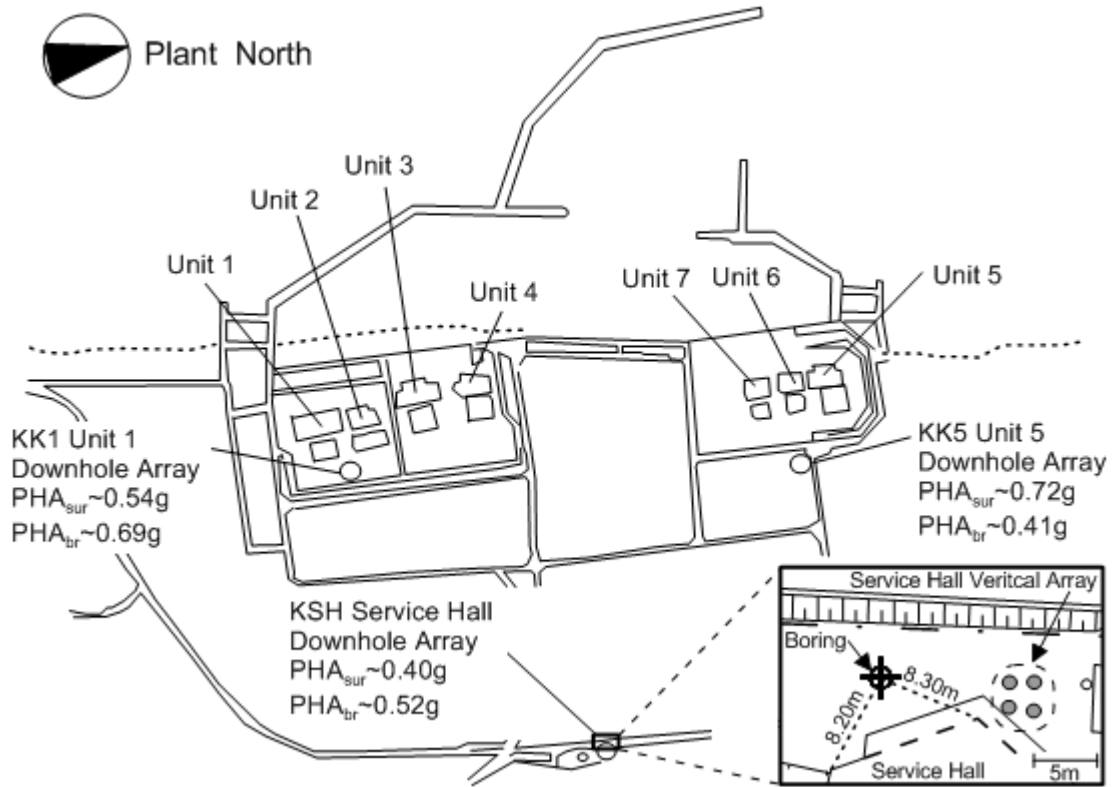


Figure 1.1 Map of Kashiwazaki area showing location of KKNPP site relative to fault rupture plane by Miyake et al. (2010). Shading on fault plane indicates slip in meters.

As shown in Figure 1.1, the Kashiwazaki-Kariwa Nuclear Power Plant (KKNPP) is located on the hanging wall of the fault above a region of relatively high slip. Accordingly, the distance of this site to the surface projection of the fault (the Joyner-Boore distance) is  $R_{jb} = 0$  km, whereas the rupture distance is  $R_{rup} = 16$  km. As described in Tokimatsu et al. [2009], the KKNPP suspended operations due to earthquake damage until partially re-opening in 2009. Figure 1.2 shows a map of the KKNPP including its seven generators (marked as Units 1-7) and three free-field downhole seismic arrays near Units 1 and 5 and the Service Hall. Recordings from the Unit 1 and 5 downhole arrays were overwritten with aftershock data and only peak accelerations remain. The Service Hall Array (SHA) recordings are intact, and as shown in Figure 1.3, this array contains four three-component accelerometers at depths of 2.4 m (Holocene dune sand), 50.8 m (Pleistocene Banjin Formation), 99.4 m (Pliocene Nishiyama Formation), and 250 m (Pliocene Nishiyama Formation) [Tokimatsu and Arai 2008]. Figure 1.2 also shows the peak near surface geometric mean accelerations, which are 0.54, 0.72, and 0.40g for vertical arrays at Unit 1, 5, and SHA, respectively. Motions near the top of the Pliocene bedrock (Nishiyama formation) were 0.69, 0.41, and 0.52g for vertical arrays at Unit 1, 5, and SHA, respectively. The lowering of peak accelerations from bedrock to surface in the Unit 1 array and SHA indicates nonlinear site response for those soil columns. In contrast, downhole to surface motions are amplified in the Unit 5 array, which is in rock. The data shown in Figure 1.2 for instruments other than the SHA are taken from Tokimatsu [2008] and TEPCO [2007].

Access to the KKNPP site was limited following the earthquake, but reconnaissance was performed by Sakai et al. [2009] and Tokimatsu [2008], who observed widespread settlement both in free-field areas and adjacent to reactor structures. Settlement near the reactors was especially large, damaging utility connections. The settlements occurred in unsaturated sandy soils, some natural and some backfilled. In the vicinity of the SHA, two lines of evidence suggest settlements of approximately  $15 \pm 5$  cm. First, as shown in Figure 1.4a, the top of one of the deep steel pipes housing a vertical array instrument extended above the ground surface by 15 cm. We infer that the pipe, whose toe is founded in competent materials, remained essentially in place while the surrounding soil settled. We are uncertain why other deep pipes housing different accelerometers in the array did not show similar extensions above the ground surface. Second, as shown in Figure 1.4b, settlement was evident around the pile-supported Service Hall building structure by amounts ranging from 10 to 25 cm. Settlements were larger immediately adjacent to

the structure, presumably because of poorly compacted backfill around the basement walls for this structure.



**Figure 1.2** Map of Kashiwazaki-Kariwa nuclear power plant showing locations of downhole arrays and geometric mean peak accelerations from 2007 Niigata-ken Chuetsu-oki earthquake. Peak accelerations are shown for surface ('sur') and bedrock ('br') conditions.

The data set from the SHA site at KKNPP is uniquely valuable in two respects. First, prior to the 2011 Tohoku Japan earthquake, the SHA recorded the strongest motions for a vertical array in soil. Vertical array recordings enable validation of ground response analysis codes and studies of dynamic soil behavior under *in situ* conditions (e.g., Zeghal et al. [1995]; Cubrinovski et al. [1996]; Kwok et al. [2008]; Tsai and Hashash [2009]). With the exception of a few arrays in liquefiable materials, previous vertical array data has generally been at low to modest shaking levels that would not be expected to induce large shear strains associated with strongly nonlinear soil behavior. It is the nonlinear condition where the need for code validation is greatest, and the strong ground motions at SHA are known to have produced nonlinear site response.

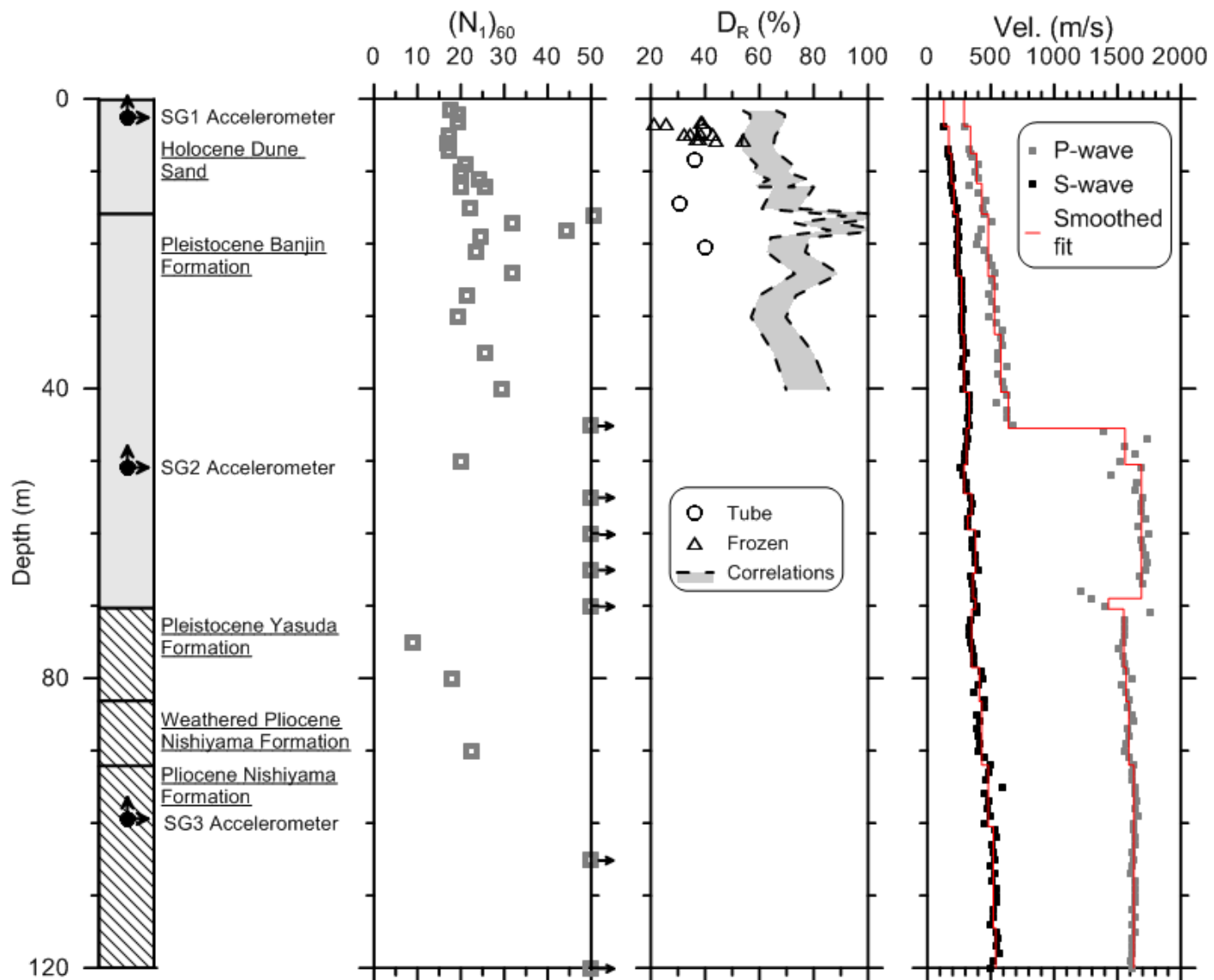
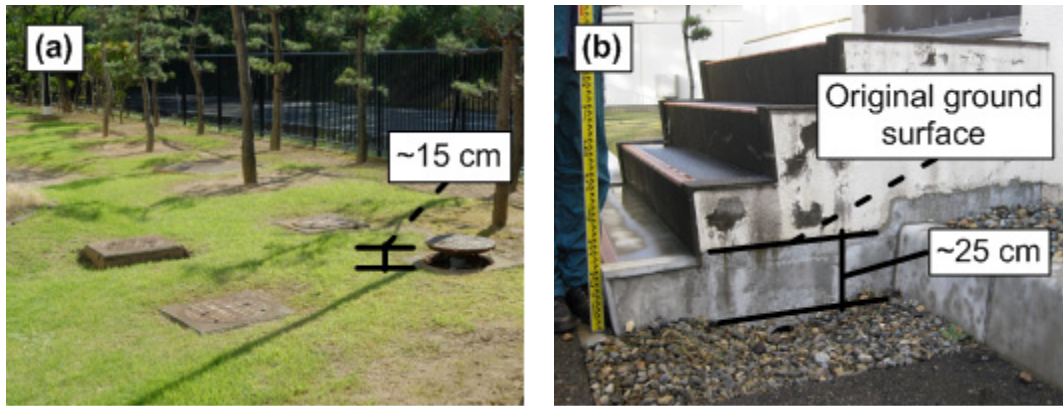


Figure 1.3 Geologic log at SHA site including instrument locations and results of penetration and suspension logging geophysical testing.



**Figure 1.4** Photographs of (a) raised pile at vertical array, showing ground settlement; and (b) settlement around Service Hall building.

Second, while ground settlements in unsaturated soils have been observed previously in strongly shaken filled ground (e.g., Pyke et al. [1975]; Stewart et al. [2002]; Wartman et al. [2003]), there are very few cases in which the pre-earthquake ground elevations are known so that grade changes induced by the earthquake can be measured [Stewart et al. 2004]. Moreover, there are no previous seismic compression case studies in which ground motions were recorded at the site. Because the SHA site has both reasonably well-defined ground settlements and vertical array recordings, it is a unique resource for validating seismic compression analysis procedures (e.g., Tokimatsu and Seed [1987]; Duku et al. [2008]).

Following this introduction, we provide a brief review of previous studies on nonlinear site response at vertical array sites and seismic compression case histories. We then describe the geotechnical characterization of materials from the SHA site and the recorded ground motions followed by a description of equivalent linear and nonlinear ground response analyses and their ability to replicate the observed near-surface recordings. Using shear strains predicted from these analyses, we then estimate ground settlement based on material-specific testing of the shallow soil materials at the SHA site and compare those predictions to the observed settlement of  $15 \pm 5$  cm.



## 2 Previous Studies

It is important to place the value of this case history in context by comparing it to previously available case studies for nonlinear site response and seismic compression. This is undertaken in the following sections.

### 2.1 NONLINEAR SITE RESPONSE

With regard to nonlinear site response, Stewart and Kwok [2008] led a multi-investigator project developing parameter selection and code usage protocols for nonlinear ground response analysis. The codes/protocols were tested against the best available vertical array data not involving soil liquefaction (because the codes are for total stress analysis). The arrays utilized were a series of stiff soil sites in Japan (Kiknet), the Lotung array in Taiwan (soft silts), the La Cienega array in California (soft clay), and the Turkey Flat array in California (shallow, stiff soil). At the Turkey Flat site [Kwok et al. 2008], peak velocities from the 2004  $M_w$  6.0 Parkfield earthquake were in the range of 7 to 8 cm/sec and calculated peak ground strains were as large as  $10^{-2}\%$ . Figure 2.1 compares predicted and observed acceleration histories at the surface and an intermediate depth, showing good comparisons.

At the other sites considered by Stewart and Kwok [2008], peak velocities were 11 to 18 cm/sec (La Cienega), 5-6 cm/sec (Kiknet), and 17-31 cm/sec (Lotung). Ground strains from these other sites were of the same order as those at Turkey Flat (slightly larger at Lotung). The level of strain is important, because one of the key attributes of the parameter selection protocols is the manner by which soil backbone curves are extended from the small strain range where dynamic soil testing is reliable (strains  $< 0.5\%$ ) to relatively large strains associated with the shear strength (1% or more). This is of considerable practical significance, because it is for these large strain problems that nonlinear ground response analysis procedures are selected for use in practice in lieu of simpler equivalent-linear methods. The SHA site provides the first example of

highly nonlinear soil behavior not involving liquefiable soils in which the induced ground strains are likely in the range of 1%.

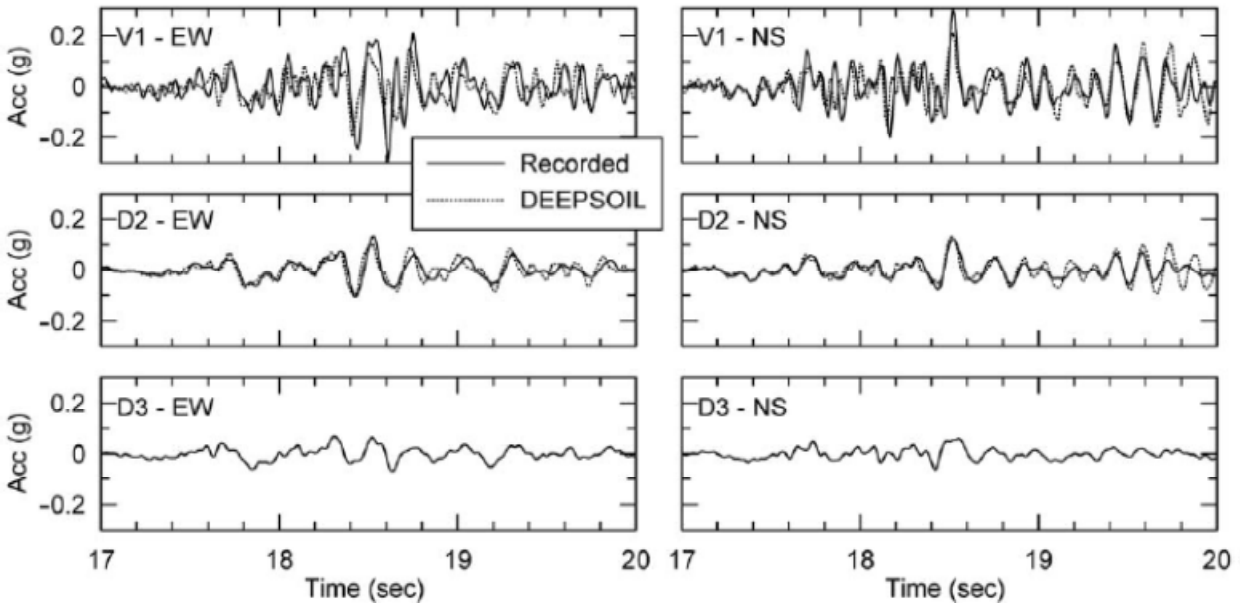


**Figure 2.1** Acceleration histories for data from the 2004 Parkfield earthquake and simulation results from site response program DeepSoil. Results are shown for two horizontal directions and two elevations (V1, ground surface; D2, 10 m depth) with the recorded input motions at elevation D3 [Kwok et al. 2008].

Tsai and Hashash [2009] used some of the same vertical array data as Stewart and Kwok [2008] in a neural network based inverse analysis of vertical arrays to extract soil properties. Their analyses were not constrained by model-based assumptions of soil behavior and hence hold the potential to provide new insights into *in situ* soil behavior. However, the approach does have the potential to map modeling errors unrelated to soil behavior (e.g., lack of one-dimensional response) into inverted soil properties. The approach was applied to the Lotung and La Cienega arrays. Shear wave velocity models were slightly adjusted from data in the “learning” process and stress-strain loops were extracted. As shown in Figure 2.2, modulus reduction and damping curves were then computed from the loops, which demonstrate stronger nonlinearity than lab-based curves (lower modulus reduction, higher damping). The higher damping is also in agreement with system identification of Lotung data from Elgamal et al. [2001]. We note in Figure 2.2 that the damping increase from the vertical array analysis seems to affect the small strain damping ( $D_{min}$ ) but not the overall shape of the damping-strain relationship.

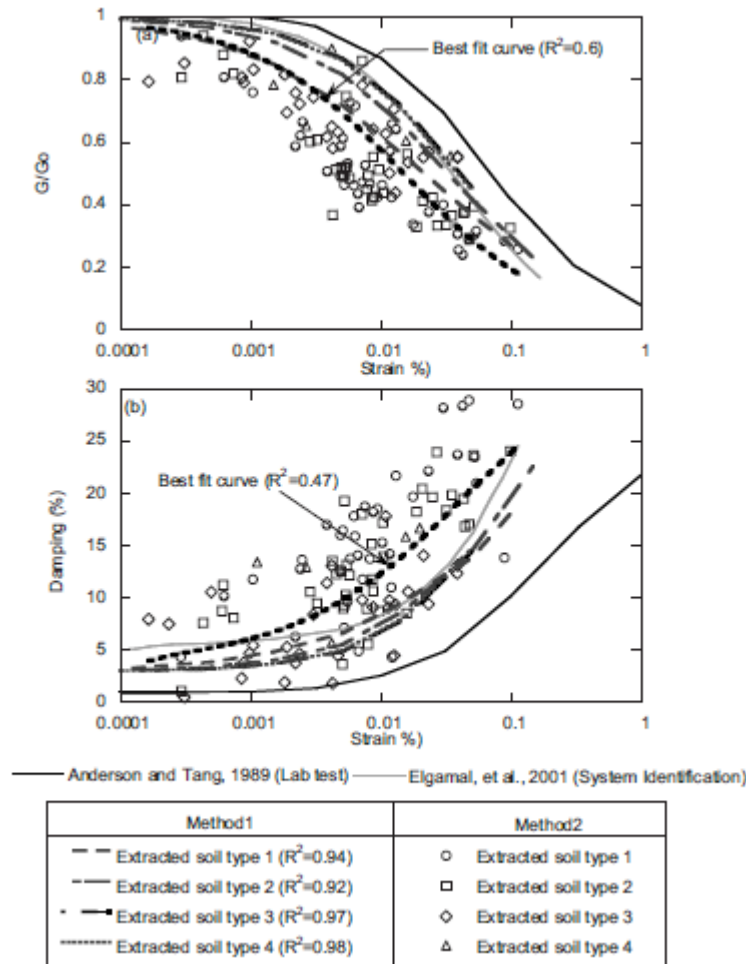


**Figure 2.2 Comparison of interpreted soil behavior by extracting soil parameters using two different methods, with curves from laboratory tests [Anderson and Tang 1989] and those from system identification [Elgamal et al. 2001], Lotung array [Tsai and Hashash 2009].**

Baise et al. [2011] examine weak motion data from a large number of sites in the Kiknet vertical array network in Japan to investigate event-to-event consistency in site transfer functions (surface/downhole) and the degree to which those transfer functions are compatible with theoretical models for one-dimensional vertical shear wave propagation (SH1D). Figure 2.3 shows examples of small and large event-to-event variability in weak motion amplification from their analysis, while Figure 2.4 shows examples of good and poor fit of the SH1D model to data. Of the seventy-four sites considered, only eleven had good fits to the SH1D model, although an unknown number of the misfits may be simply associated with modest errors in the shear wave velocity profile. Nonetheless, large misfits as shown in Figure 2.4 (right side) indicate a clearly

more complex site response than SH1D. Sites such as those would not be good candidates for calculating one-dimensional nonlinear site response for comparison to observation.

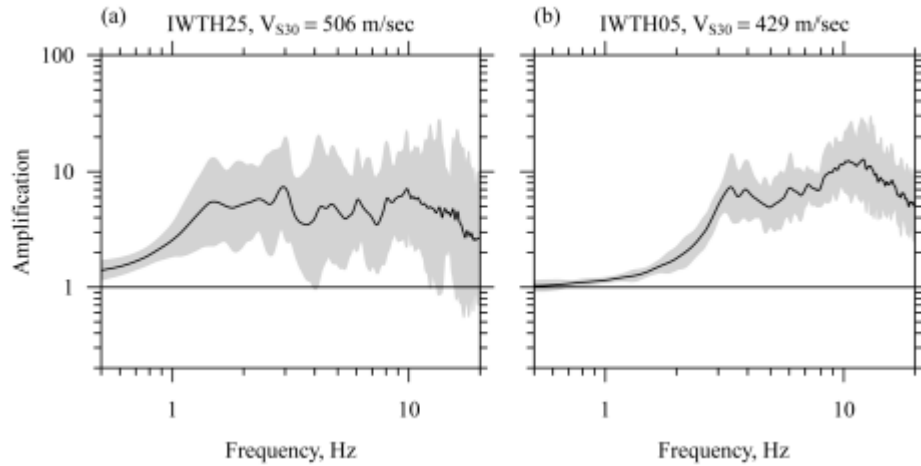


**Figure 2.3** Transfer functions at two stations, illustrating inter-event variability: (a) IWTH25 is characteristic of a site with a large degree of inter-event variability, and (b) IWTH05 is characteristic of a site with low inter-event variability. The median prediction of the transfer function is shown as a black line, and the 95% confidence band is shown in gray [Baise et al. 2011].

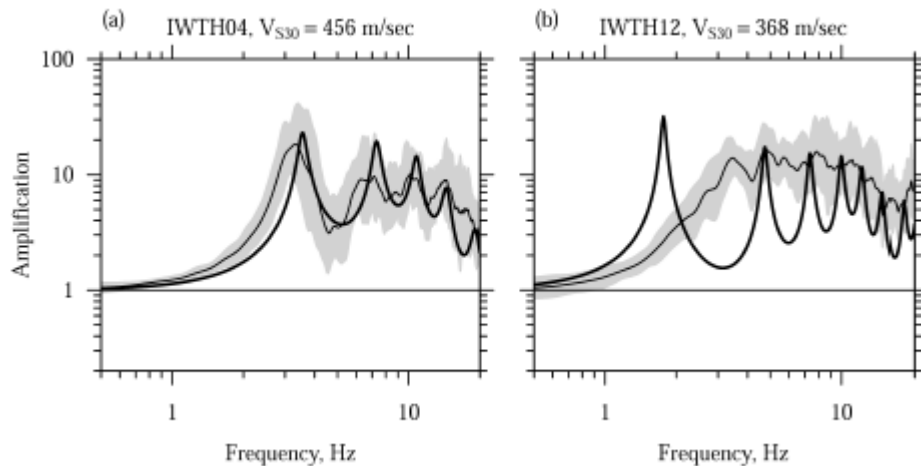


**Figure 2.4** Transfer functions at two stations, illustrating goodness-of-fit: (a) IWTH04 is characteristic of a site where the SH1D model accurately predicts the transfer functions, and (b) IWTH12 is characteristic of a site where the SH1D model poorly predicts a transfer function [Baise et al. 2011].

## 2.2 SEISMIC COMPRESSION CASE STUDIES

There are several well-documented field case histories of settlements from seismic compression. These include the Jensen Filtration Plant shaken by the 1971 San Fernando earthquake [Pyke et

al. 1975], two sites in Santa Clarita shaken by the 1994 Northridge earthquake [Stewart et al. 2004], damaged embankments from the 2001 Southern Peru earthquake [Wartman et al. 2003], and ground failure patterns from the 2003 Colima earthquake [Wartman et al. 2005].

The Joseph Jensen Filtration Plant site in Granada Hills, California, was formed by a cut-and-fill operation. The compacted clayey sand fill was up to 17 m thick overlying 1.5 to 6 m of alluvium. The groundwater table was located in the alluvial layer, which liquefied from estimated peak horizontal accelerations of about 0.5-0.6g from the  $M_w$  6.6 San Fernando earthquake. As shown in Figure 2.5, recorded settlements were about 12.7 cm along a survey baseline. However, Pyke et al. [1975] attributed some of the observed settlement to lateral spreading and estimated settlements due to seismic compression to be around 8.9 to 10.2 cm, which was about 0.7% of the fill thickness.

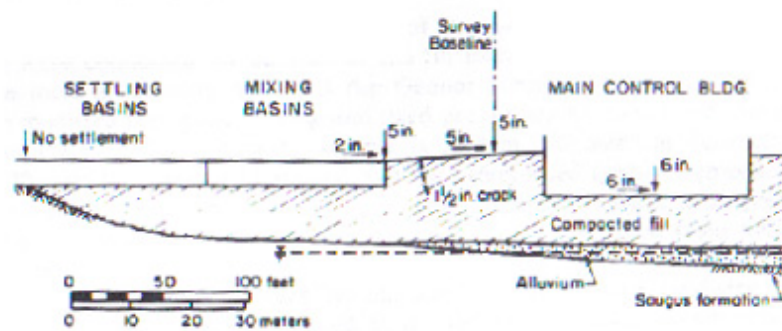


**Figure 2.5 Jensen Filtration Plant profile [Pyke et al. 1975].**

In their analysis, Pyke et al. [1975] conducted a series of strain-controlled cyclic simple shear tests on the site fill material. Subsurface investigations revealed the clayey sand fill to be uniformly compacted with an average dry density of  $1937 \text{ kg/m}^3$  and an average water content of 10%. This equated to a relative compaction of approximately 92%. The strain histories from their site response analysis were used to determine the equivalent number of uniform shear strain cycles, which they found to be five with a shear strain of two-thirds the peak value. Applying these values to the simple shear tests produced an estimate of settlement that was approximately one third of that observed in the field. As shown in Figure 2.6a, Pyke et al. [1975] went on to conduct multi-directional shake table tests and found that the total settlement caused by the combined horizontal motions are approximately equal to the sum of the settlements caused by the horizontal motions acting separately. As shown in Figure 2.6b, the application of vertical

shaking combined with horizontal further increased measured settlements by amounts ranging from approximately 20% to 50% for effective vertical accelerations ranging from 0.15-0.3g. Considering this, Pyke et al. [1975] applied a correction factor for multi-directional loading that increased their computed settlement to within the range of observed field settlements.

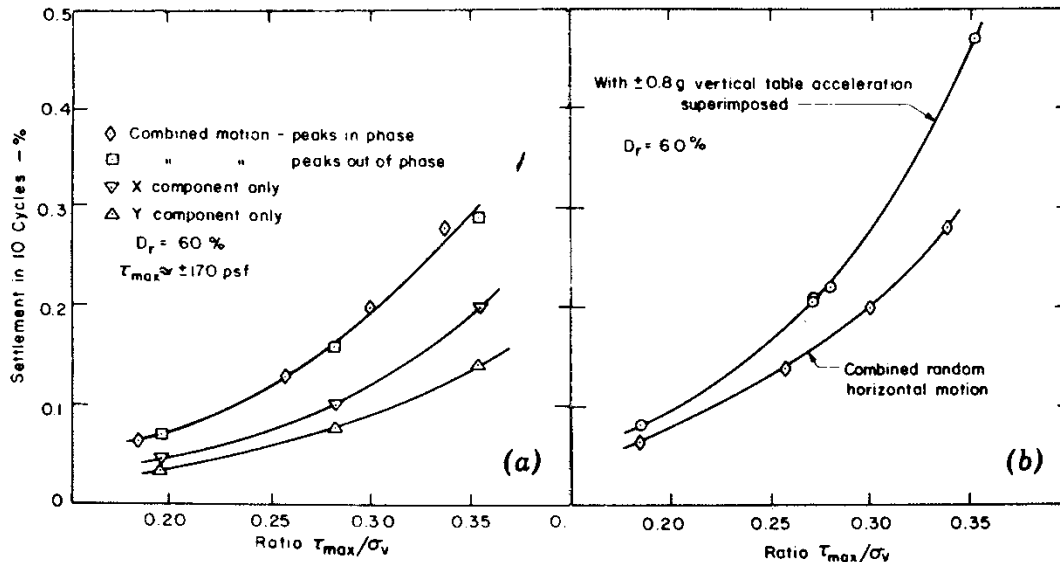


**Figure 2.6 Comparison of settlements under (a) components and combined random motions and (b) in three-dimensional shake table tests [Pyke et al. 1975].**

After the 1994  $M_w$  6.7 Northridge earthquake, two sites in Santa Clarita, California, (denoted Sites A and B) had settlements from seismic compression that could be reliably estimated. For Santa Clarita Site A, the soils consisted of a sandy clay and clayey sand fill up to 24 m thick underlaid by shallow alluvium and rock. Soil conditions show the fill generally being compacted to approximately 88% modified Proctor relative compaction and dry of optimum. Stewart et al. [2004] estimated peak horizontal accelerations of 0.5 to 0.7g with measured settlements of up to 22 cm from pre and post-earthquake surveys. For Santa Clarita Site B, the soils consisted of a silty sand fill 15 to 30.5 m thick lying over rock. Soil conditions indicate modified Proctor relative compactations of about 92%-93% near the surface and about 95% at depth. Stewart et al. [2004] estimated peak horizontal accelerations of 0.8 to 1.2 g with measured settlements of 1.3 to 6.1 cm from pre and post-earthquake surveys. Figure 2.7 shows a plan of Site B indicating fill depths and measured settlements.

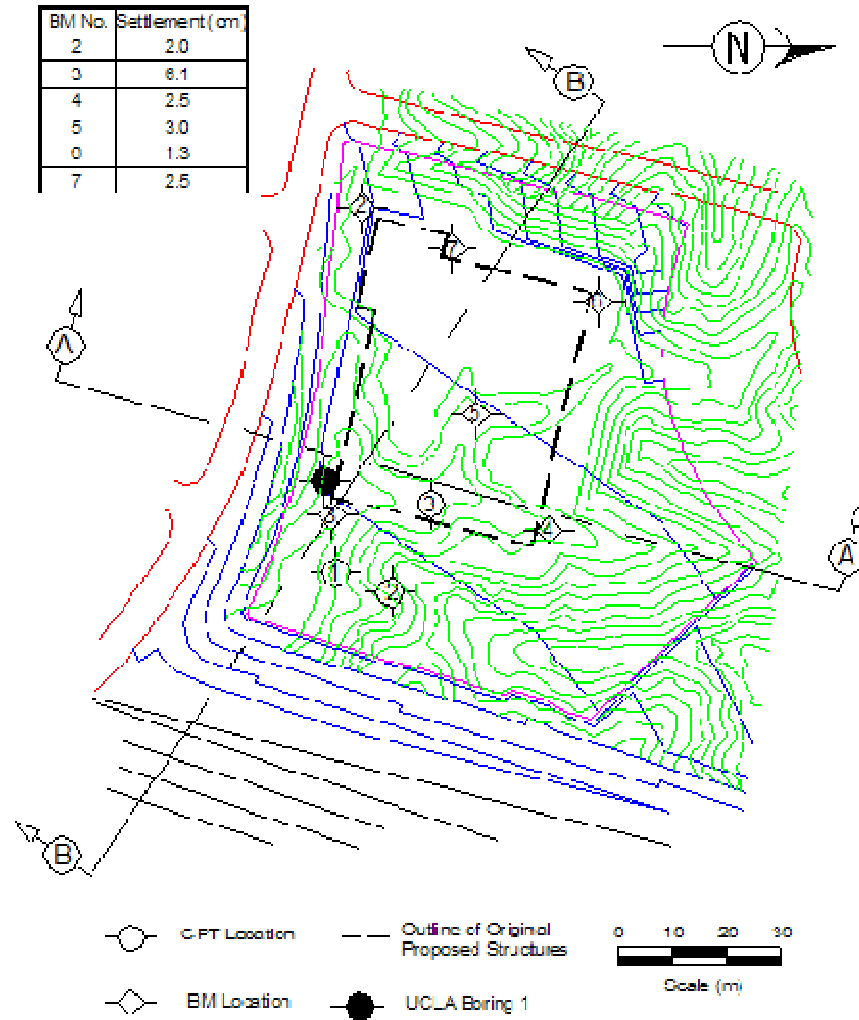


**Figure 2.7 Plan and settlement of Santa Clarita Site B [Stewart et al. 2004].**

In their analysis, Stewart et al. [2004] used an approach that was similar to Pyke et al. [1975]. For each site, they performed decoupled analyses of shear and volumetric strain. Shear strain was calculated using one-dimensional and two-dimensional ground response analyses, while volumetric strain was evaluated from shear strain using material-specific models derived from simple shear laboratory testing that incorporated important effects of fines content and as-compacted density and saturation. Figure 2.8 shows the material-specific model used to estimate vertical strains for Site B. These vertical strains were integrated over the height of the fill to estimate the total settlement from seismic compression. Figure 2.9 summarizes this process for a cross section at Site B. The top plot in Figure 2.9 displays the shear strain profile from two-dimensional ground response analyses while the bottom plot displays the estimated settlement

obtained when the shear strain results are combined with the material-specific volumetric strain model from Figure 2.8. Overall, the computed settlements were in good agreement with the observed settlements at both Site A and Site B.

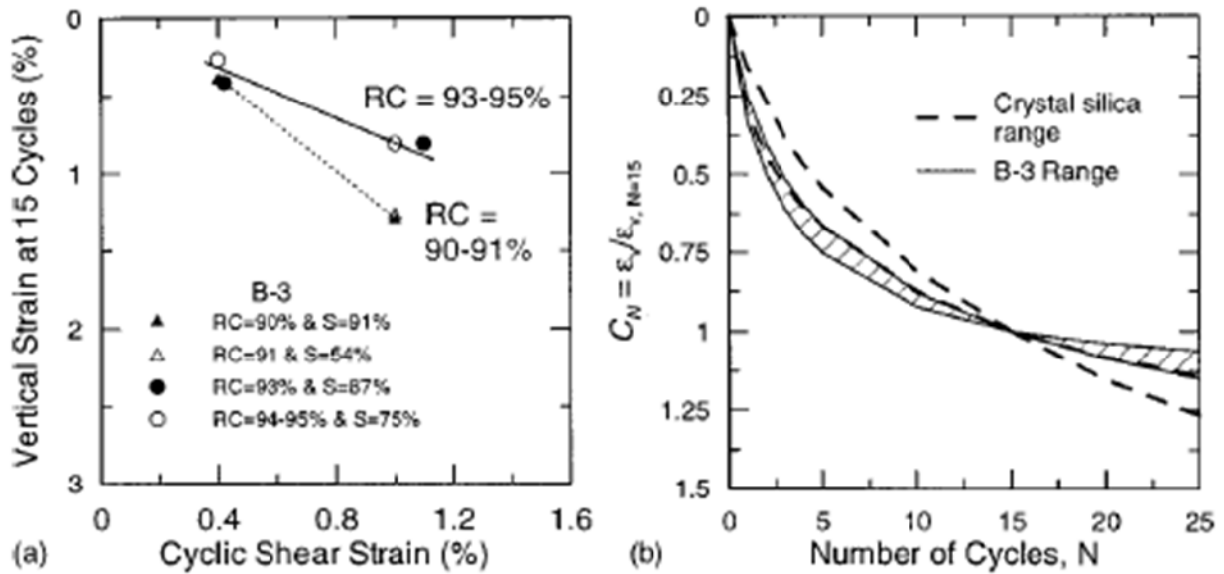


**Figure 2.8 (a) Seismic compression and (b) variation of normalized vertical strain with number of cycles of soil from Site B [Stewart et al. 2004].**

In the 2001  $M_w$  8.4 Southern Peru earthquake, many highway embankment sites were damaged due to seismic compression and these damaged areas were almost entirely underlain by fill materials. Wartman et al. [2003] described these fills as consisting of gravelly, sandy, and silty soils with measured settlements of at least 10 cm for 2- to 4-m-high embankments. The investigators noted that settlements were typically proportional to the height of the embankment and uniform across the road; Figure 2.10 shows a sample schematic of observed ground deformations. Wartman et al. [2003] also observed seismic compression in a natural silty fine Aeolian sand overlaid by a highway road. Measured settlement was about 10 to 25 cm with lateral offsets of 5 to 10 cm. The investigators found that newer embankments performed better than older embankments and attributed it to improved compaction. Detailed back-analyses to evaluate the predictability of these deformations have not been completed.

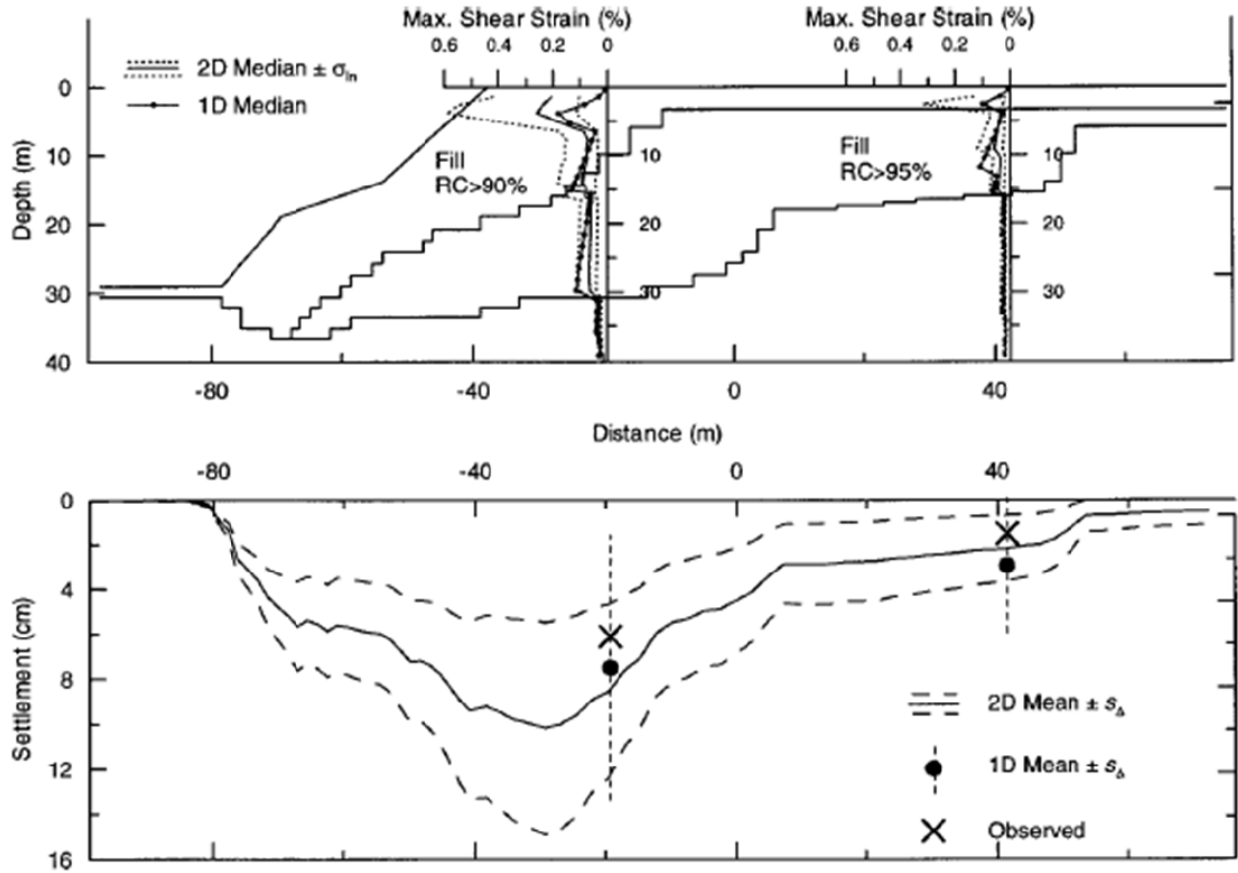


**Figure 2.9** Vertical profiles of shear strain from site response analyses (top frame) and lateral profiles of observed and calculated settlement (bottom frame) along a cross section for site B [Stewart et al. 2004].

Wartman et al. [2005] also observed seismic compression induced damage at bridge embankments from the 2003  $M_w$  7.6 Colima earthquake. These embankments were typically 7 to 8 m high and were constructed of local sandy and silty soils compacted to 90 to 95% relative compaction, based on the modified Proctor standard. Earthquake induced settlements were uniform across the width of the roadway, with differential settlements of 4 to 10 cm at the bridge-embankment interface. They also found widespread ground failures in a neighborhood that was developed on top of uncontrolled fill consisting of sandy and gravelly soils. Portions of this neighborhood underlain by a shallow groundwater table typically liquefied, while portions founded on unsaturated soils experienced seismic compression, manifested through ground cracking and settlements ranging from 5 to 20 cm. Additionally, several similarly backfilled mining pits also experienced seismic compression. These settlements were typically 15 to 30 cm,

with certain areas settling as much as 1.5 m. Detailed back-analyses to evaluate the predictability of these deformations have not been completed.

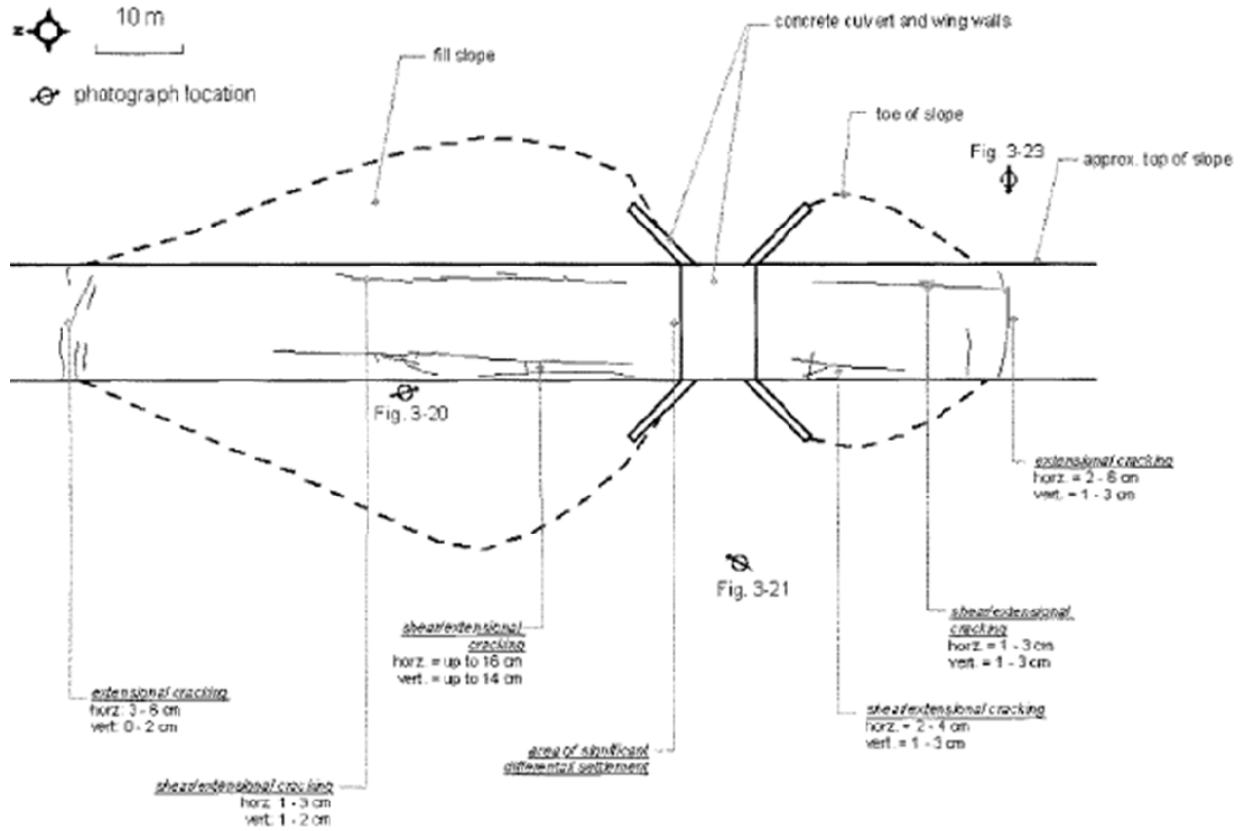


Figure 2.10 Schematic of observed ground deformation at a highway embankment site [Wartman et al. 2003].

## 3 Site Characterization

We undertook a site exploration program for the Service Hall site at the Kashiwazaki-Kariwa Nuclear Power Plant site that included review of prior investigations, the drilling of a borehole including standard penetration testing with energy measurements, and suspension logging of seismic velocities. The results of this work are described in this chapter. Our field exploration work was performed in October 2009 under contract with Tokyo Soil Research.

### 3.1 RESULTS OF GEOTECHNICAL EXPLORATION (CURRENT AND PRIOR STUDIES)

The location of the borehole drilled at the SHA site is shown in the inset of Figure 1.2. The borehole was drilled using rotary wash procedures with a hole diameter of 116 mm for the upper 20 m and a hole diameter of 86 mm thereafter. The exploration reached a maximum depth of 120.4 m after eleven days of drilling. A relatively detailed boring log—summarized in Figure 1.3—is provided in Appendix A (Electronic Supplement). The surface geology consists of the Holocene Arahama sand dune formation. This sand overlies the Pleistocene Banjin formation, the Pleistocene Yasuda formation, and the Pliocene Nishiyama formation. We also obtained selected results from previous geotechnical and geophysical site characterization that was conducted about 170 m from the Service Hall site [Tokyo Soil Research 2009]. Those data are generally consistent with the stratigraphy revealed by our exploration (see Figure 1.3).

We sampled soil materials using an SPT sampler driven with an automatic trip-release safety hammer with mass 63.5 kg dropping 75 cm. The SPT sampler had an outer diameter of 51 mm and an inner diameter of 35 mm. Additional relatively undisturbed samples were obtained by pushing a triple-barrel pitcher sampler (similar to a Shelby tube) with an outer diameter of 76 mm and an inner diameter of approximately 74 mm. The SPT samples were used for classification purposes only, whereas specimens from the pitcher sampler were used for dynamic

testing as described below. The boring logs from the previous investigation include blowcounts, but do not indicate the energy delivered. Average compression and shear wave velocities are also shown, but they appear to be at low resolution. Moreover, a limited number of shallow frozen samples have been collected in the vicinity of the SHA site.

For SPT sampling, we measured the percentage of the total theoretical energy delivered to the split-spoon sampler—or energy ratio—using procedures in ASTM D6066-98 and ASTM D1586 (see also Abou-Matar and Goble [1997]). The rods used in SPT sampling conformed with Japanese Industrial Standards (JIS), which are slightly different from AW rods (JIS rod outer diameter equals 40.5 mm and inner diameter equals 31 mm). The instrumented rod section used for energy measurement was AW, and couplers were machined to connect it to the JIS rods. Additionally, Japanese practice has the driller tap the first 10 cm of sampler penetration from the bottom of the borehole before the SPT is conducted. The SPT blowcount is then taken as the total number of blows to lower the rod 30 cm in 10 cm intervals. Refusal was set at 60 blows. As shown in Figure 3.1, the energy ratios obtained in these tests range from 84% to 94% with an average of 87%. There does not appear to be a strong, systematic depth-dependence to the energy ratios. Energy-corrected blow counts were then calculated as:

$$N_{60} = N \times \frac{ER}{60} \quad (3.1)$$

Overburden corrections were then applied as:

$$(N_1)_{60} = N_{60} \times \left( \frac{p_a}{\sigma'_v} \right)^m \quad (3.2)$$

where  $m$  is a function of relative density per Boulanger [2003],  $p_a$  is equal to 101.3 kPa, and  $\sigma'_v$  is the effective vertical stress at the sample depth (approximated as the total stress above the water table, which neglects matric suction). The resulting energy and overburden-corrected blow counts generally range from 15 to 30 in the sandy materials, as shown in Figure 1.3. No clean sand corrections are applied because fines contents are low (< 5%).

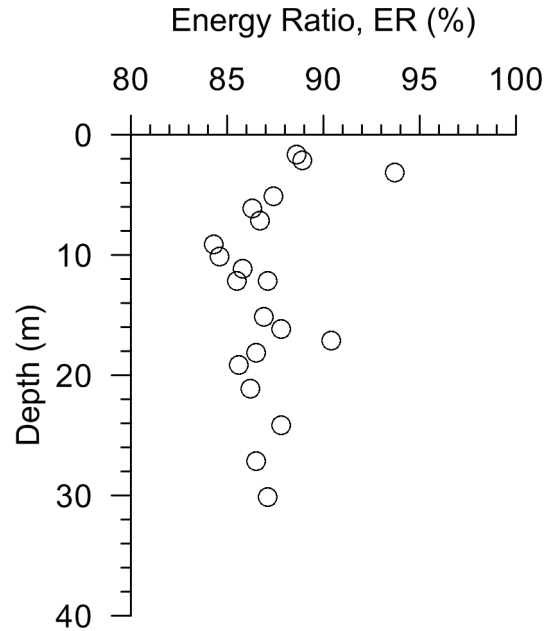


**Figure 3.1** Variation with depth of energy ratio in standard penetration tests.

Relative densities ( $D_R$ ) can be estimated from the corrected blow count data as [Idriss and Boulanger 2008]:

$$D_R = \sqrt{\frac{(N_1)_{60}}{C_d}} \quad (3.3)$$

where  $C_d$  has been proposed as 44 by Tokimatsu and Yoshimi [1983]; 55 to 65 for fine and coarse sands, respectively, by Skempton [1986]; 26 and 51 for silty and clean sands, respectively, by Cubrinovski and Ishihara [1999]; and 46 for generic clean sands by Idriss and Boulanger [2008]. Given the low fines content and small mean grain size ( $D_{50}$ ) of the sandy soils (see following section for data), we estimated an applicable range of  $C_d$  of 40 to 60. This produces the relative densities shown in Figure 1.3, which generally range from about 50% to 80%.

Suspension logging was performed in our borehole to measure P and S wave velocities at 1-m intervals [Nigbor and Imai 1994]. Resulting interval velocities are shown in Figure 1.3. The results show the Holocene dune sand (0 to 16 m deep) to have  $V_s = 130$ -240 m/sec. Underlying Pleistocene materials (16 to 70 m deep) have  $V_s = 240$ -390 m/sec and the bedrock materials have velocities increasing from  $V_s = 330$ -450 m/sec (70-83 m) to  $V_s = 400$ -600 m/sec (> 83 m). The P-wave profile indicates a groundwater depth of about 45 m.

## **3.2 LABORATORY TESTING**

### **3.2.1 Index Tests**

Soil materials recovered from the SPT split spoon sampler were combined to form bulk samples for index tests including grain size distribution, Atterberg Limits, and maximum and minimum unit weight. One bulk sample was prepared from sandy materials (from the Holocene and Pleistocene materials in the upper 70 m), whereas SPT samples from two relatively cohesive materials (Pleistocene mudstone from 70-83 m and Pliocene mudstone from 83 m to 120 m) were kept in individual packages. Results of these index tests are given in Table 3.1. The Holocene and Pleistocene sands are classified as poorly graded sands (SP) using the unified soil classification system with a fines content of 4.1%. Mean grain size  $D_{50}$  is approximately 0.25 mm and coefficient of uniformity,  $C_u$  is approximately 2.55. The two cohesive Pleistocene samples had liquid limits of 65 to 69 and plasticity indices of 22 to 33. The cohesive Pliocene sample had a liquid limit of 69 and a plasticity index of 22. Maximum and minimum dry unit weights (and void ratios) were evaluated for the sand bulk sample using the Japanese method and dry tipping (ASTM D4253 and D4254, respectively).

### **3.2.2 Relative Densities**

Triple-barrel pitcher samples were obtained at depths of 4, 8, 14, and 20 m. Dry unit weights and water contents were measured from these samples, from which void ratios could be computed using a specific gravity of  $G_s = 2.74$ . Results of these index tests are shown in Table 3.1. As shown in Figure 1.3, these results can be combined with the minimum and maximum densities from the bulk sample to evaluate relative densities, which are mostly near 40%. These  $D_R$  are smaller than those estimated from penetration resistance correlations. Additional  $D_R$  from shallow frozen samples obtained in a separate investigation elsewhere near the Service Hall site range from 20% to 50%, as shown in Figure 1.3.

### **3.2.3 Shear Strength and Modulus Reduction and Damping Relations**

Soil specimens were carefully extracted from the sample tubes, trimmed, and re-consolidated for monotonic and cycle shear testing. Because the specimens are unsaturated, no B-value

measurements were made and volume change was allowed during shear. Soil specimens were found to have sufficient cementation/cohesion to maintain their integrity upon extraction.

Consolidated-drained triaxial compression tests were performed in the Tokyo Soil Research Laboratory after consolidating three specimens from each tube to isotropic stresses of 0.5, 1.0, and 2.0× $\sigma_v$ , where  $\sigma_v = in situ$  total stress. Table 3.1 summarizes the test results, which indicate drained friction angles of 36 to 39° (average of 37.6°) for the confining pressures considered. These results are comparable to estimates from  $\phi'$ -blow count correlations by Hatanaka and Uchida [1996], which are 35 to 41° for  $(N_I)_{60} = 15$  and 30, respectively.

**Table 3.1 Summary of soil index tests, triaxial compression shear strength tests, and resonant column-torsional shear tests for dynamic soil properties.**

Sample									Triaxial		RCTS	
Depth	$\sigma_c$	$\gamma_{dry}$	w	LL	PI	e	$e_{min}$	$e_{max}$	$\phi$	$G_{max}$	$D_{min}$	$\gamma_r$
(m)	(kPa)	(kN/m <sup>3</sup> )	(%)						(°)	(MPa)	(%)	(%)
4-5 <sup>P</sup>	81	14.95	19.9		NP	0.794			39.4	50	1.3	0.057
8-9 <sup>P</sup>	153	14.23	15.0		NP	0.886			36.4	74	0.9	0.1
14-15 <sup>P</sup>	256	14.42	23.3		NP	0.859			38.7	88	1.7	0.15
20-21 <sup>P</sup>	361	14.18	11.9		NP	0.899			35.9	112	0.8	0.163
Bulk (sand) <sup>S</sup>			16.6		NP		0.538	0.930				
75.15 <sup>S</sup>				69	33							
80.15 <sup>S</sup>				65	22							
90.15 <sup>S</sup>				69	22							

P – Pitcher sample

S – SPT samples

Using the same triple-barrel pitcher samples from the four sample depths, additional specimens were prepared for resonant column/torsional shear testing in the Tokyo Soil Research Laboratory. These specimens were isotropically consolidated to *in situ* stresses prior to cyclic testing. Each individual sample was subjected to a series of 10 cycles at 12-13 strain amplitudes. The small-strain shear modulus ( $G_{max}$ ) and material damping ( $D_{min}$ ) were taken from the resonant column tests per ASTM D4015. At each respective strain amplitude from the torsional shear tests, secant modulus ( $G$ ) and material damping ( $D$ ) were evaluated at the fifth and tenth cycle

per Japanese Standard JGS 0543-2000 (similar to ASTM D4015). We did not observe significant changes in  $G$  and  $D$  between cycles. Figure 3.2 plots the modulus reduction ( $G/G_{max}$ ) and damping curves for the fifth loading cycle. The pseudo reference strain from these tests,  $\gamma_r$ —which is the shear strain at which  $G/G_{max} = 0.5$ —is listed in Table 3.1.

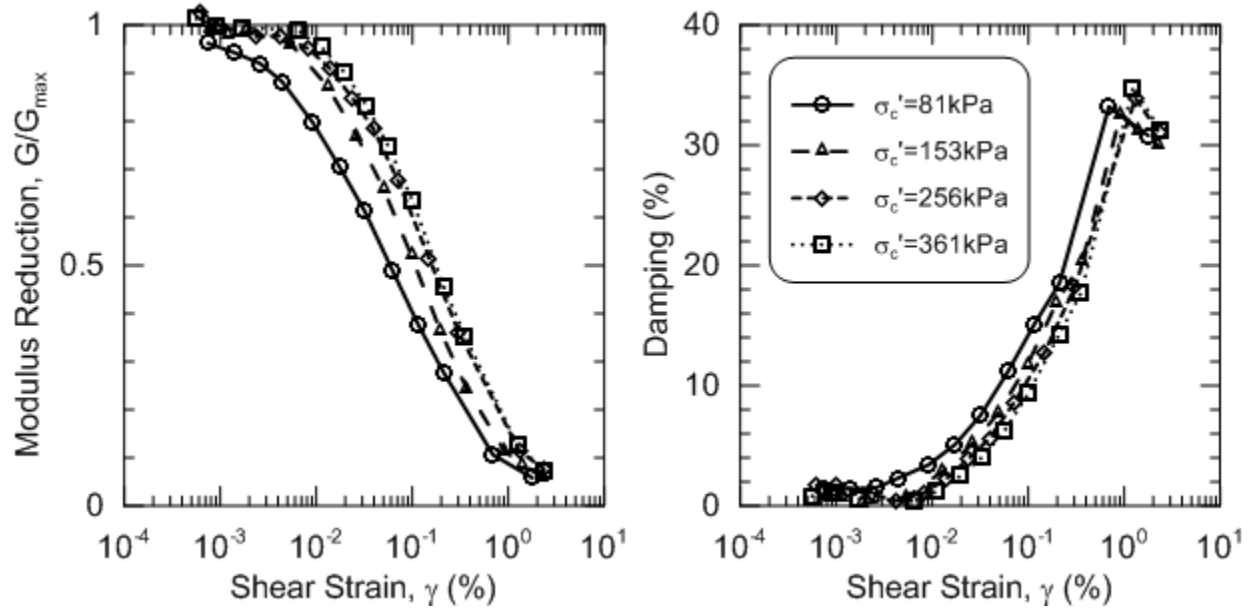


**Figure 3.2** Modulus reduction and damping curves from resonant column and torsional shear tests performed on specimens from four samples.

### 3.2.4 Cyclic Volume Change

In order to estimate cyclic volume change of the Holocene and Pleistocene sand materials, reconstituted specimens were prepared from the bulk samples for cyclic simple shear testing at a range of strain amplitudes. While volume change also occurred during the torsional shear tests, they are not suitable for estimation of seismic compression because of the successively larger strain cycles applied to the specimens, which biases volumetric strains relative to what would occur in virgin loading for the same shear strain amplitude (e.g., Seed et al. [1977]). While it would be preferable for the simple shear tests to be on intact specimens, we anticipate the results are suitable because fabric effects on dynamic soil properties have been found to be modest for strain-controlled testing (e.g. Dobry and Ladd [1980]; National Research Council [1985]; Polito and Martin [2001]).

Specimens for simple shear testing were prepared to field moisture contents (6% to 18%) and compacted via moist tamping to target relative densities near 35% and 65% to reflect the

possible range of *in situ* conditions as revealed by laboratory tests and SPT correlations. Other sample preparation procedures match those described by Duku et al. [2008]. Specimens were confined laterally by a wire-reinforced Norwegian Geotechnical Institute (NGI) membrane with a diameter of 102 mm. Specimens were consolidated under vertical stresses of  $\sigma_v = 50, 100, 200,$  or 400 kPa and then sheared under constant displacement amplitudes (corresponding to shear strains between 0.01% to 1%) at a frequency of 1 Hz using the digitally controlled simple shear device described by Duku et al. [2007]. Figure 3.3a and Figure 3.3c summarize the vertical strain at 15 cycles  $[(\varepsilon_v)_{N=15}]$  from these tests and show no apparent influence of water content. Power law fits to the data were established as [Duku et al. 2008]:

$$(\varepsilon_v)_{N=15} = a(\gamma - \gamma_{tv})^b \quad (3.4)$$

where  $a$  and  $b$  are regression coefficients listed in Table 3.2 and  $\gamma_{tv}$  is the volumetric threshold shear strain estimated from test data using the method by Yee et al. [2011].

Parameter  $b$  can be thought of as the slope of the best fit line through test data in log-log space, while parameter  $a$  can be thought of as the vertical strain at about 1% shear strain. Figure 3.4 illustrates the effect of relative density on parameter  $a$  with slope parameter  $b$  fixed to 1.2. The value of  $b = 1.2$  is an average obtained from prior testing of 16 clean sands [Duku et al. 2008] and represents reasonably well the SHA data as well. As shown in Figure 3.4, the SHA data are consistent with a  $D_R$ - $a$  model for clean sands by Duku et al. [2008].

Equation (3.4) represents the vertical strains from seismic compression at a total stress overburden pressure of  $\sigma_v = 100$  kPa. For other overburden pressures, a correction factor  $K_{\sigma,\varepsilon}$  can be applied to parameter  $a$ , which has been found in previous work [Duku et al. 2008] to be reasonably represented as:

$$K_{\sigma,\varepsilon} = \left( \frac{p_a}{\sigma_v} \right)^{0.29} \quad (3.5)$$

Parameter  $K_{\sigma,\varepsilon}$  represents of the ratio of  $a$  for arbitrary  $\sigma_v$  to  $a$  at  $\sigma_v = 100$  kPa. Figure 3.3e shows that test results for the SHA soils fit this overburden model well.

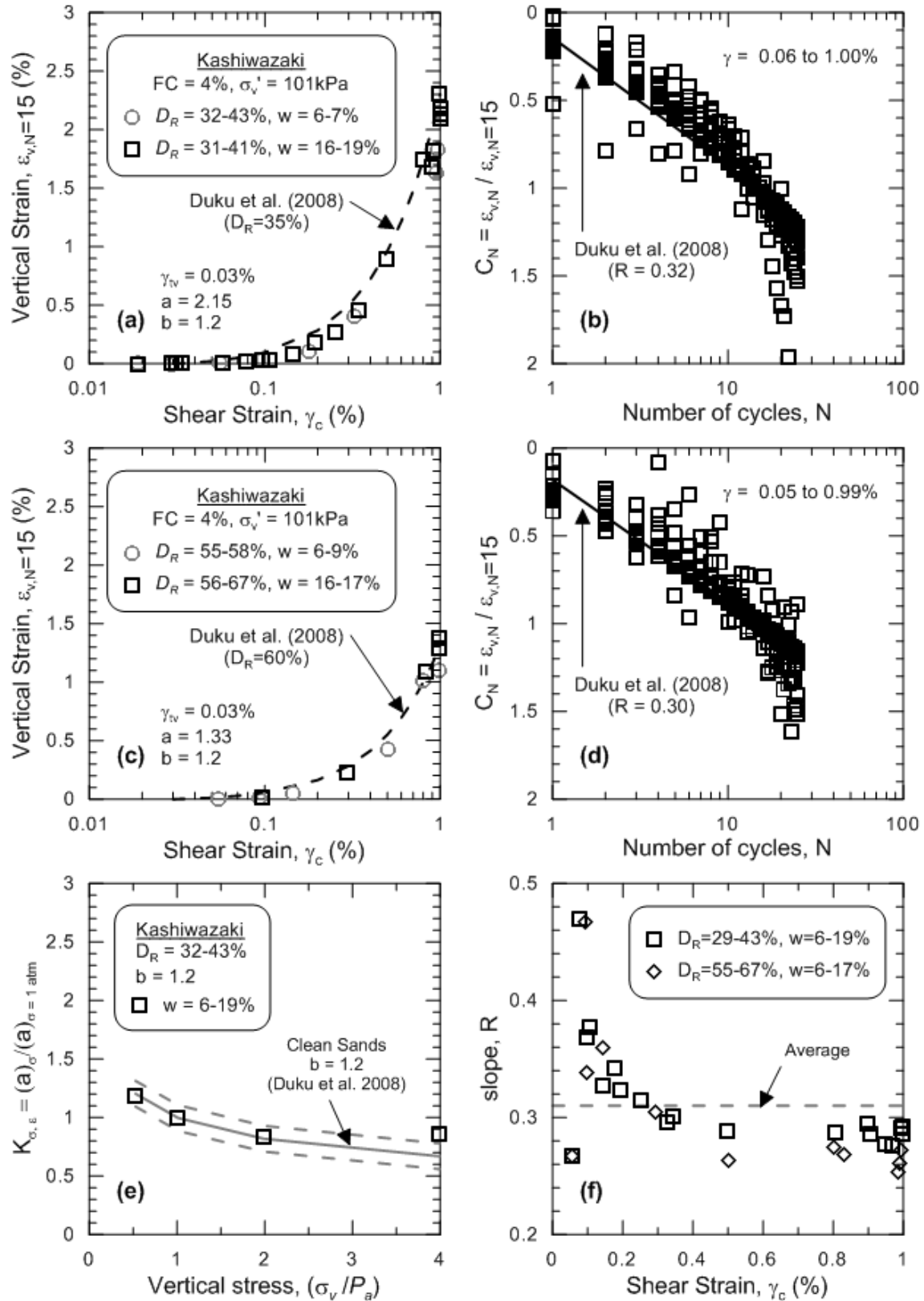


**Figure 3.3** Results of simple shear tests showing cyclic volume change characteristics of sandy materials in upper 70 m of SHA site.

**Table 3.2 Suites of cyclic simple shear tests and regressed parameters.**

$D_R$	$w$	$\sigma_v$	$a$	$b$	$\gamma_{tv}$	$a^{**}$
(%)	(%)	(kPa)			(%)	
32-43	6-7	100	1.91	1.34	0.03	1.88
28-42	17-18	50	2.50	1.11	0.038	2.56
31-41	17-19	100	2.27	1.33	0.034	2.23
33-43	17-18	200	1.86	1.42	0.03*	1.79
31-41	17-18	400	1.95	1.54	0.044	1.86
55-58	6-9	100	1.24	1.28	0.03*	1.22
56-67	16-17	100	1.42	1.33	0.03*	1.40
62-62	17-18	400	0.82	1.39	0.05*	0.63

\* assumed values due to lack of data for  $\gamma_{tv}$

\*\*  $b$  fixed at 1.2

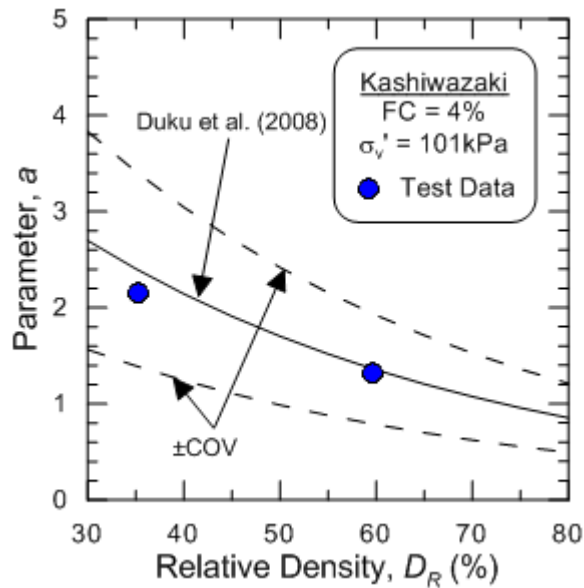


**Figure 3.4 Comparison of parameter  $a$  for KKNPP sand with slope parameter  $b = 1.2$  against the clean sand model by Duku et al. [2008].**

Duku et al. [2008] also provided a relationship to describe the effect of the number of loading cycles, given as:

$$C_N = R \ln N + c \quad (3.6)$$

where  $C_N$  equals  $(\varepsilon_v)_N / (\varepsilon_v)_{N=15}$ ,  $R$  is the regressed slope parameter,  $N$  is the number of loading cycles, and  $c$  equals  $1 - [\ln(15)R]$ . Data for  $C_N$  and  $R$  is shown in Figure 3.3b, d, and f, giving an average value around 0.31, which is close to the average value of 0.29 obtained by Duku et al. [2008].

Equation (3.4) and its modifiers (Equations. 3.5 and 3.6) apply for ground shaking in a single horizontal direction. We examined the degree to which multi-directional shaking affects seismic compression behavior through a series of one-dimensional and two-dimensional simple shear tests. As shown in Figure 3.5, sample shear strain histories computed from preliminary ground response analyses at about 8 m depth for orthogonal fault normal (FN) and fault parallel (FP) directions were imparted to three similarly prepared soil specimens under three conditions: (1) both FN and FP applied together in a two-dimensional test; (2) FN only applied in a one-dimensional test; (3) FP only applied in a one-dimensional test. The vertical strain histories resulting from this sequence of three tests are shown in Figure 3.5, indicating that the cumulative vertical strain from multi-direction shaking is practically identical to summation of vertical strains evaluated independently in the two one-dimensional tests. These results support the findings of Pyke et al. [1975], described previously in Section 2.2.

The results of these tests, as parameterized above, comprise a material-specific volumetric strain material model (VSMM) for the dune sand materials at the SHA site conditional on a relative density of about 35% and 65%. This VSMM will be used subsequently for estimation of settlement from seismic compression.

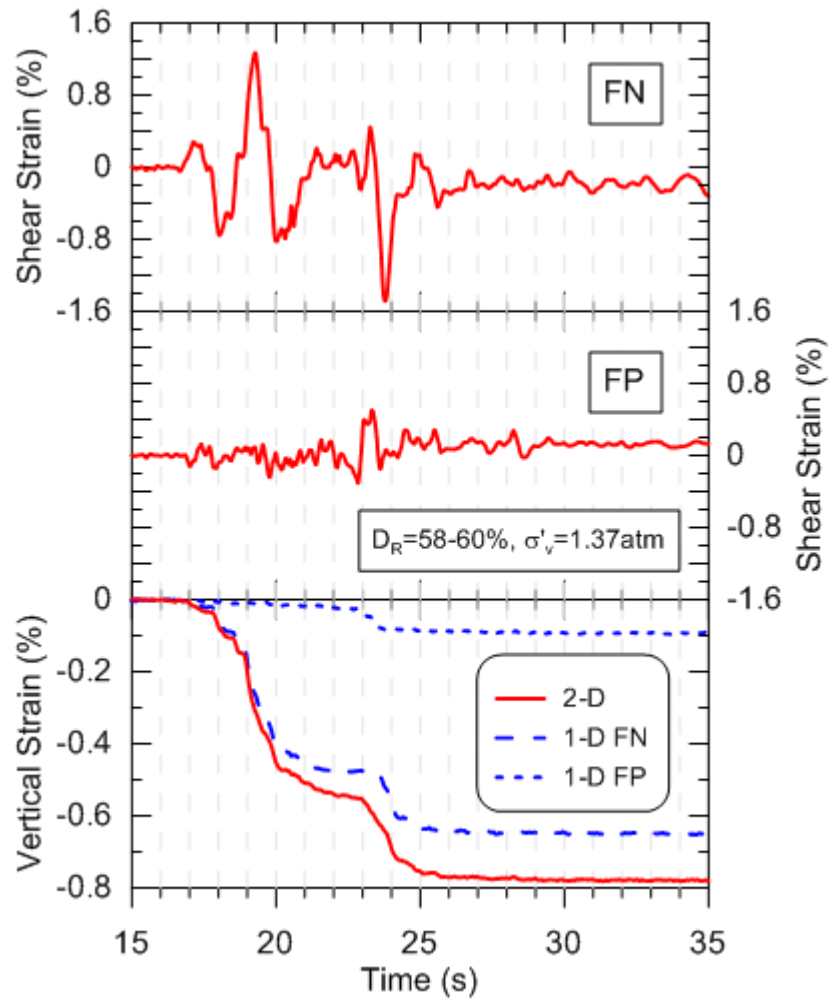


**Figure 3.5** Simple shear results from applying ground motions at 8.2 m depth taken from site response analyses and the resultant settlement time history. The FN and FP ground motions were also applied separately.



## 4 Ground Motion Data from Service Hall Array

Accelerometers at the KKNPP are owned and maintained by the Tokyo Electric Power Company (TEPCO). The horizontal accelerometers have azimuths of  $18.9^\circ$  and  $108.9^\circ$  (measured east from due north to reflect the power plant's orientation). These data, which have not been publically released, were made available to the third author and approved for use in the present work. These data include acceleration recordings for the main shock and two subsequent aftershocks, named L and S herein, with their epicentral and hypocentral information listed in Table 4.1. The SHA accelerometer data provided by TEPCO was in digital form and had engineering units, but was otherwise unprocessed. The unprocessed data has baseline drift, which necessitated corrections to remove low-frequency noise. We employed the data processing procedures described by Boore [2005] and Boore and Bommer [2005]:

- Zero pads were added to the beginning and end of each record. The number of zeros added was equal to  $1.5n/(f_c \cdot dt)$  where  $n$  is the Butterworth filter order (integer),  $f_c$  is the filter corner frequency, and  $dt$  is the sampling interval (0.01 sec).
- An acausal high-pass filter was applied at a specified corner frequency. The frequency was selected on a record-by-record basis so as to remove baseline drift while minimally affecting the amplitudes of velocity and displacement histories. These frequencies ranged from 0.03 to 0.10 Hz. We utilized a high-pass acausal Butterworth filter of order 4 as implemented in Matlab. These frequencies are presented in Table 4.2.
- The filtered acceleration history was integrated to velocity and displacements using the full duration of the time series.

Acceleration, velocity, and displacement histories are shown in Appendices B, C, and D, for the main shock and two subsequent shocks, L and S, respectively (Electronic Supplement). The same filter frequencies—presented in Table 4.2—were also used for the subsequent

aftershocks. Summary velocity histories are shown for the main shock in Figure 4.1 after rotation into the FN and FP directions. Resultant peak ground accelerations (PGA) and peak ground velocities (PGV) are also shown in Table 4.3 for each seismic event. Figure 4.2 shows the main shock 5% damped pseudo-acceleration response spectra at each instrument in the FN, FP, and vertical directions. For each component, the spectra are similar at depths of 99.4 m and 250 m (both in bedrock). As the motions travel upwards through the soil column, low-period ( $T < \sim 0.6$  sec) horizontal components are reduced and longer period horizontal components are progressively amplified as shown in the spectra at 50.8 and 2.4 m. Comparing the FN and FP response spectra, we see larger accelerations in the FN direction, particularly in bedrock motions at 0.1 to 0.2 sec and near 2.0 sec in bedrock and surface motions. The FN amplification near 2.0-sec period could be a forward directivity pulse period because it lies in the range of previously observed pulse periods for shallow crustal earthquakes ( $\sim 1.3$  to 4.0 sec, with median of 2.2 sec; Shahi and Baker [2011]).

**Table 4.1 Ground motions used for this study.**

Event	Magnitude			Distance				
	$M_w$	Latitude	Longitude	Depth	$R_{rup}$	$R_{jb}$	$R_{epi}$	$R_{hyp}$
				(km)	(km)	(km)	(km)	(km)
Main shock	6.6	37.53	138.45	9	16	0		
Aftershock L	5.7	37.50	138.47	15			15	21
Aftershock S	4.4	37.51	138.63	20			9	22

**Table 4.2 Filter frequencies applied to vertical array data.**

Array Sensor Depth	Filter corner frequency		
	EW	NS	UD
	(m)	(Hz)	(Hz)
2.4	0.05	0.10	0.10
50.8	0.03	0.05	0.10
99.4	0.03	0.05	0.05
250	0.03	0.10	0.05

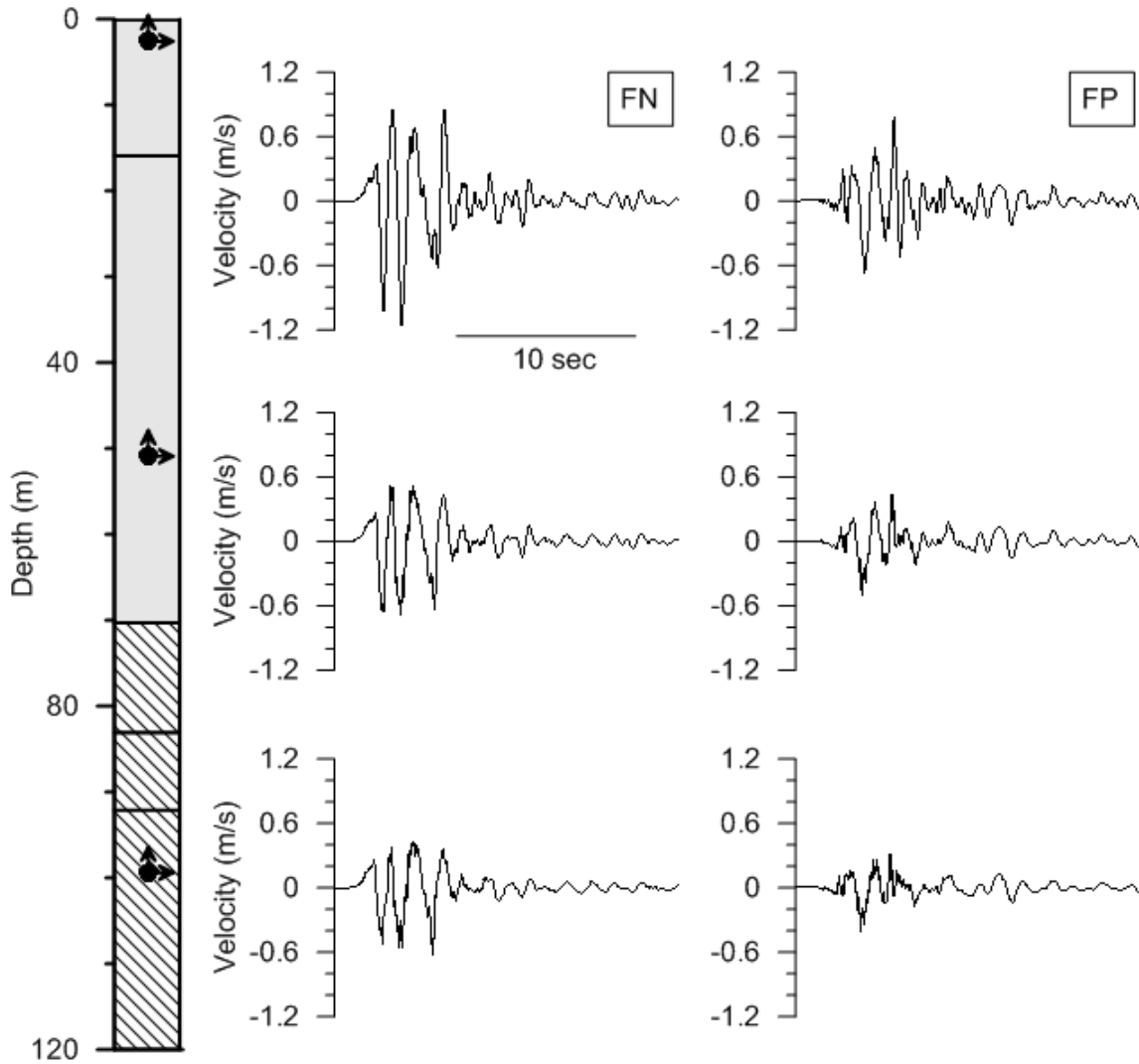


**Figure 4.1** Main shock velocity histories from the upper three instruments at the SHA site rotated into the FN and FP directions.

**Table 4.3** PGA and PGV from rotated motions.

Event	FN		FP		UD	
	PGA	PGV	PGA	PGV	PGA	PGV
	(g)	(cm/sec)	(g)	(cm/sec)	(g)	(cm/sec)
Main shock	0.42	116	0.38	79	0.6	44
Aftershock L	0.18	24	0.17	10	0.2	9
Aftershock S	0.04	1	0.04	1	0.04	1

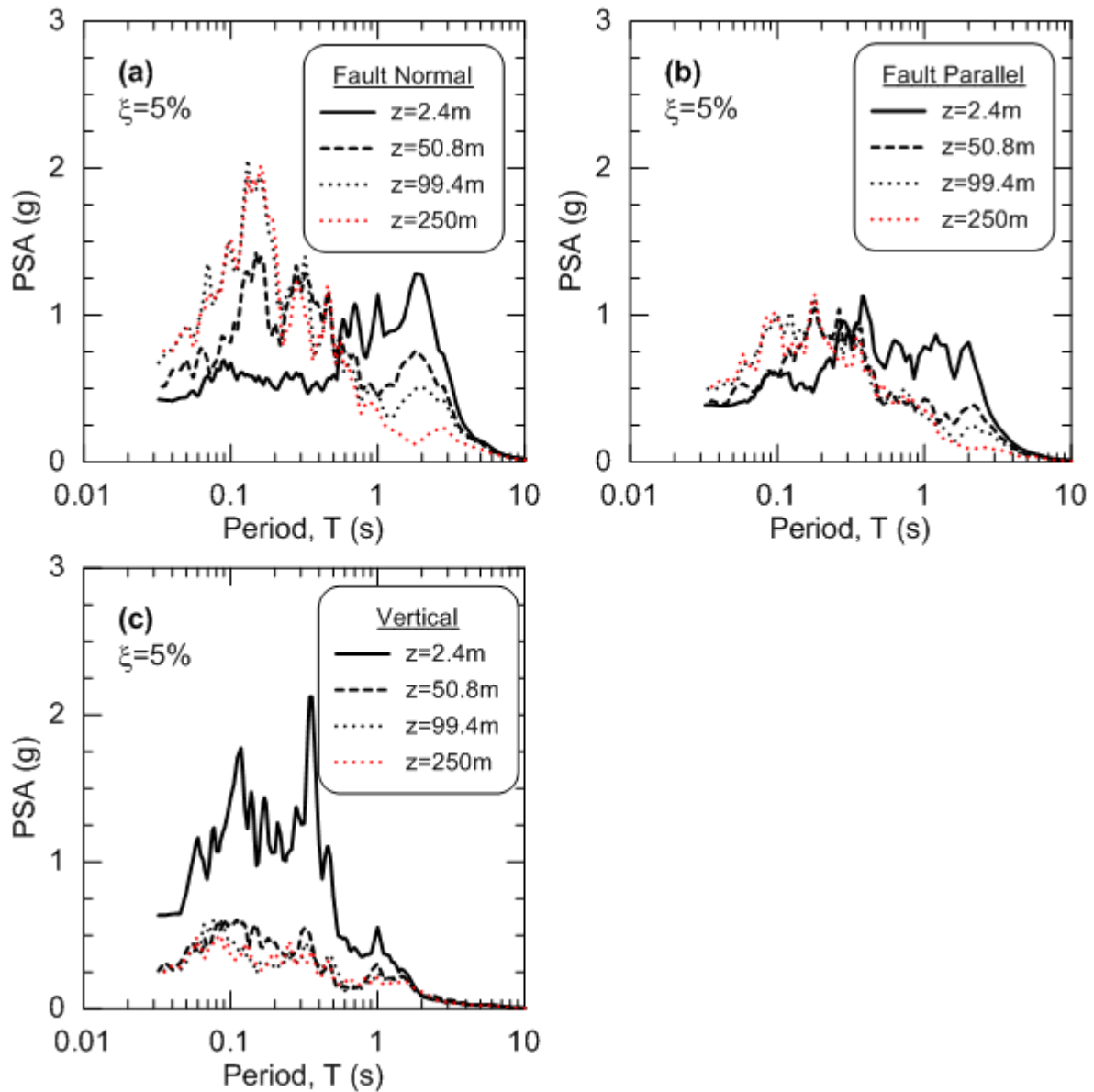


**Figure 4.2** Pseudo-acceleration response spectra for the three components of recorded main shock ground motions at SHA site.

In Figure 4.2c, although the vertical spectra are relatively consistent at 50.8, 99.4, and 250 m, significant amplification occurs across all periods near the surface. The vertical bedrock response spectra are lower than either of the horizontal bedrock response spectra at all periods. Near the surface, the vertical spectra for  $T < 0.4$  sec exceed the horizontal spectra, which are typical of near-fault recordings [Bozorgnia and Campbell 2004].

Figure 4.3 shows surface-to-rock (SR) transfer functions of horizontal components of the ground motions from 2.4 m and 99.4 m depth as well as horizontal-to-vertical (H/V) spectral ratios of the surface (2.4 m) recordings. Transfer functions were computed from power spectral density functions and time-domain smoothing procedures with an effective bandwidth of 0.195 Hz using procedures described by Mikami et al. [2008]. The SR transfer functions exhibit relatively similar shapes for the three events. The lowest frequency peak (indicating the first-mode site frequency) is consistently lower in the FN direction relative to the FP direction, which may be due to complexities in the geologic structure. In the FN direction, the fundamental mode frequency ranges from about 0.75 Hz for the main shock to 0.8 to 1.0 Hz for the aftershocks. In the FP direction, this frequency is approximately 1.0 Hz, with less change between events. The H/V spectral ratios are also relatively consistent between events and suggest similar site periods as the SR transfer functions. The general similarity of the SR transfer functions and H/V spectral ratios from event-to-event indicates relatively consistent site response, aside from the effects of nonlinearity on the site period in the FN direction.

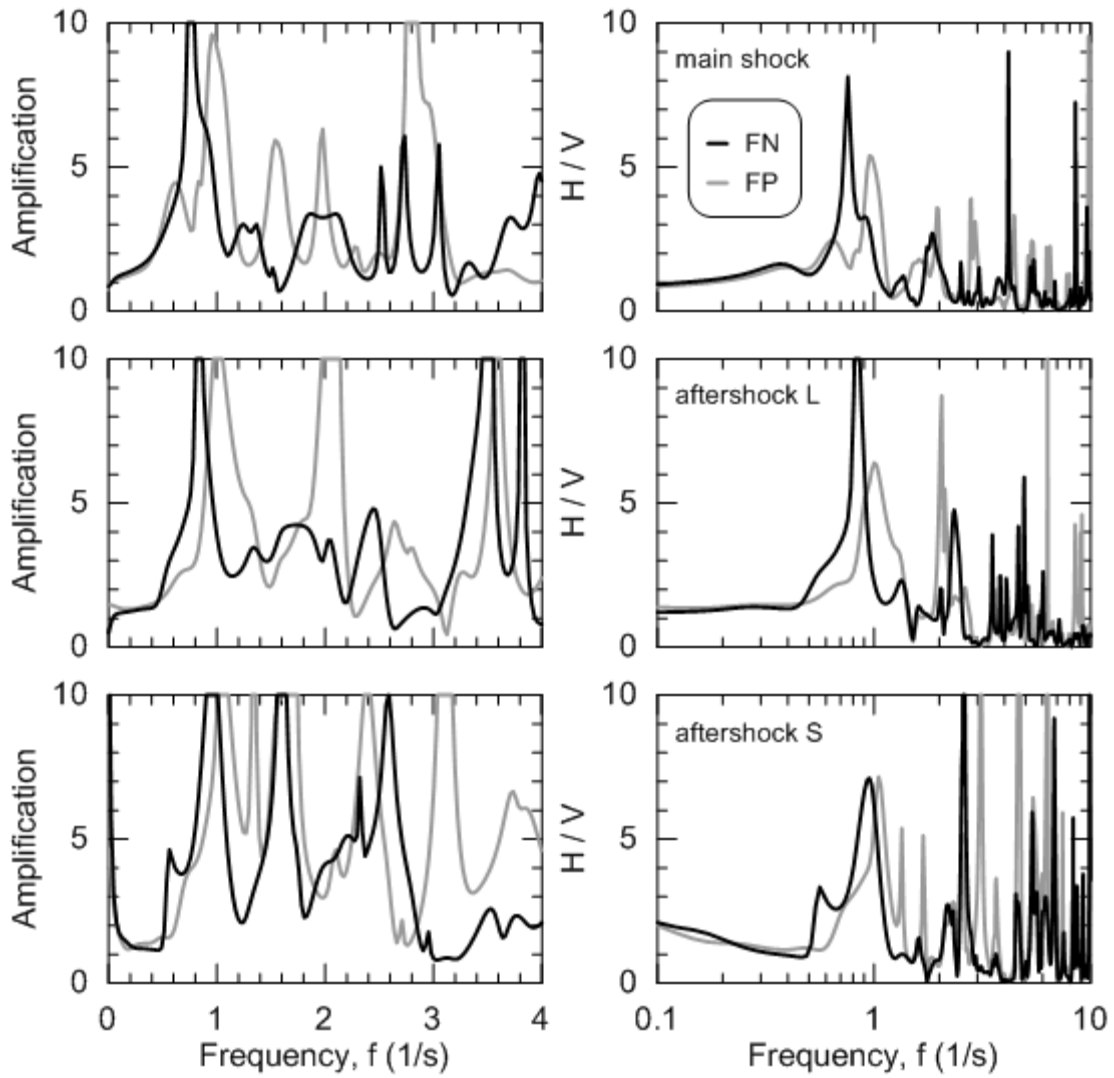


Figure 4.3 Surface-to-rock (2.4 m/99.4 m) transfer functions and surface (2.4 m) H/V spectral ratios for main shock and aftershock recordings.

## 5 Ground Response Analysis

Ground response analyses are used to predict one-dimensional shear wave propagation through the soil column at the SHA site. These analyses are performed using an equivalent linear (EQL) method in which the wave equation is solved in the frequency domain (e.g., Kramer [1996]) and a nonlinear method in which the soil column is represented as a multiple-degree-of-freedom system whose response to a base input motion is solved in the time domain using numerical integration. For SHA, the input motion is taken as the corrected ground motion recording within bedrock at 99.4 m depth. As recommended by Kwok et al. [2007], the recorded motions are used as recorded (“within” condition) with a rigid base assumed below 99.4 m. Subsequent sections describe the soil properties used for these analyses (small strain modulus and nonlinear modulus and damping relations). Both one-dimensional EQL and nonlinear ground response analysis are performed in DeepSoil 4.0 [Hashash et al. 2011]. The desired outcome of the analyses are (1) to be able to predict ground motions through the soil column for comparison to recordings and (2) to construct profiles of predicted shear strains for use in seismic compression analysis.

### 5.1 DYNAMIC SOIL PROPERTIES FOR ANALYSIS

As shown in Figure 1.3, the initial shear wave velocity profile used for analysis is smoothed relative to the interval velocities from suspension logging. At a depth of about 50 m—just below the water table—there is a slight dip in the velocity profile that impacts the analysis results. Surrounding materials have shear wave velocities above 300 m/sec, whereas at 50 m, shear wave velocities are about 270 m/sec. Mass densities are taken from measured moist unit weights, which were approximately 16 kN/m<sup>3</sup> to a depth of 4 m and 17.75 kN/m<sup>3</sup> from 4 to 45 m. A saturated unit weight of 20.8 kN/m<sup>3</sup> was used from 45 to 70 m. Maximum shear modulus was computed from shear wave velocity and mass density as:

$$G_{\max} = V_s^2 \rho \quad (5.1)$$

The nonlinear constitutive models in DeepSoil utilize a hyperbolic backbone curve described by:

$$\tau = \frac{G_{\max} \gamma}{1 + \beta \left( \frac{\gamma}{\gamma_r} \right)^\alpha} \quad (5.2a)$$

where  $\gamma$  is shear strain,  $\gamma_r$  is pseudo-reference strain, and  $\beta$  and  $\alpha$  are fitting coefficients generally taken as  $\beta = 1.0$  and  $\alpha \sim 0.92$  [Darendeli 2001; Zhang et al. 2005]. The representation of the backbone curve as shown in Equation (5.2a) is equivalent to taking the modulus reduction curve as:

$$\frac{G}{G_{\max}} = \frac{1}{1 + \beta \left( \frac{\gamma}{\gamma_r} \right)^\alpha} \quad (5.2b)$$

We adopt this hyperbolic model for the backbone curve with  $\beta = 1.0$ . Values for parameter  $\alpha$  are adjusted to fit the curvature of the laboratory modulus reduction curves, as described further below. With this framework, the only required parameters for a given depth in the soil column are  $G_{\max}$  and pseudo-reference strain  $\gamma_r$ . Parameter  $\gamma_r$  can be evaluated from cyclic test data (or empirical models calibrated from test data), which describe the backbone curve at small strains ( $\gamma < \sim 0.5-1.0\%$ ). However, the hyperbolic model breaks down at large strains, where it typically produces stress estimates biased relative to the shear strength. In this section, we make first-order estimates of  $\gamma_r$  using available test data and models, which can be used for preliminary ground response analyses. Problematic depth intervals for which large strains develop are then identified in a subsequent section.

The RCTS test data described above provides measurements of  $\gamma_r$  at the sample depths of 4, 8, 14, and 20 m, with the results in Table 3.1. Figure 5.1 shows the pseudo-reference strains from RCTS tests performed in this study and for the neighboring site compared with predictions from empirical models by Menq [2003] and Darendeli [2001]. The Darendeli [2001] model was developed from a large database taking into account both plastic and non-plastic soil materials, while the Menq [2003] model was derived specifically for granular soil materials. The Menq

[2003] model is considered more directly applicable to the granular materials present in the upper 70 m of the SHA site.

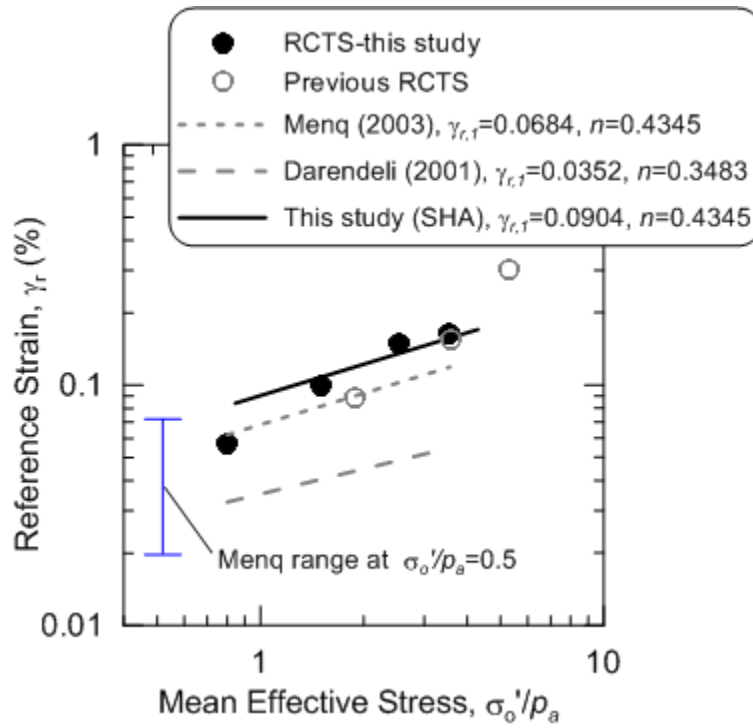


**Figure 5.1** Variation of pseudo reference strain with mean confining pressure from RCTS tests (this study), previous RCTS tests (neighboring site), and model predictions.

Figure 5.1 shows that  $\gamma_r$  from the RCTS tests to generally be higher than the Menq [2003] and Darendeli [2001] model predictions. The variability of data around the Menq model has not been formally evaluated, but an approximate range of data at an overburden pressure of 0.5 atm is shown in Figure 5.1 [Menq 2010]. Based on this preliminary result, it appears that test results from the SHA site lie near the upper range of the data considered by Menq [2003]. One possible reason for the difference is that the Menq [2003] testing involved dry sands without matric suction, whereas our RCTS tests are partially saturated; the resulting matric suction may increase the effective confinement relative to what is reported based on the isotropic cell pressure in the device. A power fit to the tube sample pseudo-reference strains was derived according to:

$$\gamma_r = \gamma_{r,1} \left( \frac{\sigma'_0}{p_a} \right)^n \quad (5.3)$$

where  $\sigma'_0$  is the mean effective confining pressure (same as cell pressure in RCTS tests),  $p_a$  is the atmospheric pressure (101.3 kPa),  $n$  is taken from Menq (2003) as 0.4345, and  $\gamma_{r,1}$  is a regression coefficient {0.0904±0.0565 for present work (range indicates 95% confidence interval); 0.0684 for sands [Menq 2003] and 0.0352 for sands [Darendeli, 2001]}. The resultant fits are shown in Figure 5.1.

Equation (5.3) was used to estimate pseudo-reference strains through most of the sand column above the water table, as shown in Figure 5.2. Below the ground water table, where test data is not available and matric suction is zero, we anticipate that the Menq [2003] model is more accurate than the projection from Equation (5.3). Accordingly, we transition the  $\gamma_r$  used for analysis from the projected value at the deepest sample (20 m) to the Menq estimate at the base of the sand column (70 m). To estimate the  $\alpha$  parameter in Equation (5.2), pseudo-reference strains from Figure 5.1 at depths of 4.5, 8.5, 14.5, and 20.5 m were entered into Equation (5.2b), and  $\alpha$  was adjusted so that the predicted modulus reduction curves match the curvature from laboratory tests. The resulting  $\alpha$  values were found to vary with overburden pressure as:

$$\alpha = \alpha_1 + \alpha_2 \log \left( \frac{\sigma'_0}{p_a} \right) \quad (5.4)$$

where  $\alpha_1 = 0.82 \pm 0.10$  and  $\alpha_2 = 0.34 \pm 0.27$ . Our model for  $\alpha$  scales more strongly with  $\sigma'_0$  than the  $\alpha$  equation provided by Menq [2003] ( $\alpha_1 = 0.86$  and  $\alpha_2 = 0.1$ ), which is reported to be poorly constrained [Menq 2010]. While our model for  $\alpha$  captures the trends with depth in modulus reduction behavior,  $\alpha$  also affects damping, so we alternatively could have used an  $\alpha$  model that optimizes the fit to laboratory damping data. The model provided by Equation (5.4) and our coefficients is generally well-behaved for damping at strains < 0.3%, but is judged to be unrealistic for strains > 1.0% because model damping at large strain increases with depth. Menq's  $\alpha$  model provides a more realistic trend to the damping curves (decreasing with depth over a wider strain range), but at the expense of modulus reduction misfit. We chose to minimize modulus reduction misfit through the use of Equation (5.4) with our  $\alpha$  coefficients, which is checked subsequently to see if damping trends are problematic for the strain range of interest.

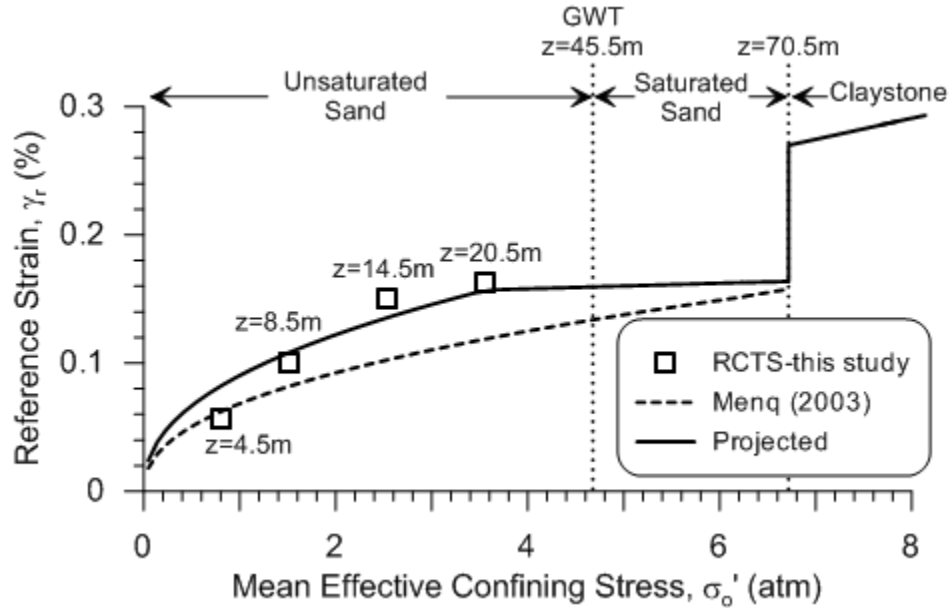


**Figure 5.2** Values of pseudo reference strain used for analysis as function of with confining pressure and depth through the soil column.

Figure 5.3a compares the aforementioned model to RCTS test data for the sample at 20 m. Also included are the modulus reduction curves from the Darendeli [2001] and Menq [2003] models. Figure 5.3b shows that RCTS damping data for the 20 m depth sample exceeds the Darendeli [2001] and Menq [2003] model predictions at large strains. As shown in Figure 5.4, the damping models are good for  $D_{min}$ , so the misfit is associated with the component of the material damping model above the minimum value (i.e.,  $D-D_{min}$ ). In the Darendeli [2001] and Menq [2003] models, the model for  $D-D_{min}$  depends on the shape of the modulus reduction curve (as required by Masing's rules). The Darendeli [2001] and Menq [2003] model predictions in Figure 5.3b use their respective modulus reduction curves. For application at the SHA site, we utilized the  $D-D_{min}$  component of the Menq's [2003] model with two modifications (1) use the modulus reduction curves from this study in the  $D-D_{min}$  equations; and (2) we increased the  $D$  above  $D_{min}$  by 40% to achieve a reasonable match to the data at 20m (as shown in Figure 5.3b) and other depths as well.

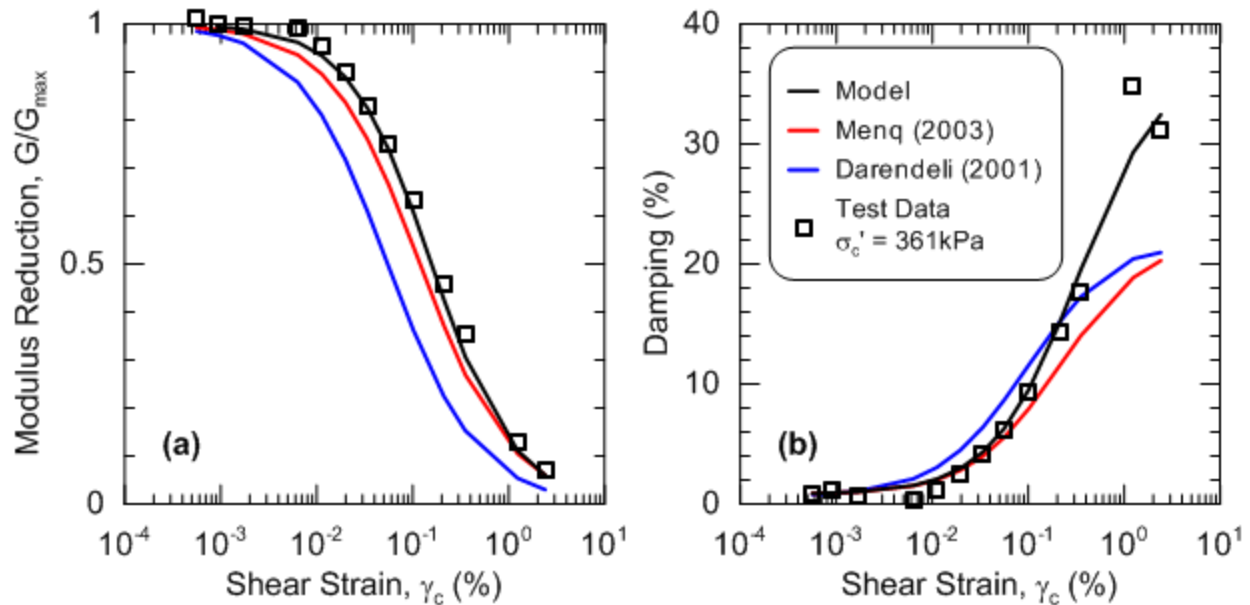


Figure 5.3 Comparison of the Darendeli [2001] and Menq [2003] (a) modulus reduction and (b) damping curve models to sample test data from 20 m deep. Resultant modulus reduction and damping curves are labeled as “Model”.

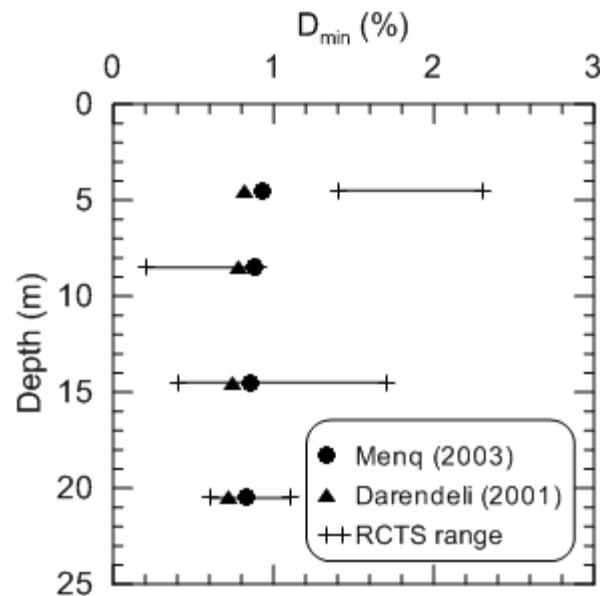


Figure 5.4 Comparison of Menq [2003] minimum damping and the range of damping values at shear strains less than 0.05% from RCTS testing.

To generate modulus reduction and damping curves for the relatively plastic soil and rock materials, two modifications were applied to the Menq [2003] model. The term that considers plasticity was taken from the Darendeli [2001] pseudo-reference strain and minimum damping models, and added into the aforementioned granular model. Additionally, parameter  $\alpha$  was set to

0.92 as was used in the Darendeli [2001] model. These modifications were used to generate pseudo-reference strains and minimum damping for modulus reduction and damping curves for the relatively plastic materials below 70 m depth. The resulting pseudo-reference strains for plastic materials below 70 m depth are shown in Figure 5.2.

## 5.2 GROUND RESPONSE ANALYSIS USING AFTERSHOCK DATA

This section describes the results of initial ground response analyses utilizing the smoothed version of the suspension logging data as shown in Figure 1.3 and modulus reduction/damping relations derived from RCTS laboratory testing, as described in Section 5.1. It will be shown that problems were encountered in these analyses, and final runs were performed using strength adjustments to the modulus reduction curves and increases to small strain damping  $D_{min}$ . Those adjustments and their effect on the results are described in Sections 5.4.1 to 5.4.3.

Both EQL and nonlinear ground response analysis in DeepSoil 4.0 requires sub-layering that addresses: (1) stratigraphic boundaries and changes in the  $V_s$  profile; (2) depths of accelerometers, such that output depths are comparable; and (3) minimum layer thicknesses that allow waves with maximum frequencies between 25 to 50 Hz to propagate without artificial damping (see Kwok et al. [2007] and Hashash et al. [2011] for details). Each sub-layer of the SHA profile was assigned modulus reduction and damping curves taken from the pseudo reference strain and damping formulations described above. Following the recommendations of Kwok et al. [2007] for input motion selection for vertical arrays, the FN and FP ground motions from the accelerometer at 99.4 m were taken as input with a rigid base. For EQL analysis, the effective shear strains for soil property iteration were taken as 56, 47, and 34% of the peak strain for the main shock, aftershock L, and aftershock S, respectively, which are consistent with the recommendations of Idriss and Sun [1992].

We began our analysis using the aftershock data to gain insight into the degree to which one-dimensional analysis can capture the site response without the complications of highly nonlinear soil behavior. As noted previously in Table 4.1, the two aftershocks are labeled L and S. Figure 5.5 through Figure 5.7 present accelerograms and response spectra (data and simulation results), strain profiles, and maximum horizontal acceleration (MHA) profiles, respectively, for aftershock L. Figure 5.8 through Figure 5.10 present similar results for aftershock S. Figure 5.11 shows predicted and observed SR transfer functions for the aftershocks. We note that the

predicted transfer function provides a reasonable match to the shape and resonant frequencies of the observed transfer functions, although the data is clearly too limited to establish statistically significant empirical trends for small-strain site response. Nonetheless, following the logic of Baise et al. [2011] as described in Section 2.1, these results are encouraging regarding the suitability of SH1D analysis for capturing site response at the SHA site.

As shown in Figure 5.6 and Figure 5.9, strain levels for the aftershocks, while relatively small, are large enough that some modulus reduction effects are expected. Model-data comparisons are favorable at 50.8 m depth but show some over-prediction of motions at 2.4 m. The overprediction of shallow motions suggests that damping ratios are underestimated from the laboratory tests, which is generally consistent with previous findings by Tsai and Hashash [2009] and Elgamal et al. [2001], as described in Section 2.1. Accordingly, ground response analyses were repeated with small strain damping levels in soil increased to  $D_{min} = 2\%$  and  $5\%$  (generally from approximately  $1\%$  in the original models). This increase in  $D_{min}$  causes the entire damping-strain curve to increase (the  $D-D_{min}$  component is not affected) upwards by about  $1\%$  and  $4\%$  for  $D_{min} = 2\%$  and  $5\%$ , respectively. As shown in Figure 5.12 and Figure 5.13, the resulting spectra better matched the recorded data, especially in the FN direction and for the shallower accelerometers. The results do not strongly support either the  $2\%$  or  $5\%$  small strain damping levels as the preferred choice.

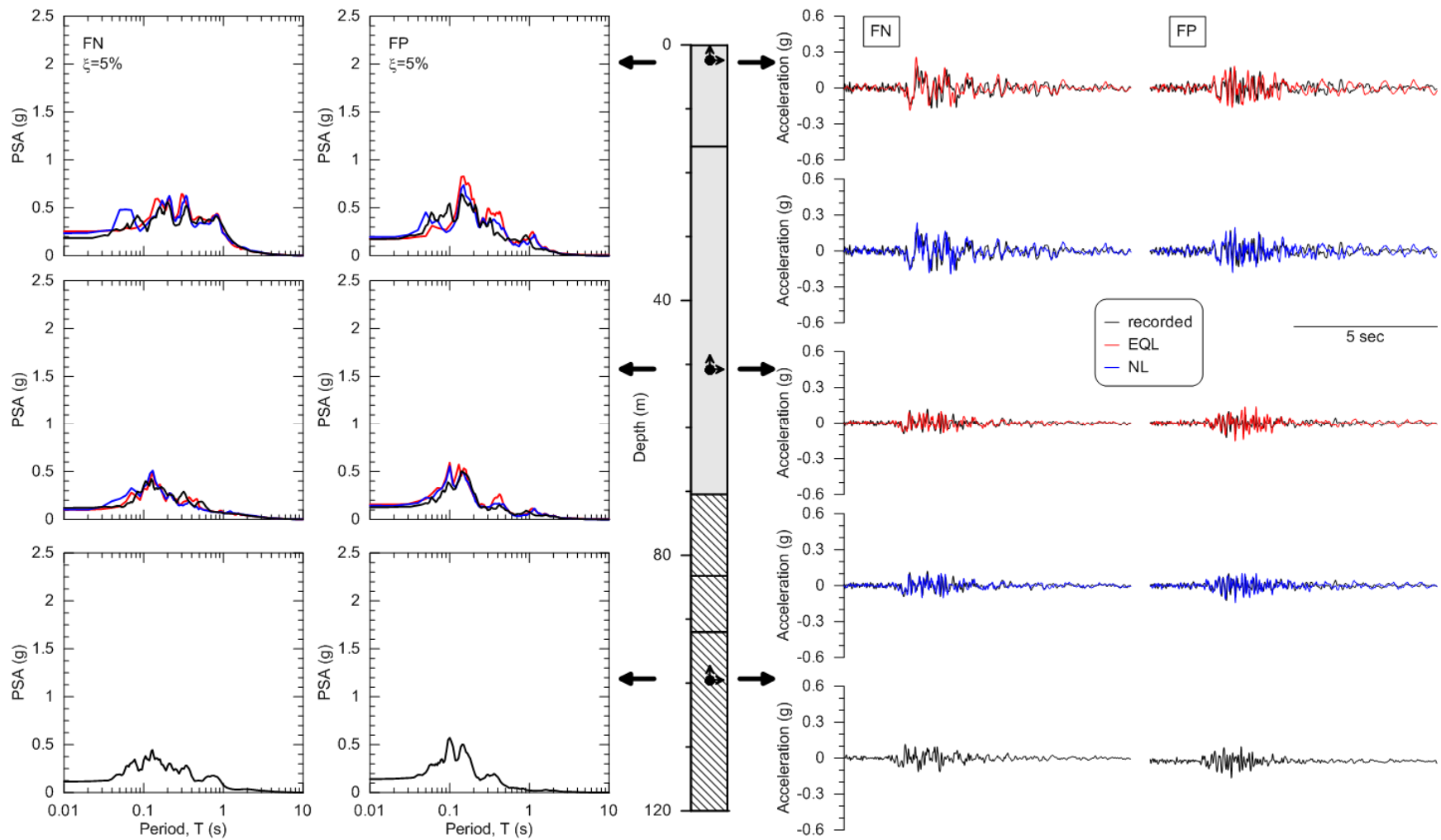


Figure 5.5 Results of EQL and nonlinear ground response analyses for aftershock L.

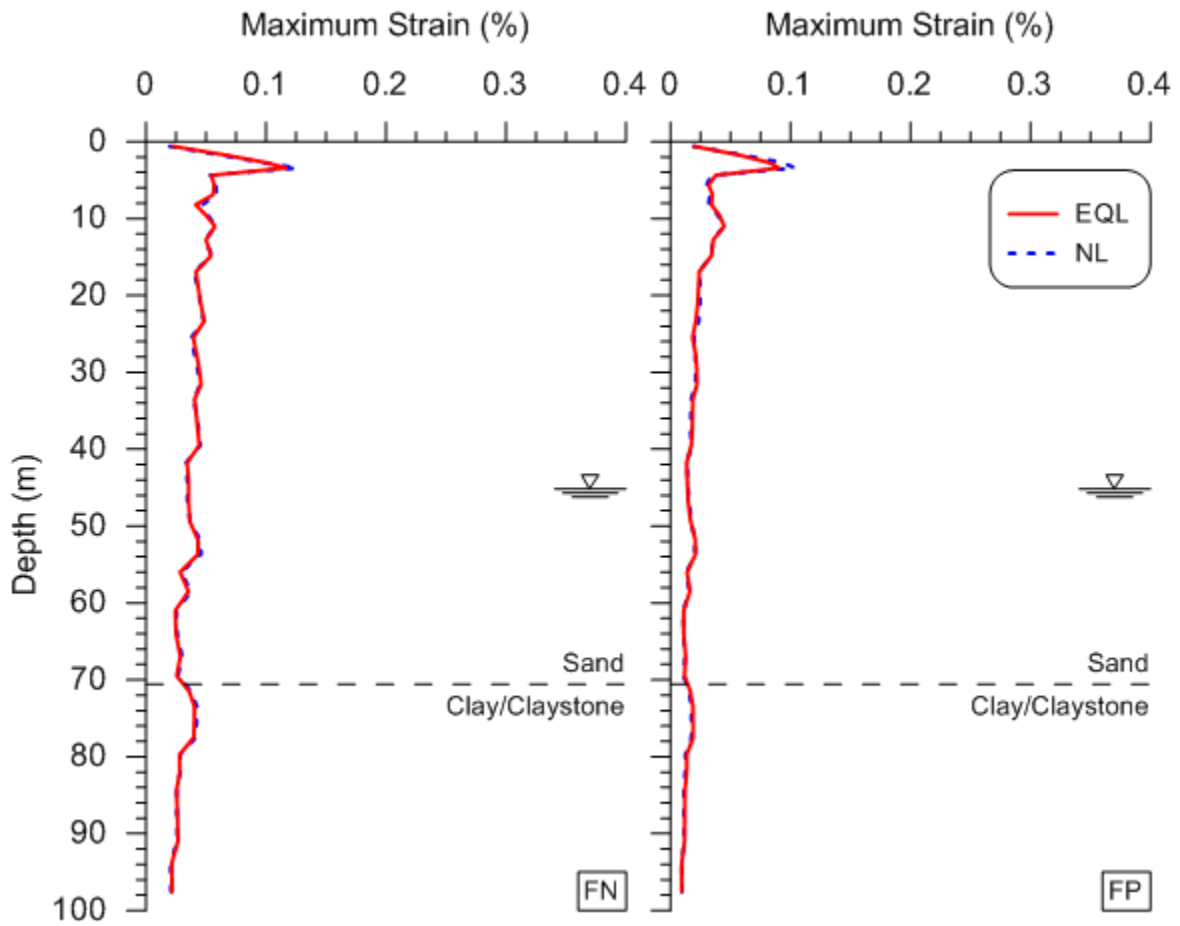


Figure 5.6 Peak strain profiles from EQL and nonlinear analyses for aftershock L.

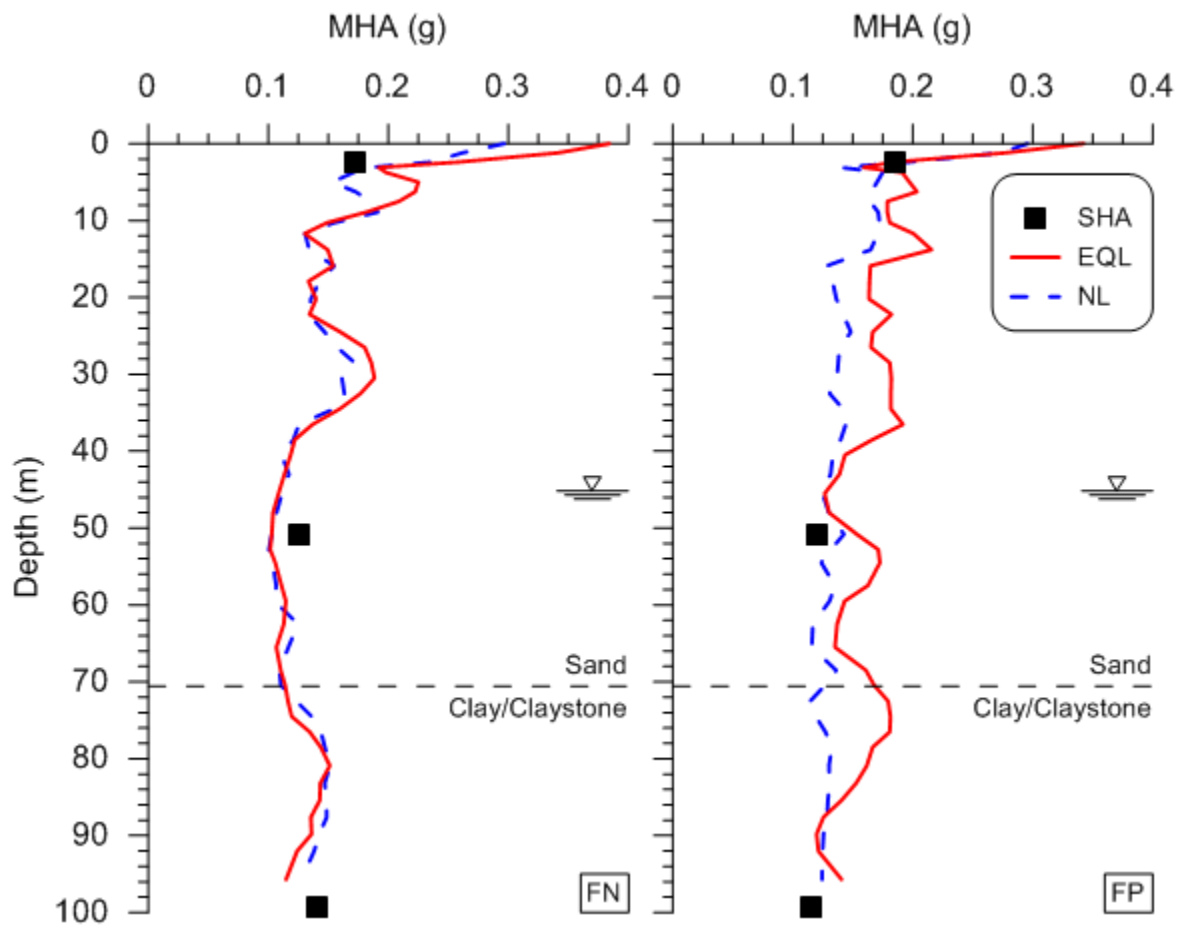


Figure 5.7 Peak accelerations from EQL and nonlinear analyses for aftershock L.

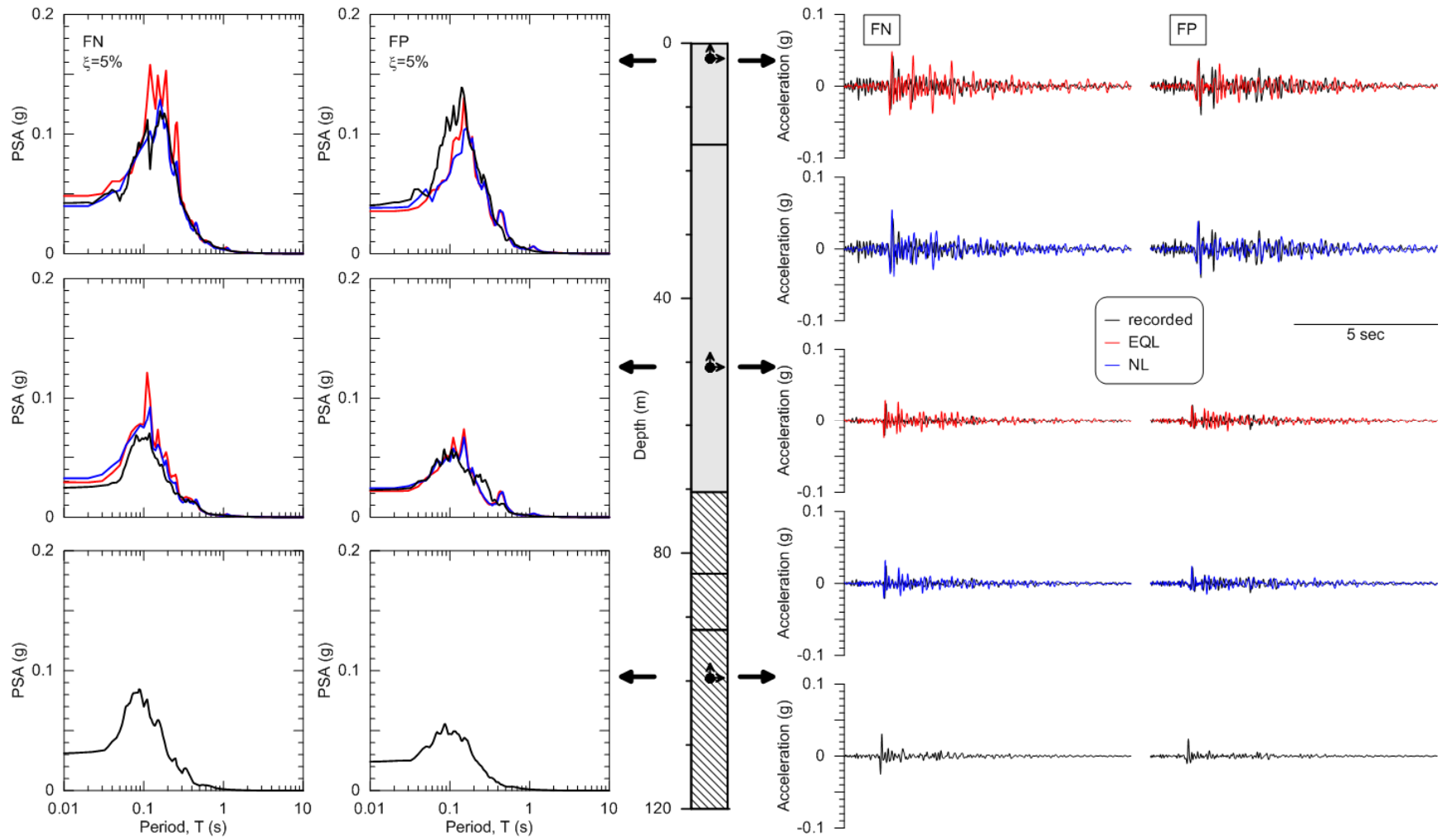


Figure 5.8 Results of EQL and nonlinear ground response analyses for aftershock S.

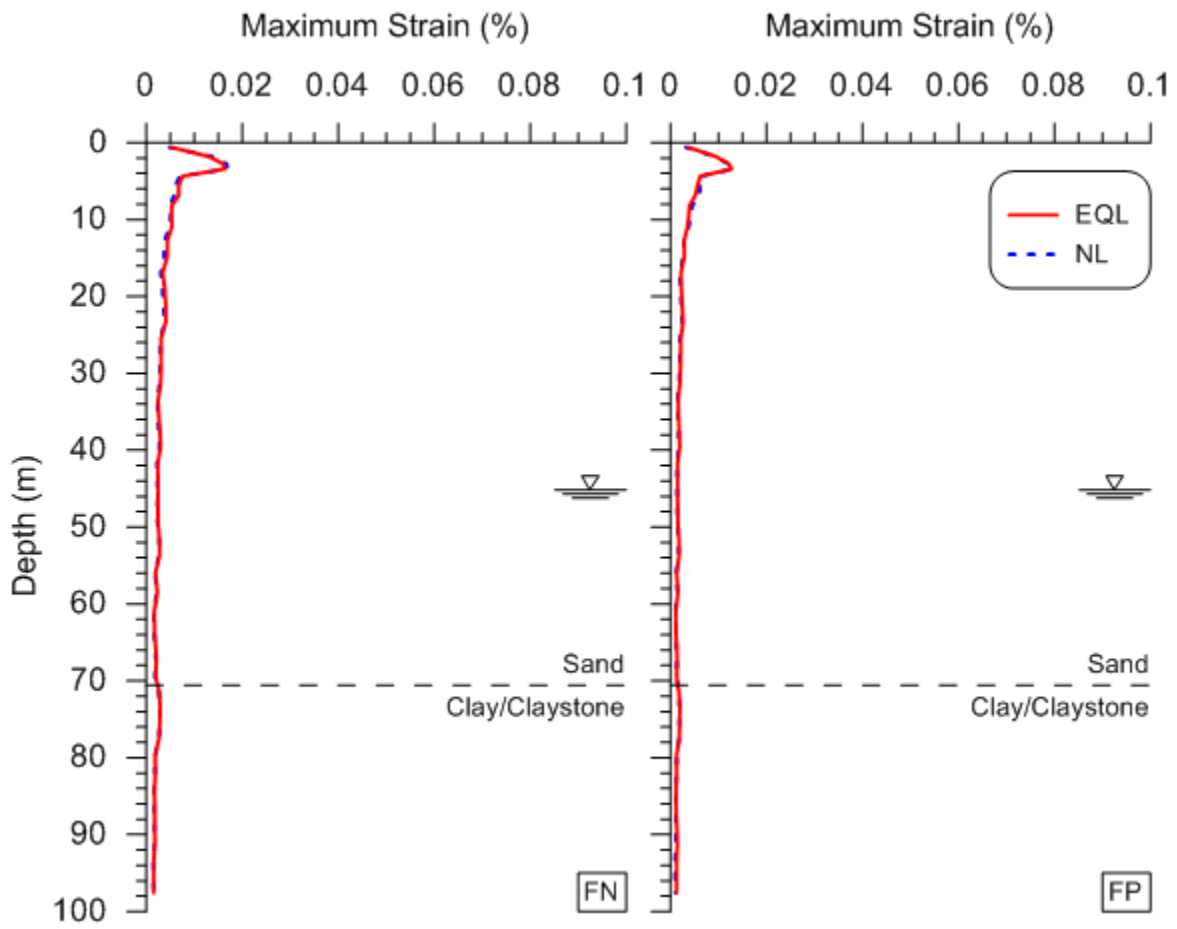


Figure 5.9 Peak strain profiles from EQL and nonlinear analyses for aftershock S.

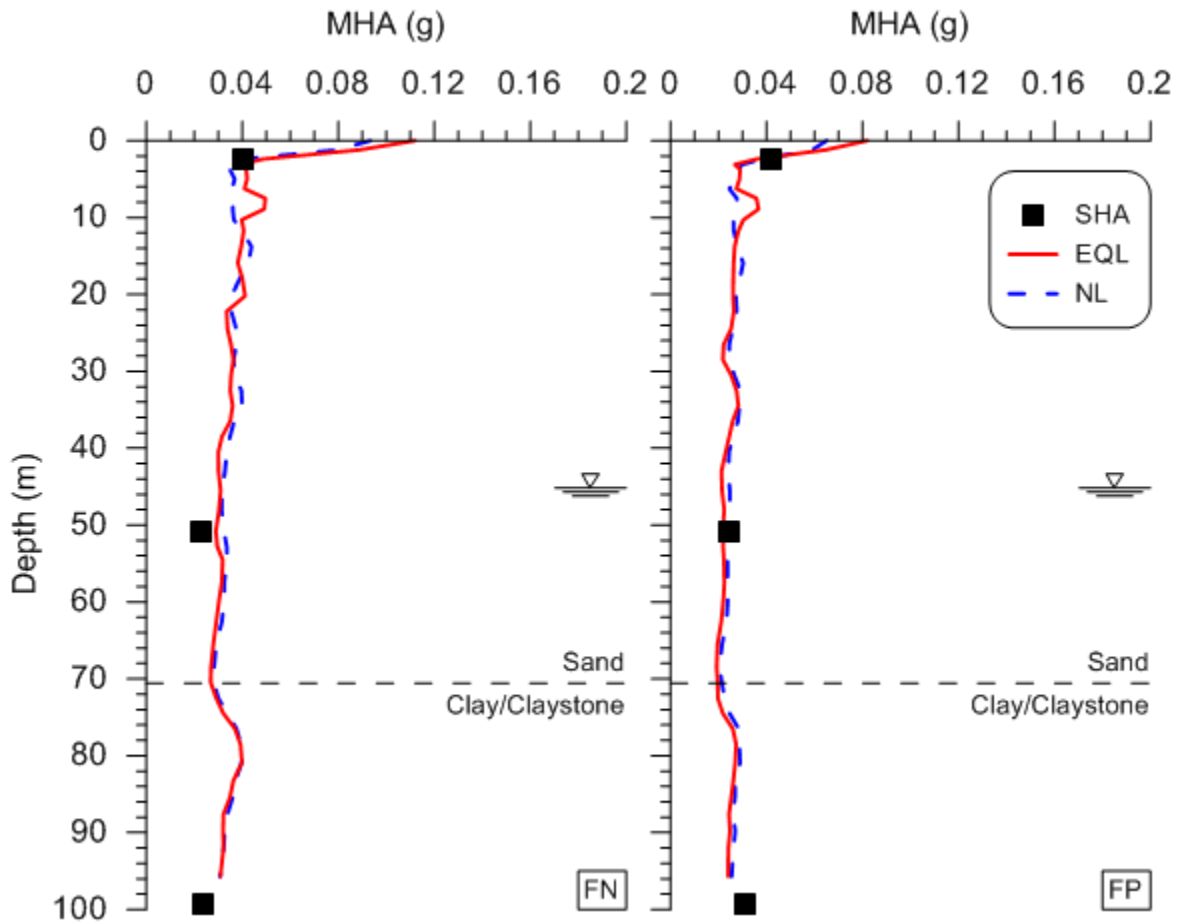


Figure 5.10 Peak accelerations from EQL and nonlinear analyses for aftershock S.

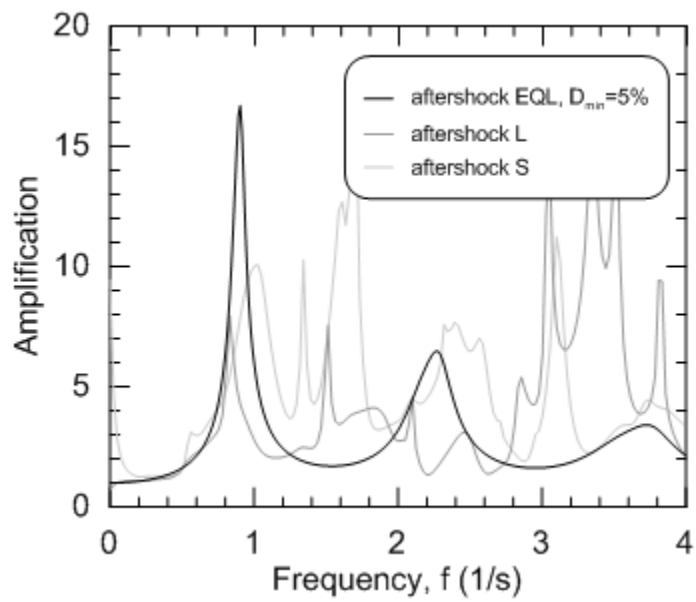


Figure 5.11 Transfer function and coherence for the main shock and two aftershocks.

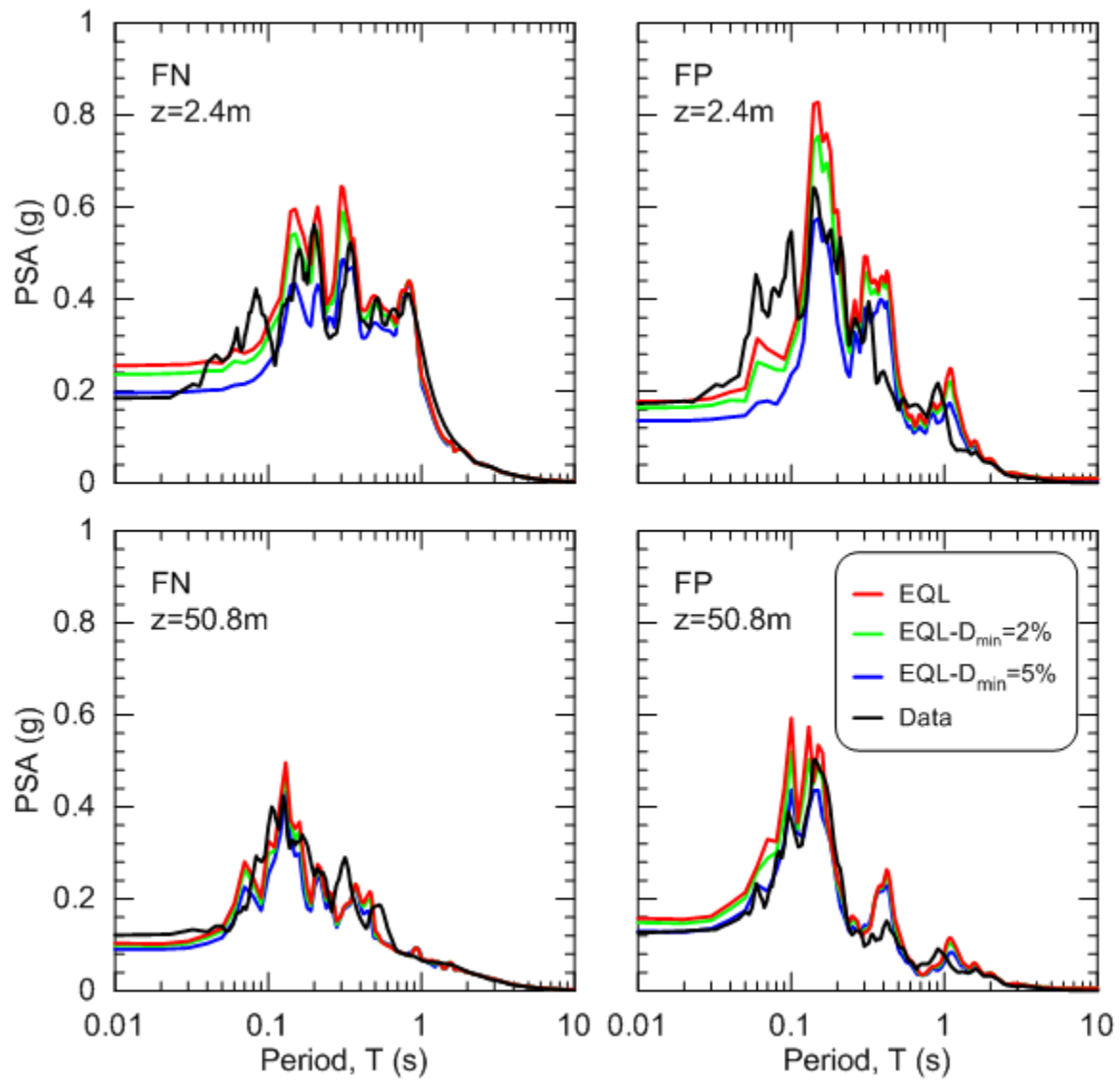


Figure 5.12 Response spectra at 5% damping for aftershock L and EQL analysis results for varying levels of small strain damping.

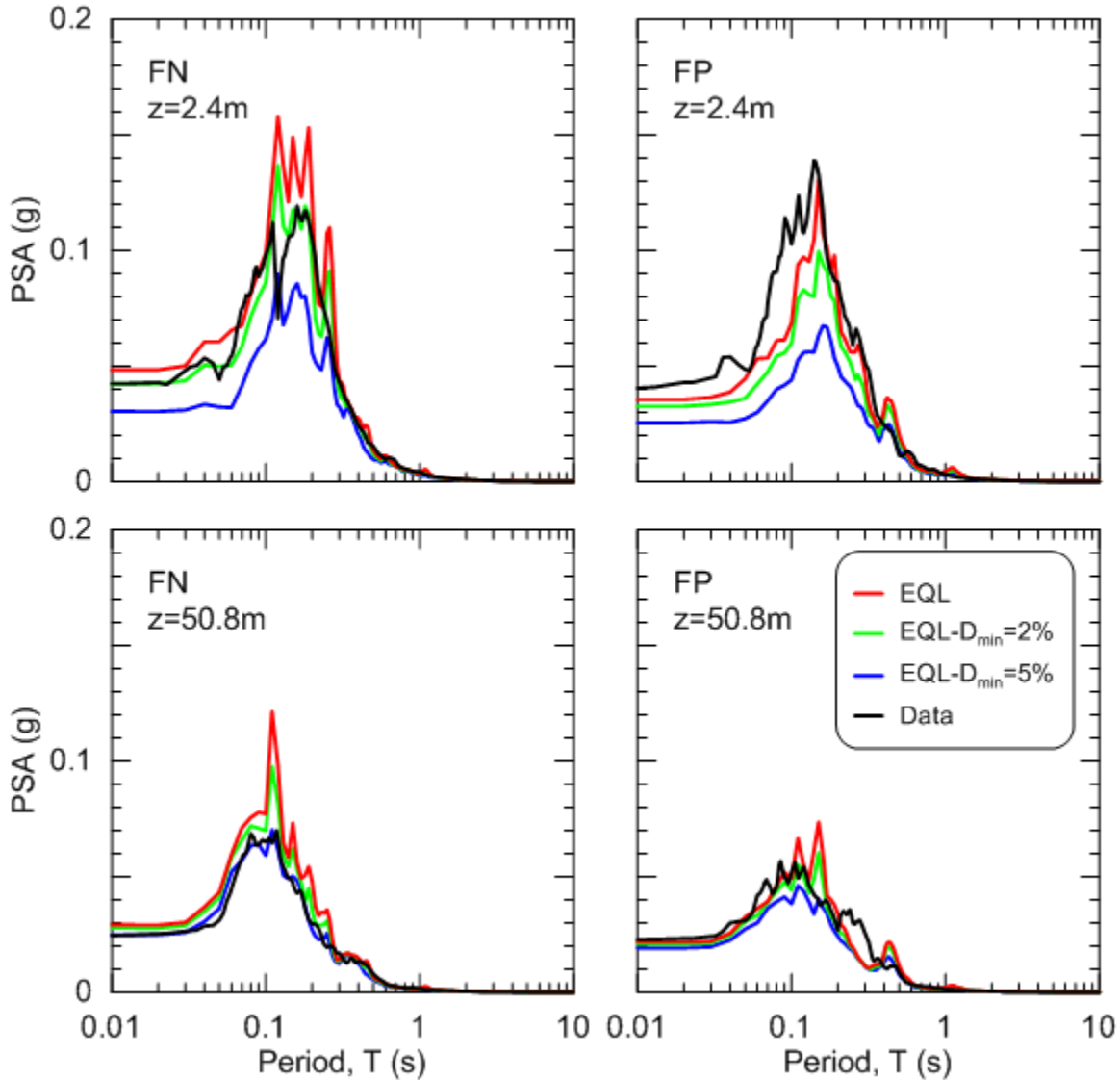


Figure 5.13 Response spectra at 5% damping for aftershock S and EQL analysis results for varying levels of small strain damping.

### 5.3 INITIAL GROUND RESPONSE ANALYSIS USING MAIN SHOCK RECORDINGS

Main shock ground response analyses were performed using the soil properties described in Section 5.1 with the exception of increased small strain material damping to  $D_{min} = 2\%$ , which corresponds to an additive increase to the damping curves of  $\Delta D_{min} \sim 1\%$ . This adjustment approximately doubles the small strain damping from the lab-based models, which was motivated by the aftershock analysis described in Section 5.2.

Figure 5.14 compares main shock results of the EQL and nonlinear analyses with the SHA recordings at 2.4 and 50.8 m depth. The waveform comparisons indicate a relatively good fit during the 15 sec to 25 sec time interval plotted, which is the principal shear wave arrival window. Based on the waveforms and pseudo-acceleration response spectra (left side of figure), low-frequency features of the motions are well predicted at both depths (50.8 m and 2.4 m) but high frequencies are slightly underestimated at 50.8 m and significantly overestimated at 2.4 m. The 2.4-m response spectra illustrate saturation of the EQL results to peak acceleration (as evidenced by flat short period spectral ordinates) for  $T < \sim 0.1$  sec. This saturation effect is evidence of poor performance of the EQL model at large strain, and is not present in the nonlinear results or the data.

Insight into the causes of these trends is provided in Figure 5.15, which shows peak strain profiles from EQL and nonlinear analysis. Computed peak strains in the sandy materials overlying rock are generally around 0.35 to 0.6%, although there is a spike in strains at about 50 m that exceeds the usable limit of the backbone curves (i.e., the upper bound strains from the RCTS tests). In Figure 5.16, we plotted the backbone curve at 50 m depth obtained from the hyperbolic model along with the anticipated drained shear strength. The shear strength in Figure 5.16 is based on  $\tau_{ff} = \sigma_v \tan \phi'$ , where  $\sigma_v$  is the vertical effective stress and  $\phi'$  is the average friction angle from Table 3.1. Clearly the model significantly underestimates the soil shear capacity in this depth range, which causes unrealistic strain localization. This localization is caused by the aforementioned dip in the  $V_s$  profile, as shown in Figure 1.3.

We also investigated the use of alternative smoothed velocity profiles in which there is no velocity dip at 50 m. Results from these analyses show a reduction in peak shear strains at 50 m, but significant increases in peak shear strains at other depths where the smoothed velocity profile has abrupt reductions. Hence, our conclusion is that the strain localization problem is for all practical purposes unavoidable with the backbone curves formulated in Section 5.1. In the next section we take additional steps to remove the strain localization effect and then re-examine the fit of the simulation results to data.

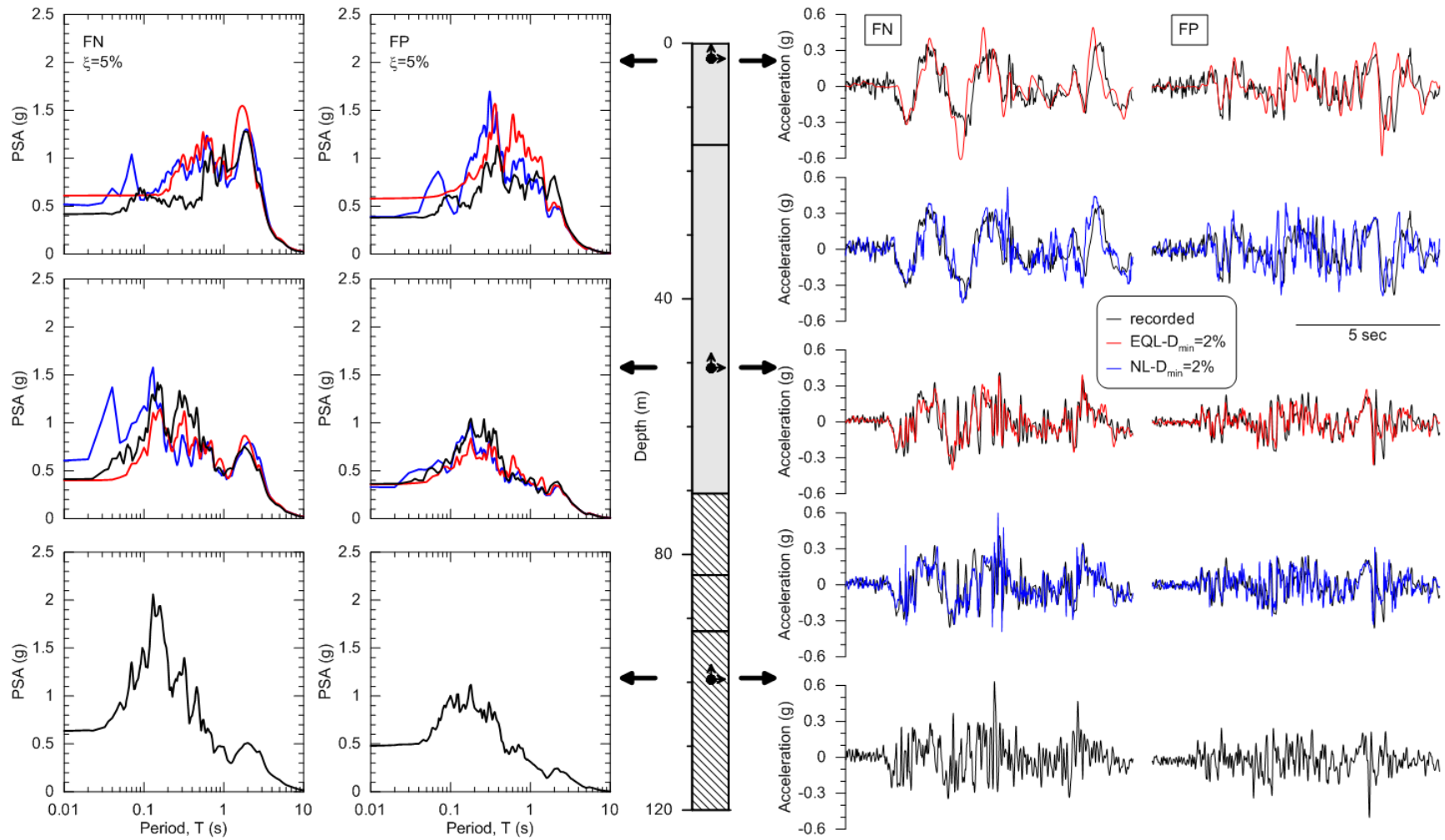


Figure 5.14 Results of EQL and nonlinear ground response analyses using increased damping ( $D_{min}=2\%$ ).

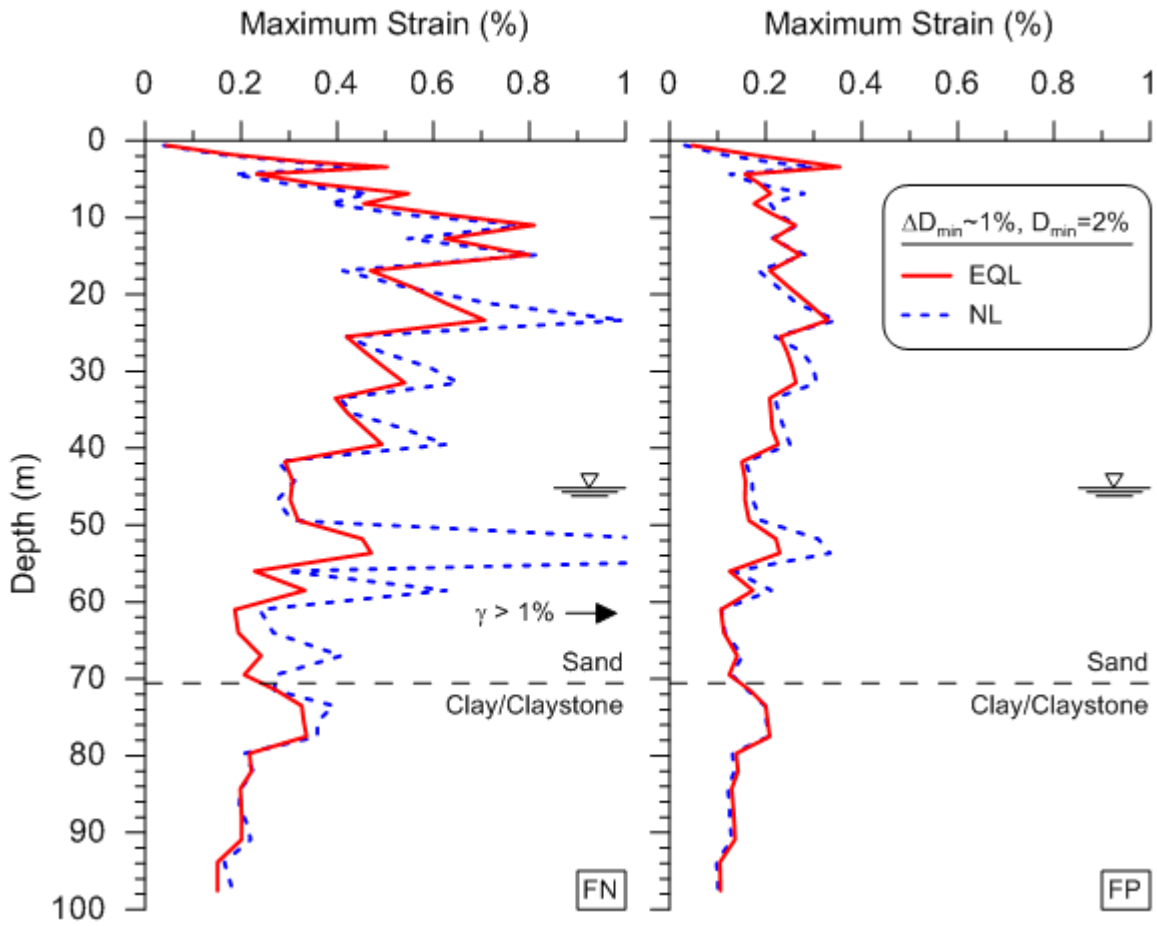


Figure 5.15 Peak strain profiles from EQL and nonlinear analyses with increased damping ( $D_{min}=2\%$ ).

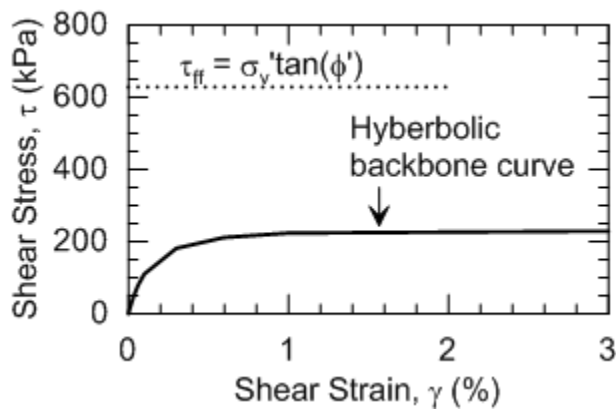


Figure 5.16 Comparison of backbone curve from FN nonlinear site response analysis at 50.8 m depth and estimated drained shear strength.

## 5.4 REVISED GROUND RESPONSE ANALYSIS CONSIDERING STRENGTH ADJUSTED BACKBONE CURVES AND INCREASED DAMPING

The shear localization that occurs at 50 m depth is evident from large maximum strains that are beyond the limits of the soil backbone curves developed from laboratory testing. This localization is considered unrealistic because the maximum shear stresses mobilized in the analyses are much lower than the shear strength as illustrated in Figure 5.16. To more properly reflect the soil strength, we propose a procedure to adjust the soil backbone curve to transition towards a specified shear strength at large strains while preserving the “small strain” behavior from modulus reduction curves. In this section, we describe this procedure, its implementation in DeepSoil, and the results of the analysis. The sensitivity of analysis results to small strain damping is also investigated.

### 5.4.1 Modification of Backbone Curve to Capture Shear Strength

Figure 5.17 schematically illustrates the proposed approach for incorporating shear strength into the backbone curve. The procedure utilizes the traditional hyperbolic backbone curve described by Equation (5.2) at shear strains  $\gamma < \gamma_l$ , where  $\gamma_l$  is a user-specified transitional shear strain. We refer to this as the *first hyperbola*. For  $\gamma > \gamma_l$  a *second* hyperbola is used having an initial modulus that is the tangent modulus of the first hyperbola at  $\gamma_l$  (denoted  $G_{\gamma_l}$ ), which ensures continuity of slope between the two hyperbolas. The second hyperbola asymptotically approaches the shear strength ( $\tau_{ff}$ ) at large strain. The equation of the second hyperbola can be written as:

$$(\tau - \tau_1) = \frac{G_{\gamma_l} \gamma'}{1 + \frac{\gamma'}{\gamma'_{ref}}} \quad (5.5)$$

where  $\gamma' = \gamma - \gamma_l$  and  $\gamma'_{ref} = (\tau_{ff} - \tau_1) / G_{\gamma_l}$ . Equation (5.5) matches Equation (5.2a) except that  $\beta = \alpha = 1$ , the ordinates are expressed relative to a shifted set of axes with an origin at  $(\gamma_l, \tau_1)$ , and pseudo reference strain has been replaced by an adjustment of the classical reference strain of Hardin and Drnevich [1972] [ $\gamma'_{ref}$ ]. Tangent shear modulus  $G_{\gamma_l}$  is obtained as a derivative of Equation (5.2a) evaluated at  $\gamma_l$  as:

$$\frac{G_{\gamma_1}}{G_{\max}} = \frac{1 + (1 - \alpha) \left( \frac{\gamma_1}{\gamma_r} \right)^\alpha}{\left( 1 + \left( \frac{\gamma_1}{\gamma_r} \right)^\alpha \right)^2} \quad (5.6)$$

For  $\gamma > \gamma_1$  the secant modulus corresponding to points on the second backbone curve at  $(\gamma', \tau')$  can be evaluated as the sum of  $\tau_1$  (from Equation 5.2) and  $\tau - \tau_1$  (from Equation 5.5) normalized by the sum of  $\gamma_1$  and  $\gamma'$ . After manipulation to an equivalent modulus reduction relation we have:

$$\frac{G}{G_{\max}} = \frac{\frac{\gamma_1}{1 + (\gamma_1/\gamma_r)^\alpha} + \frac{(G_{\gamma_1}/G_{\max})\gamma'}{1 + (\gamma'/\gamma'_{ref})}}{\gamma} \quad \text{for } (\gamma > \gamma_1) \quad (5.7)$$

Strain  $\gamma_1$  must be selected such that  $\tau_1$  is less than  $\tau_{ff}$ .

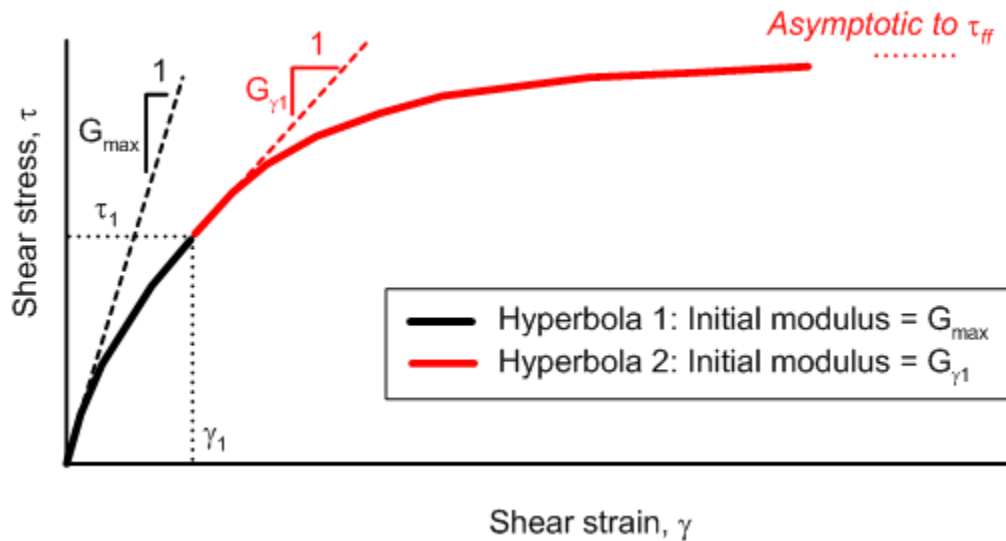


**Figure 5.17 Diagram for constructing shear strength adjusted modulus reduction curves.**

DeepSoil cannot accept the backbone curve functional form given above because it cannot be represented by a single hyperbola over the full range of strains. We use the fitting option in DeepSoil in which a target curve is specified as given above, and the best fit hyperbola is internally generated within the program.

#### 5.4.2 Effects of Modified Backbone Curves on Analysis Results

These new backbone curves were input into DeepSoil; the resultant fitted curves with no  $D_{min}$  adjustments are shown in Figure 5.18. Figure 5.18a, c, and e compare the initial model and strength adjusted modulus reduction curves at depths of 2.4, 8.2, and 50.8 m, respectively, while Figure 5.18b, d, and f, compare the damping curves at depths of 2.4, 8.2, and 50.8 m, respectively. The initial model tends to overestimate strength in shallow layers while underestimating strength in deeper layers. As described in Section 5.1, the damping curves have an unrealistic increase of large strain damping (e.g., at  $\gamma=1\%$ ) with depth due to the selected relation for  $\alpha$  (see Equation 5.4), although this trend is not present at smaller damping levels ( $\gamma < \sim 0.3\%$ ).

Based on the aftershock calibration, we performed ground response analyses using main shock motions, strength adjusted backbone curves, and damping curves in soil modified to  $D_{min} = 2\%$ . Results of these simulations are shown in Figure 5.19 through Figure 5.21. Figure 5.20 shows that the strain localization problem has been removed with the strength adjustment to the backbone curves. Figure 5.19 shows both strength adjusted EQL and nonlinear analyses to over-predict response spectral ordinates across the majority of periods from PGA to 2 sec at shallow depths. At 50 m the predicted and recorded response spectral shapes match well, although there are some misfits in amplitude; particularly noteworthy is the FN peak near 0.1 sec that is captured well with the strength adjusted curves but is lost in prior analysis due to strain localization. Comparison of the FP predictions in Figure 5.19 and Figure 5.14 indicates that the strength adjustments are less important for this direction because of the lower strain levels. Examining the waveforms, we see in Figure 5.19 that nonlinear analyses better represent the high frequency energy content in the initial portions of the strong shaking interval relative to EQL analysis.

Figure 5.21 compares the peak accelerations within the soil column from the EQL and nonlinear analyses and from recordings. Results are shown for analyses before and after strength adjustment to the backbone curves. In the FN direction, peak accelerations from nonlinear analysis are over-predicted at both depths (consistent with the findings from response spectra), and the strength adjustment to the backbone curves significantly increases the overprediction. This behavior is not evident in the FP direction where strains were lower. Peak accelerations from EQL analyses are closer to observed values for the FN direction.

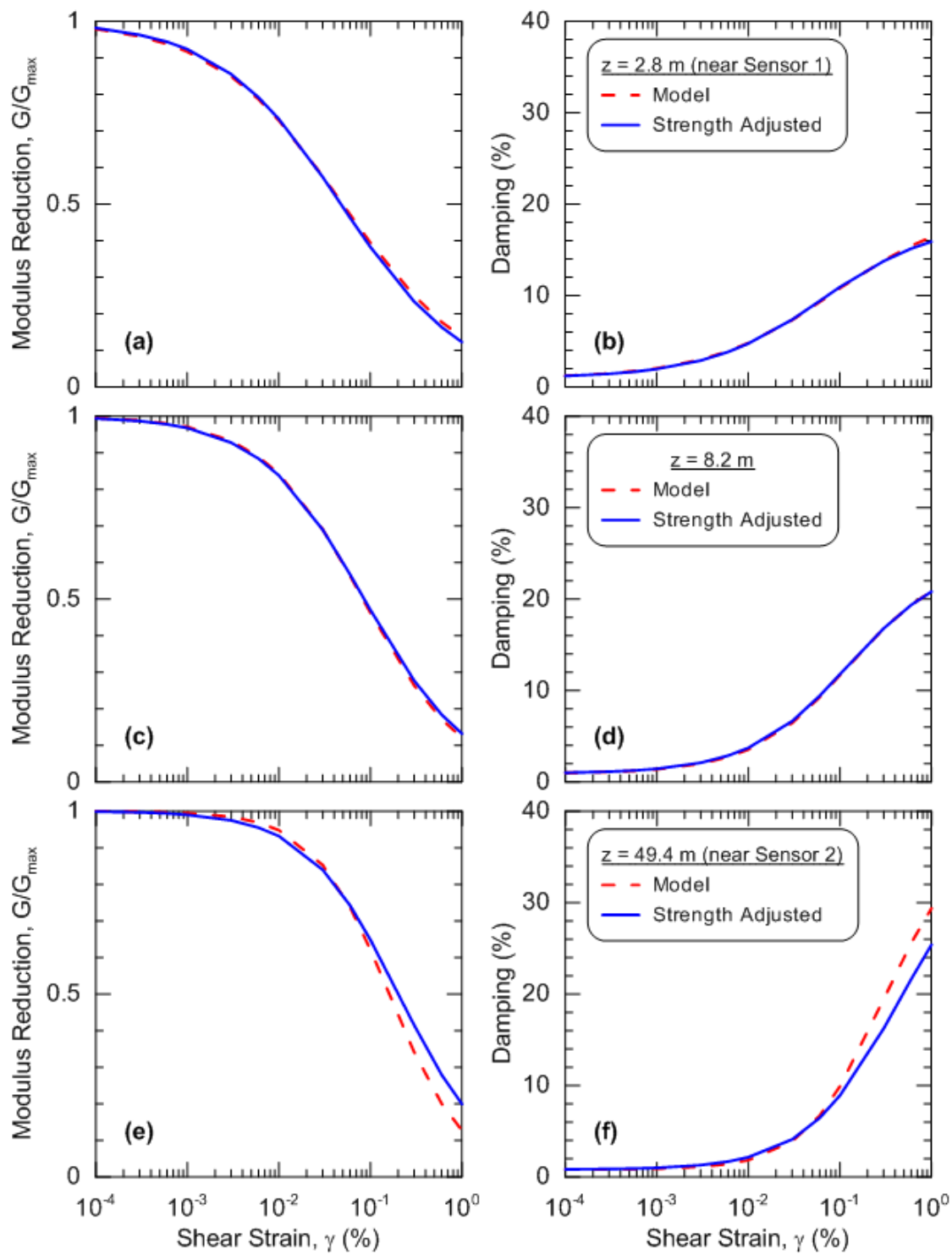


Figure 5.18 Comparison of the original and strength adjusted (a) modulus reduction and (b) damping models for the layer of soil containing the first sensor, (c) modulus reduction and (d) damping models for a layer at 8.2 m depth, and (e) modulus reduction and (f) damping models for the layer of soil containing the second sensor.

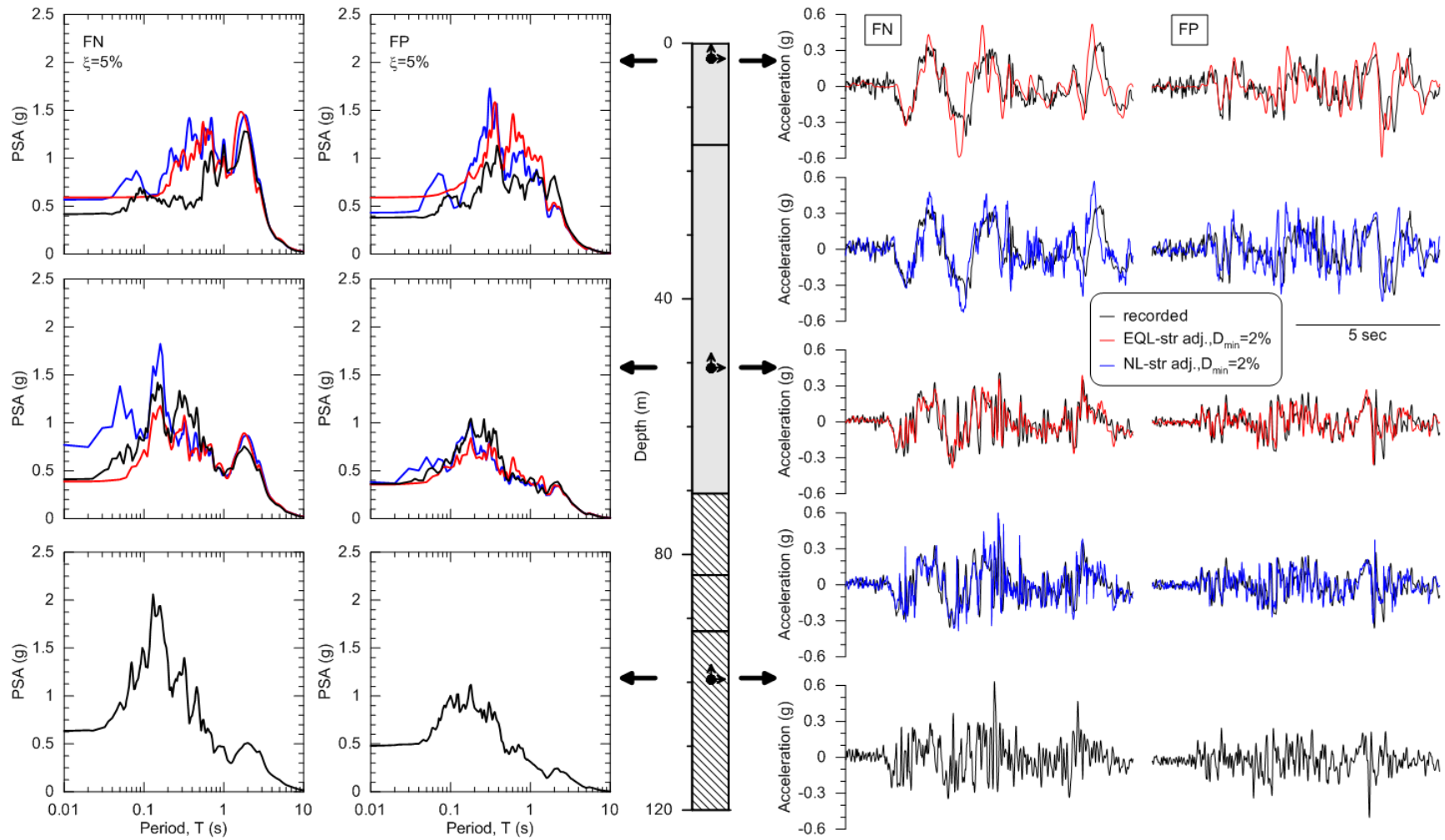


Figure 5.19 Results of strength adjusted EQL and nonlinear ground response analyses.

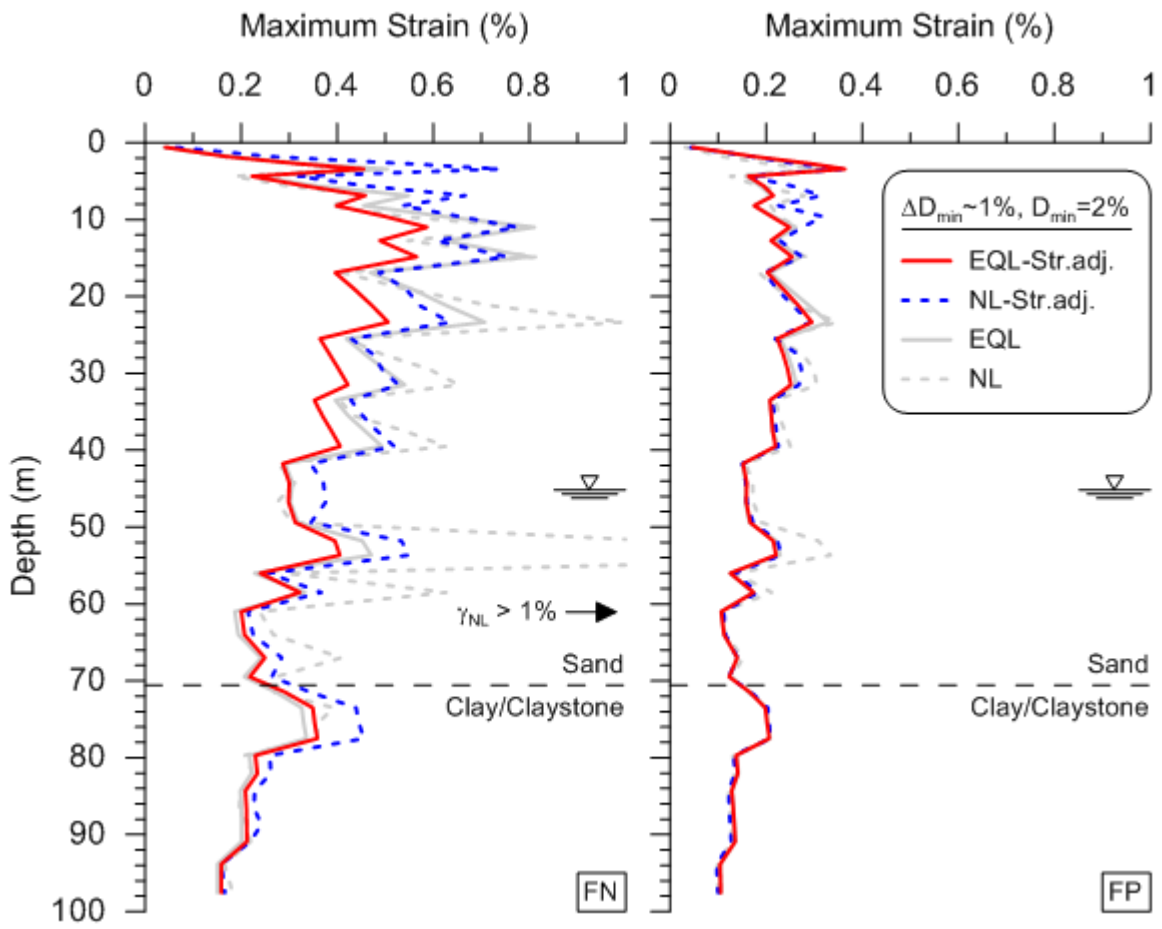


Figure 5.20 Peak strain profiles from strength adjusted EQL and nonlinear analyses.

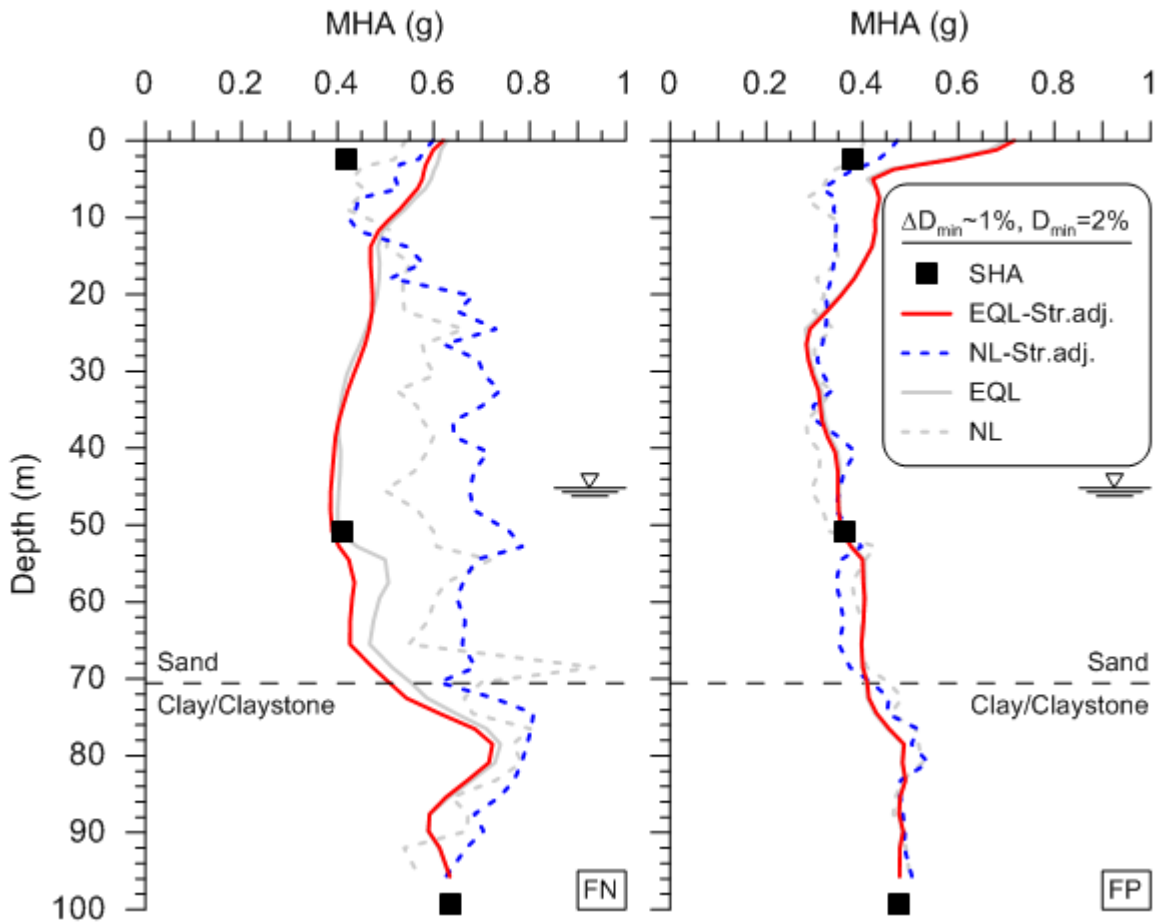
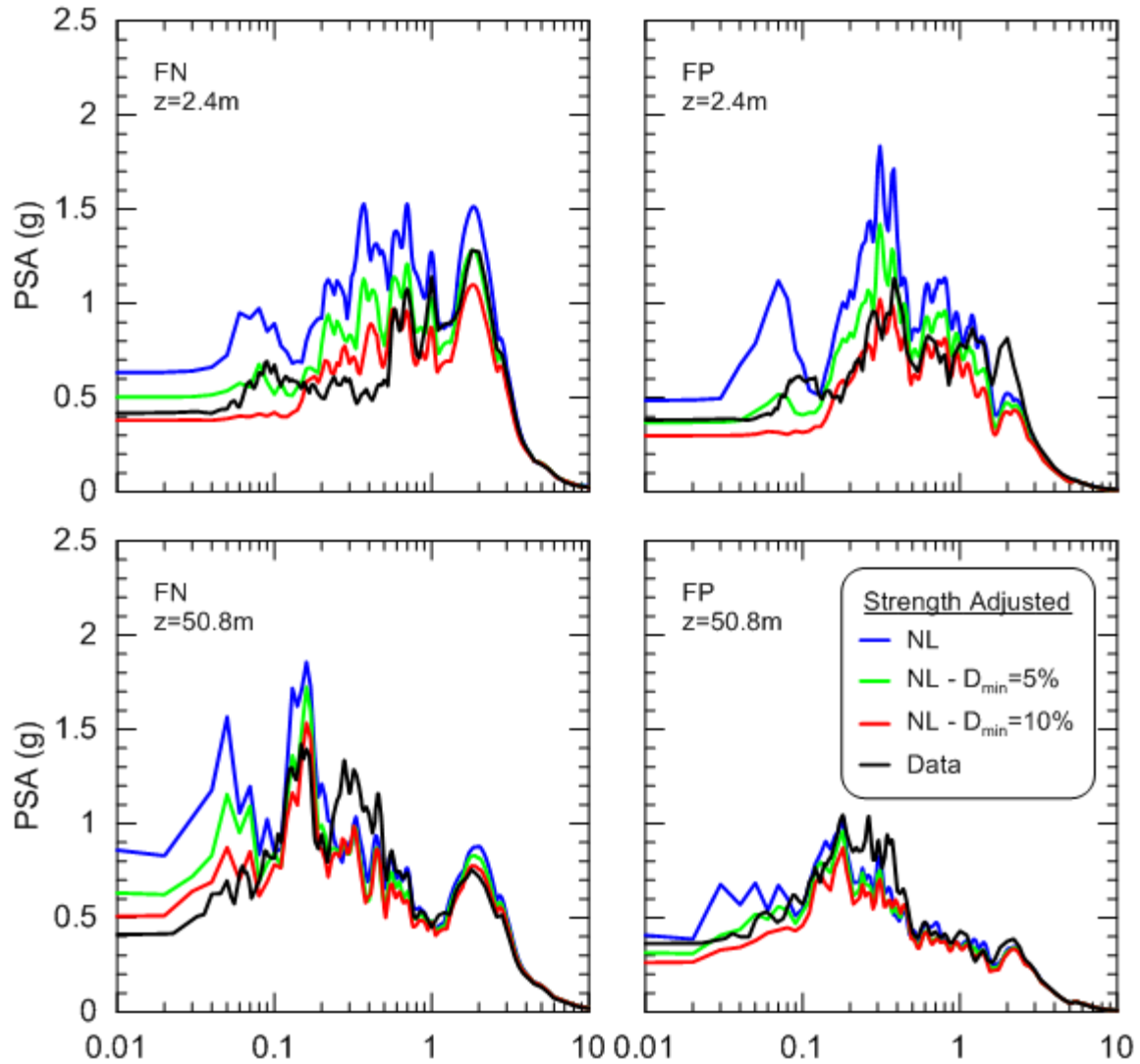


Figure 5.21 Peak accelerations from strength adjusted EQL and nonlinear analyses.

### 5.4.3 Damping Adjustment

The discrepancies in response spectra and peak acceleration profiles further support the need to increase damping (see Section 5.2). We evaluated the sensitivity of the Deepsoil results to small strain damping in soil by increasing  $D_{min}$  from 2% to 5% and 10%, which correspond to  $\Delta D_{min} \sim 4\%$  and  $9\%$ , respectively. The effects of these changes in damping on response spectral ordinates are shown in Figure 5.22. As expected, general spectral shapes before and after these adjustments are comparable, although high-frequency ordinates are reduced. Our interpretation of the results in Figure 5.22 is that a minimum damping of  $D_{min} = 5\%$  performs reasonably well for both directions and at both depths. This level of damping is within the range that was considered applicable from analysis of the aftershock data. Adjusting  $D_{min}$  to 10% overdamps the response, particularly for the FP direction and is also evident in the maximum horizontal acceleration profile shown in Figure 5.23.



**Figure 5.22** Response spectra at 5% damping for main shock and nonlinear analysis results using strength adjusted backbone curves and varying levels of small strain damping.

Figure 5.24 and 5.25 show MHA profiles, response spectra and wave forms, and strain profiles from strength adjusted ground response analyses with  $D_{min}$  in soil set to 5%. We do not show EQL results in these figures because the EQL MHA are shown in Figure 5.21 and are not sensitive to  $D_{min}$ . The simulation-data comparisons of waveforms, response spectra, and MHA profiles are more favorable for this set of simulations than those presented previously. The strain profile in Figure 5.25 is not significantly affected by the damping change (i.e., it is similar to that in Figure 5.20). Those strain levels are generally low enough that the unrealistic increase of large-strain damping with depth (which results from the  $\alpha$  model in Equation 5.4) is unlikely to

affect the results. The EQL analyses estimate lower peak strains than nonlinear analyses. As before, the differences between nonlinear and EQL analyses are most evident from low-period saturation of EQL spectra and the loss of high-frequency ground motion components in the EQL waveforms.

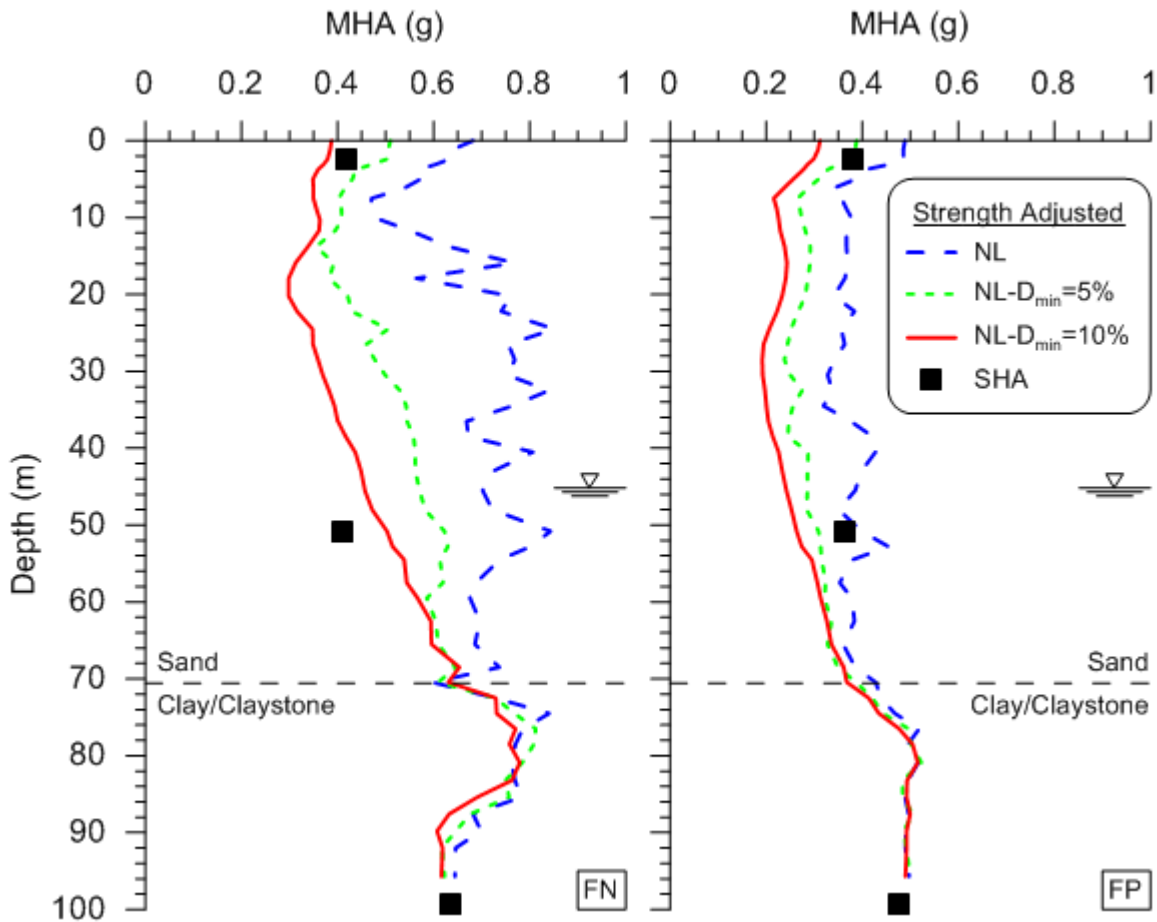


Figure 5.23 Peak accelerations from increased damping on strength adjusted nonlinear analyses.

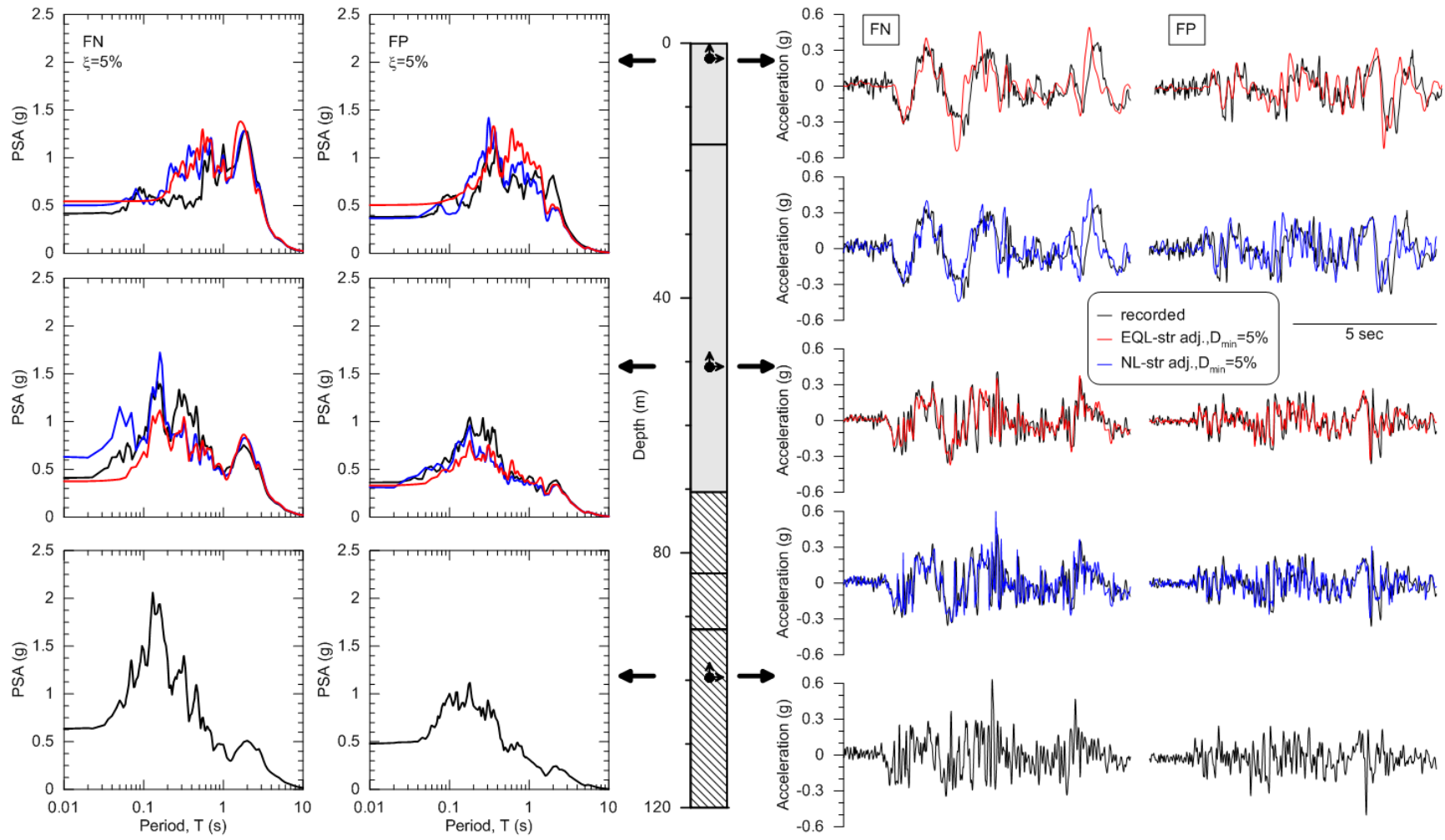


Figure 5.24 Results of strength adjusted EQL and nonlinear ground response analyses with increased damping.

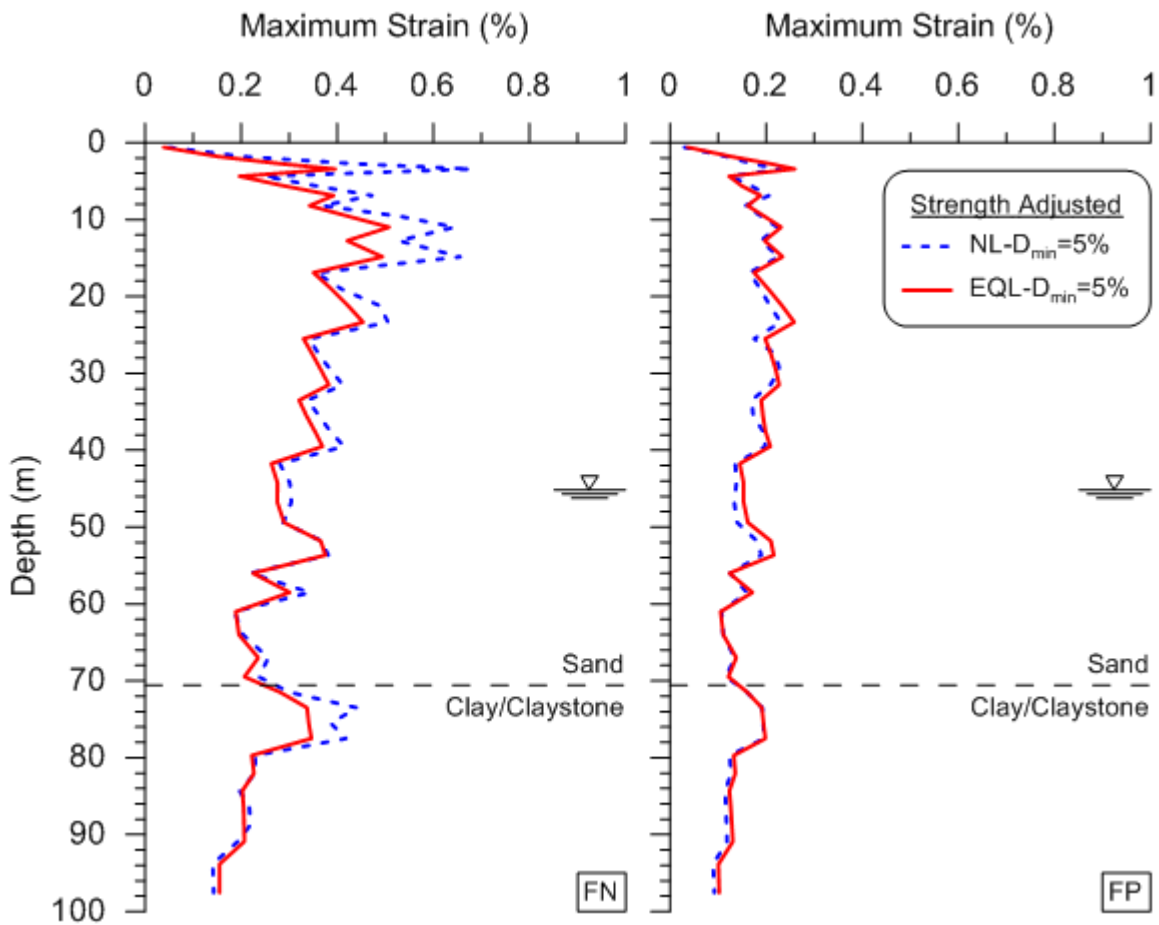


Figure 5.25 Peak strain profiles from strength adjusted EQL and nonlinear analyses with increased damping.

## 6 Ground Failure Analysis

Significant damage to utility pipelines and non-reactor structures occurred at the KKNPP that was attributed to settlement from seismic compression [Sakai et al. 2009; Tokimatsu, 2008]. The area in the immediate vicinity of the SHA experienced approximately  $15 \pm 5$  cm of settlement based on multiple sets of observations as described in Chapter 1. There was no obvious evidence of liquefaction manifest at the ground surface.

### 6.1 POTENTIAL FOR LIQUEFACTION AT DEPTH

In this section, we evaluate the potential for liquefaction of the soils below the water table, specifically at 50 m depth where a relatively low blow count was recorded [ $(N_1)_{60} \approx 20$ ] and relatively sizable strains are expected on the basis of ground response analysis (peak strains of 0.3% to 0.4%; see Figure 5.25). Seismic demand is computed as a magnitude- and overburden-adjusted Cycle Stress Ratio,  $CSR$ , computed as (modified from Seed and Idriss [1971]):

$$CSR_{M=7.5, \sigma'_v=1atm} = 0.65 \left( \frac{\tau_{max}}{\sigma'_v} \right) \frac{1}{MSF} \frac{1}{K_\sigma} \quad (6.1)$$

where  $\tau_{max}$  is the peak shear stress from ground response analysis,  $\sigma'_v$  is the vertical effective stress,  $MSF$  is the magnitude scaling factor taken as 1.3, and  $K_\sigma$  is the overburden correction factor, which depends on relative density, and ranges from 0.82 for  $D_R = 40\%$  to 0.72 for  $D_R = 65\%$  [Idriss and Boulanger 2008]. Based on Equation 6.1, we find that the  $CSR$  ranges from 0.16 to 0.18, considering the range of relative densities and stresses computed from the strength and damping adjusted nonlinear analyses. These values of  $CSR$  plot below the liquefaction triggering curves [cyclic resistance ratio  $CRR = 0.20$  for  $(N_1)_{60cs} = 20$ ], suggesting that liquefaction was unlikely to have occurred at depth at the SHA site. For the EQL analysis, the peak shear stresses are somewhat higher (this is expected given the constant shear modulus assumption in the EQL

method) and provide a *CSR* range of 0.19 to 0.21. The EQL analyses are considered less credible given the large-strain response of the soil in this depth interval.

## 6.2 SEISMIC COMPRESSION

In the remainder of this chapter, we compute ground settlement from seismic compression for comparison to the observations. Seismic compression analysis requires evaluation of seismic demand in the form of effective strain profiles and equivalent numbers of strain cycles combined with a volumetric strain material model (e.g., see Figure 3.3).

Site specific analyses utilize shear strain demands computed from ground response analyses and a site-specific VSMM. The effective shear strain at depth  $z$  is taken as 65% of the maximum strain from nonlinear site response analysis (i.e., see Figure 5.25),

$$\gamma_{eff}(z) = 0.65 \times \gamma_{max}(z) \quad (6.2)$$

The equivalent number of cycles of the ground motions at shear strain level  $\gamma_{eff}$  can be evaluated using procedures described in Liu et al. [2001]. As described in Liu et al. [2001] and Stewart et al. [2002], the relative weighting of peaks with different amplitudes is evaluated based on laboratory-derived relationships between cyclic shear strain amplitude ( $\gamma_c$ ) and the number of cycles to induce a particular level of performance (i.e., particular levels of vertical strain in the case of seismic compression problems). Those relationships tend to be linear in log-log space, as shown in Figure 6.1 for the KKNPP soil material. The weight factors assigned to peaks with different amplitudes is related to the slope of the linear relationship. As shown in Figure 6.1, this slope was taken as -0.4 from laboratory testing of the KKNPP soil material. Using these procedures, the equivalent number of cycles was computed from calculated strain histories derived from EQL analysis, with the results shown in Figure 6.2. Nonlinear analyses could not be used due to permanent offsets in the strain histories.

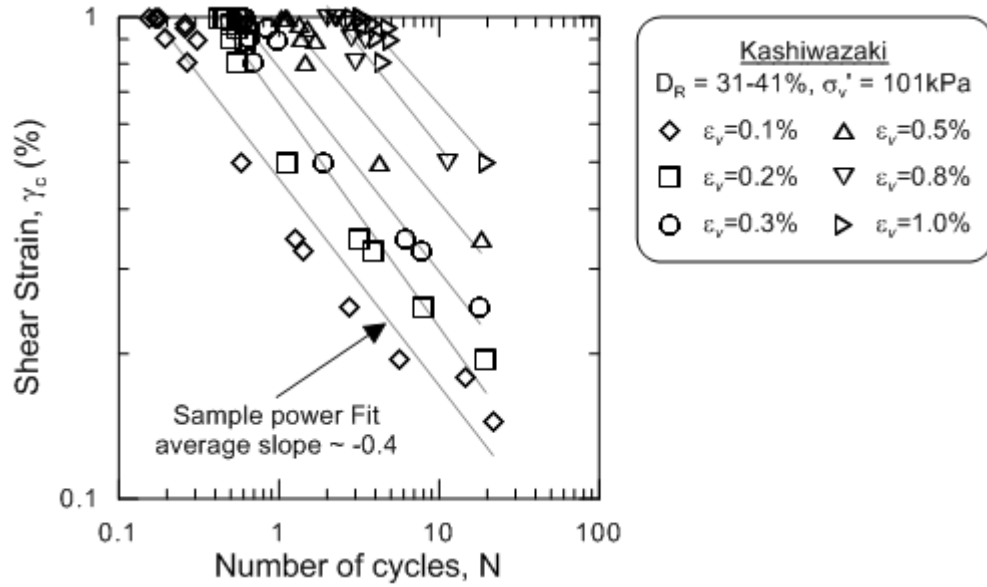


Figure 6.1 Relationship between shear strain amplitude,  $\gamma_c$ , and number of cycles,  $N$ , to cause selected amounts of vertical strain,  $\epsilon_v$ .

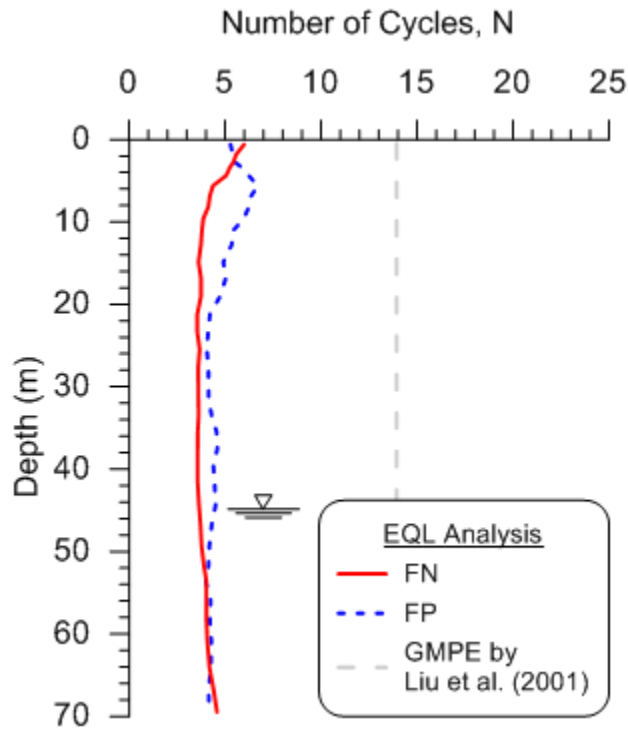


Figure 6.2 Number of cycles from strength-adjusted EQL analysis.

Vertical strains for each component of ground motion at depth  $z$  are calculated as:

$$\varepsilon_v(z) = (a \times K_{\sigma,\varepsilon}(z)) (\gamma_{eff}(z) - \gamma_{iv})^b \times C_N \quad (6.3)$$

where  $\gamma_{eff}(z)$  is taken from the ground response analysis results (shown in left plot of Figure 6.3), parameters  $a$  and  $b$  are as given in Figure 3.3 [regressed from simple shear test data; results similar to the Duku et al. [2008] relation for this material]. The overburden correction term  $K_{\sigma,\varepsilon}(z)$  is taken as a function of vertical stress from the model of Duku et al. [2008], which has been verified from material-specific testing (see Figure 3.3e). Parameter  $C_N$  is taken from Equation (3.6) with  $R=0.31$  and  $N$  taken from Figure 6.2. These analyses are repeated for both the FN and FP directions, with the resulting settlements being 9 and 3 cm, respectively for  $D_R = 40\%$  and 6 and 2 cm, respectively for  $D_R = 65\%$ . Figure 6.3 shows the distribution of vertical strain along the soil profile and indicates a majority of the deformations occurred in the upper 25 m. Following the findings from two-dimensional testing (see Section 3.2.4 and Figure 3.5), these two settlements are summed, leading to predicted settlements from horizontal ground motions of about 12 and 8 cm for  $D_R = 40\%$  and  $65\%$ , respectively.

As shown by Pyke et al. [1975] and described in Section 2.2, the application of vertical ground motion in combination with horizontal ground motion increases volumetric strains by amounts ranging from approximately 20% to 50% for effective vertical accelerations between 0.15 to 0.3g. The peak vertical accelerations at the KKNPP site (shown in Figure 4.2) are about 0.25g at depth (50 m and below) and 0.6g near the surface. Given that most of the seismic compression occurs in the upper 25 m, a reasonable value for the effective vertical acceleration in the depth range of principal interest is approximately two-thirds of 0.6g or 0.4g. This value of effective vertical acceleration supports a volumetric strain increase of approximately 50%, leading to predicted settlements in the range of 12 to 18 cm, which are reasonably consistent with the measured range of  $15 \pm 5$  cm at the site.

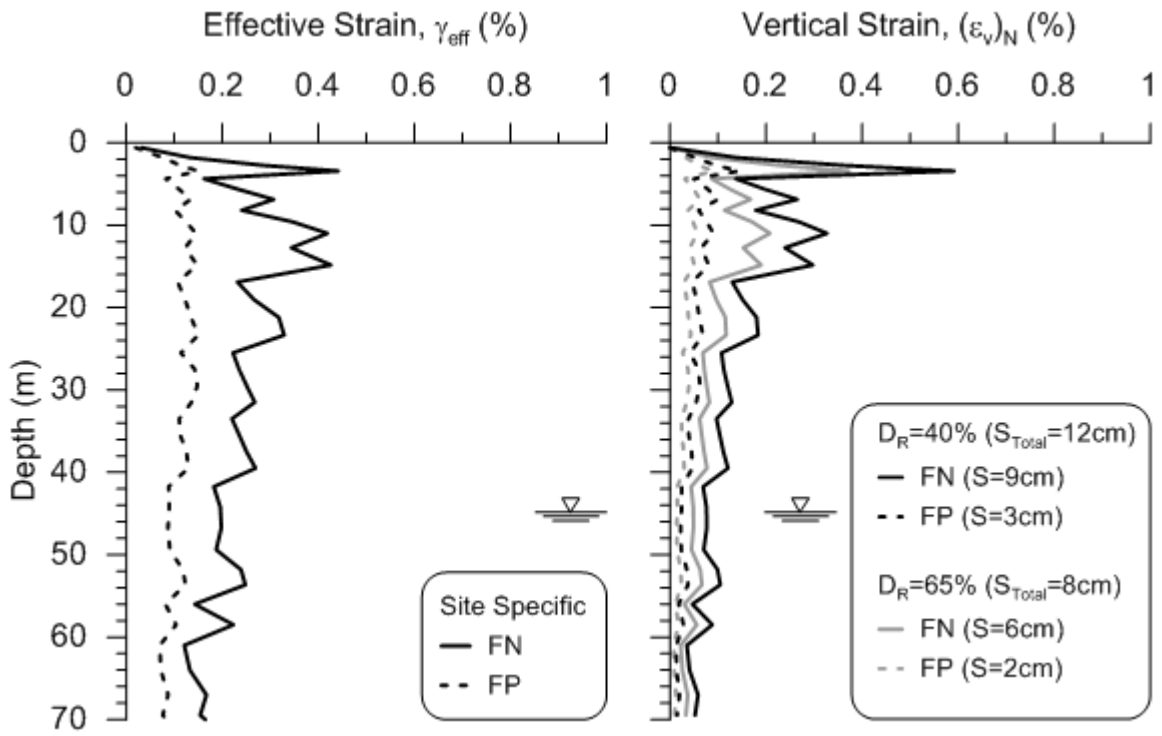


**Figure 6.3** Sample effective strain demand profiles, vertical strain profiles, and resultant settlements from a site specific analysis for  $D_R = 40\%$  and  $65\%$ .



## 7 Summary and Conclusions

The 2007 Niigata-ken Chuetsu-oki earthquake was recorded at the KKNPP site by a series of surface and downhole instruments. In this study we have focused on the data from the service hall array (SHA) site where geometric mean peak accelerations at the ground surface were 0.44g and ground settlements of about  $15 \pm 5$  cm were observed. The SHA site offers a unique opportunity to validate ground response analysis codes and seismic compression analysis procedures for strong levels of shaking similar to those that would often be applied in seismic design.

A site investigation at the SHA was conducted to obtain soil samples, SPT blowcounts with energy measurements, and a velocity profile. The site profile was found to consist of about 70 m of Quaternary sands overlying Pleistocene and then Tertiary clayey bedrock materials. Triaxial compression and resonant column/torsional shear (RCTS) tests were conducted on sand specimens to measure shear strength and cyclic modulus reduction and damping curves. Simple shear tests were also conducted on remolded sand specimens to develop a material-specific model relating volume change to amplitude and number of shear strain cycles for the unsaturated soils. This testing was performed for relative densities ( $D_R$ ) of 40% and 65%, which spans the range of estimates from Pitcher tube samples and penetration resistance correlations.

Equivalent linear and nonlinear ground response was modeled with DeepSoil 4.0 using the dynamic soil properties developed from field and laboratory testing and ground motion recordings from 100 m depth as input. We have some confidence in the use of one-dimensional modeling of site response for the KKNPP site, due to relatively consistent surface-to-bedrock transfer functions from recorded data that are reasonably well predicted by DeepSoil.

Initial ground response analyses utilizing soil dynamic properties derived from RCTS tests encounter several difficulties, including overestimation of high-frequency ground response and unrealistic strain localization at a depth of 50 m from main shock ground motions. Increases

in the small strain material damping from laboratory-based values (generally near  $D_{min} = 1\%$ ) to higher levels of  $D_{min} = 2\%$  and  $5\%$  largely solve the problem of over-prediction of high-frequency ground response. Such increases in small strain damping are consistent with previous vertical array studies in which observed soil damping levels exceed those from laboratory testing. A procedure to adjust backbone curves to approach the shear strength at large strains while retaining low-strain behavior from traditional modulus reduction curves was implemented to address the strain localization problem.

When the modified soil properties are implemented in ground response analysis, the strain localization problem is eliminated and strain demands are increased in shallower parts of the profile. At a small strain damping level (in soil layers) of  $D_{min} = 5\%$ , the ground motion predictions from both equivalent linear (EQL) and nonlinear analyses provide generally good matches to recorded response spectra from aftershock and main shock recordings at 2.4 and 50 m depths. The EQL and nonlinear results are practically identical for the relatively low-strain aftershock site response (peak shear strains in profile of  $\gamma \sim 0.12\%$  and  $0.02\%$ ). For the relatively strong main shock recordings, the EQL analyses over-damp the ground motions producing a characteristic flat spectral shape at short periods ( $T < \sim 0.1$  sec) that is not present in nonlinear analysis results or in the data. For the same reason (overdamping), the EQL waveforms lack realistic phasing outside of the main shear wave window. Despite these problems, at intermediate and long spectral periods ( $T > \sim 0.1$  sec), the EQL and nonlinear results are similar, with both providing good matches to recorded data.

Ground failure analyses for the site indicate that liquefaction was unlikely to have occurred. Near the ground surface the soils are unsaturated and hence not susceptible. At depths beyond 50 m, the soils are saturated but cyclic demands are shown to fall below the anticipated cyclic resistance. Accordingly, ground settlements appear to have resulted from seismic compression of partially saturated soils. Shear strains estimated from the nonlinear ground response analysis were combined with a material-specific volumetric strain material model that predicts vertical strains given shear strain amplitude, number of cycles, and vertical total stress. Settlements were computed using vertical strains evaluated independently for both horizontal directions. Drawing on test results showing that vertical strains from the two horizontal directions can be summed to evaluate the vertical strain from simultaneous two-dimensional strain demands, the two settlement estimates are summed to provide estimates of site-specific

ground surface settlements from horizontal ground shaking ranging from approximately 8 to 12 cm for relative densities of 65% and 40%, respectively. When vertical ground motions are considered, these estimates are increased by 50%, leading to estimated settlements ranging from 12 to 18 cm. These estimates compare reasonably well to the observed settlements of  $15 \pm 5$  cm at the SHA site.



## REFERENCES

- Abou-Matar, H. and Goble G. G. (1997). "SPT dynamic analysis and measurements," *J. Geotech. & Geoenviron. Engrg.*, ASCE 123(10), 921-928.
- Anderson, D. G., and Tang, Y. K. (1989). "Summary of soil characterization program for the lotung large-scale seismic experiment," *NP-6154*, Electric Power Research Institute, Palo Alto, Calif.
- Baise, L.G., Thompson, E.M., Kaklamanos, J., and Dorfmann, L. (2011). "Complex site response: does one dimensional site response work?" *Proc. 4<sup>th</sup> IASPEI/IAEE International Symposium*, Univ. of California, Santa Barbara.
- Boore, D.M. (2005). "On pads and filters: processing strong-motion data," *Bull. Seism. Soc. Am.*, 95(2), 745-750.
- Boore, D.M. and Bommer, J.J. (2005). "Processing of strong-motion accelerograms: needs, options and consequences," *Soil Dyn. Earthquake Engrg.*, 25(2), 93-115.
- Boulanger, R.W. (2003). "High overburden stress effects in liquefaction analysis," *J. Geotech. & Geoenviron. Engrg.*, ASCE 129(12), 1071-1082.
- Bozorgnia, Y. and Campbell, K.W. (2004). "The vertical-to-horizontal response spectral ratio and tentative procedures for developing simplified V/H and vertical design spectra," *J. Earthquake Engrg.*, 8(2), 175-207.
- Cubrinovski, M. and Ishihara, K. (1999). "Empirical correlation between SPT N-value and relative density for sandy soils," *Soils and Foundations*, 39(5), 61-71.
- Cubrinovski, M., Ishihara, K., and Tanizawa, F. (1996). "Numerical simulation of the Kobe port island liquefaction," *Proc. 11th World Conf. on Earthquake Engrg.*, Paper No. 330.
- Darendeli, M. (2001). "Development of a new family of normalized modulus reduction and material damping curves," *Ph.D. Dissertation*, Dept. of Civil Eng., Univ. of Texas, Austin.
- Dobry, R. and Ladd, R.S. (1980). Discussion to "Soil liquefaction and cyclic mobility evaluation for level ground during earthquakes," *J. of Geotech. Engrg. Div.*, ASCE, 106(GT6), 720-724.
- Duku, P.M., Stewart, J.P., Whang, D.H., Venugopal, R. (2007). "Digitally controlled simple shear apparatus for dynamic soil testing," *Geotech. Testing Journal*, ASTM, 30 (5), 368-377.
- Duku, P.M., Stewart, J.P., Whang, D.H., and Yee, E. (2008). "Volumetric strains of clean sands subject to cyclic loads," *J. of Geotech. & Geoenviron. Engrg.*, ASCE, 134 (8), 1073-1085.
- Elgamal, A., Lai, T., Yang, Z., and He, L. (2001). "Dynamic soil properties, seismic downhole arrays and applications in practice," *Proc., 4th Int. Conf. on Recent Advances in Geotechnical Earthquake Engineering and Soil Dynamics*, Univ. of Missouri-Rolla, San Diego.
- Hardin, BO and VP Drnevich (1972). "Shear modulus and damping in soils," *J. Soil Mech. & Found. Div.*, ASCE, 98 (7), 667-692.
- Hashash, Y.M.A., Groholski, D.R., Phillips, C.A., Park, D., and Musgrove, M. (2011). "Deepsoil v4.0, user manual and tutorial," 98p.
- Hatanaka, M. and Uchida A. (1996). "Empirical correlation between penetration resistance and internal friction angle of sandy soils," *Soils and Foundation*, 48(4), 1-9.
- Idriss, I.M. and Boulanger, R.W. (2008). Soil liquefaction during earthquakes. *Monograph MNO-12*, Earthquake Engineering Research Institute, Oakland, CA, 261 pp.
- Idriss, I.M. and Sun, J.I. (1992). "Shake91: a computer program for conducting equivalent linear seismic response analyses of horizontally layered soil deposits," *Users Guide*, Univ. of Calif., Davis, 13pp.
- Kayen, R., Brandenberg, S.J., Collins, B.D., Dickenson, S., Ashford, S., Kawamata, Y., Tanaka, Y., Koumoto, H., Abrahamson, N., Cluff, L., Tokimatsu, K. (2009). "Geoengineering and seismological aspects of the niigata-ken chuetsu-oki earthquake of 16 July 2007," *Earthquake Spectra*, 25(4), 777-802.
- Kramer, SL (1996). "*Geotechnical earthquake engineering*," Prentice Hall, New Jersey, 653pp.

- Kwok, A.O., Stewart, J.P., and Hashash, Y.M.A. (2008). "Nonlinear ground response analysis of Turkey Flat shallow stiff soil site to strong ground motion," *Bull. Seism. Soc. Am.*, 98(1), 331-343.
- Kwok, A.O., Stewart, J.P., Hashash, Y.M.A., Matasovic, N., Pyke, R., Wang, Z., and Yang, Z. (2007). "Use of exact solutions of wave propagation problems to guide implementation of nonlinear seismic ground response analysis procedures," *J. Geotech. & Geoenviron. Engrg.*, ASCE, 133 (11), 1385-1398.
- Liu, A.H., Stewart, J.P., Abrahamson, N.A., and Moriwaki, Y. (2001). "Equivalent number of uniform stress cycles for soil liquefaction analysis," *J. Geotech. & Geoenviron. Engrg.*, ASCE, 127(12), 1017-1026.
- Menq, F.Y. (2003). "Dynamic properties of sandy and gravelly soils." *Ph.D. Dissertation*, Dept. of Civil Eng., Univ. of Texas, Austin.
- Mikami, A., Stewart, J.P., and Kamiyama, M. (2008). "Effects of time series analysis protocols on transfer functions calculated from earthquake accelerograms," *Soil Dyn. Earthquake Engrg.*, 28 (9), 695-706.
- Miyake, H., Koketsu, K., Hikima, K., Shinohara, M., and Kanazawa, T. (2010). "Source fault of the 2007 Chuetsu-oki, Japan, earthquake," *Bull. Seism. Soc. Am.*, 100(1), 384-391.
- National Research Council (NRC). (1985). "Committee on Earthquake Engineering, Commission on Engineering and Technical Systems." *Liquefaction of soils during earthquakes*, National Academy Press, Washington D.C..
- Nigbor, R.L. and Imai, T. (1994). "The suspension ps velocity logging method," *Geophysical Characterization of Sites*, ISSMFE Special Publication TC 10, XIII ICSMFE, New Delhi, India, Richard Woods, Editor, 57-61.
- Polito, C. P. and Martin, J. R. (2001). "Effects of nonplastic fines on the liquefaction resistance of sands." *J. Geotech. & Geoenviron. Engrg.*, 127(5), 408-415.
- Pyke, R., Seed, H.B., Chan, C.K. (1975). "Settlement of sands under multidirectional shaking," *J. Geotech. Engrg.*, ASCE, 101 (4), 379-398.
- Sakai, T., Suehiro, T., Tani, T., and Sato, H. (2009). "Geotechnical performance of the Kashiwazaki-Kariwa nuclear power station caused by the 2007 Niigata ken Chuetsu-oki earthquake" *Earthquake geotechnical case histories for performance-based design*, Taylor & Francis Group, London, Kokusho (ed).
- Seed, H.B. and Idriss, I.M. (1971). "Simplified procedure for evaluating soil liquefaction potential," *J. Soil Mech. & Found. Div.*, ASCE, 97(9), 1249-1273.
- Seed, H.B., Mori, K., and Chan, C.K. (1977). "Influence of seismic history on liquefaction of sands," *J. Geotech. Engrg. Div.*, ASCE, 103(GT4), 246-270.
- Shahi, S.K. and Baker, J.W. (2011). "An empirically calibrated framework for including the effects of near-fault directivity in probabilistic seismic hazard analysis," *Bull. Seism. Soc. Am.*, 101, (2), 742-755.
- Skempton, AW (1986). "Standard penetration test procedures and the effects in sands of overburden pressure, relative density, particle size, aging, and overconsolidation," *Geotechnique*, 36(3), 425-447.
- Stewart, J.P. and Kwok, A.O. (2008). "Nonlinear seismic ground response analysis: code usage protocols and verification against vertical array data," *Geotechnical Engineering and Soil Dynamics IV*, May 18-22, 2008, Sacramento, CA, *ASCE Geotechnical Special Publication No. 181*, D. Zeng, M.T. Manzari, and D.R. Hiltunen (eds.), 24 pages (electronic file).
- Stewart J.P., Smith P.M., Whang D.H., and Bray J.D. (2004). "Seismic compression of two compacted earth fills shaken by the 1994 Northridge earthquake," *J. Geotech. & Geoenviron. Engrg.*, ASCE, 130(5), 461-476.
- Stewart, J.P., Smith, P.M., Whang, D.H., and Bray, J.D. (2002). "Documentation and analysis of field case histories of seismic compression during the 1994 Northridge, California, earthquake," *Rpt. No. PEER-2002/09*, Pacific Earthquake Engineering Research Center, U.C. Berkeley, Calif.
- Stewart, J.P., Kwok, A.O., Hashash, Y.M.A., Matasovic, N., Pyke, R., Wang, Z., and Yang, Z. (2008). "Benchmarking of nonlinear seismic ground response analysis procedures," *Rpt. No. PEER-2008/04*, Pacific Earthquake Engineering Research Center, U.C. Berkeley, Calif.

- The Tokyo Electric Power Company, Inc. (2007). "The data analysis recorded at the Kashiwazaki Kariwa Nuclear Power Plant during the 2007 Niigata-ken Chuetsu-oki earthquake", [http://www.tepco.co.jp/cc/press/betu07\\_j/images/070730d.pdf](http://www.tepco.co.jp/cc/press/betu07_j/images/070730d.pdf).
- Tokimatsu, K. (2008). "Geotechnical problems in the 2007 Niigata-ken Chuetsu-oki earthquake," *Geotechnical Engineering and Soil Dynamics IV*, May 18-22, 2008, Sacramento, CA, *ASCE Geotechnical Special Publication No. 181*, D. Zeng, M.T. Manzari, and D.R. Hiltunen (eds.), 30 pages (electronic file).
- Tokimatsu, K. and Arai, H. (2008). "Dynamic soil behavior and rock outcrop motion back-calculated from downhole array records at kashiwazaki-kariwa nuclear power plant in the 2007 niigata-ken chuetsu-oki earthquakes," *Proc. 5th Int. Conf. on Urban Earthquake Eng.*, Tokyo, Japan, Mar. 4-5, 2008, 289-294.
- Tokimatsu, K. and Seed, H.B. (1987). "Evaluation of settlements in sand due to earthquake shaking," *J. of Geotech. Engrg.*, ASCE, 113(8), 861-878.
- Tokimatsu, K. and Yoshimi, Y. (1983). "Empirical correlation of soil liquefaction based on SPT N-value and fines content," *Soils and Foundations*, 23(4), 56-74.
- Tokimatsu, K., Ibaraki, Y., and Arai, H. (2009). "Dynamic soil properties back-calculated from strong motions recorded at two downhole arrays during the 2007 Niigata-ken Chuetsu-oki earthquakes," *Proc. 6th Int. Conf. on Urban Earthquake Eng.*, Tokyo, Japan, Mar. 3-4, 2009, 485-489.
- Tokyo Soil Research (2009). "Tokyo electric power Kashiwazaki-Kariwa nuclear power plant service hall geotechnical investigation," *Rpt. by Tokyo Soil Research*, 66pp.
- Tsai, C.C. and Hashash, Y.M.A. (2009). "Learning of dynamic soil behavior from downhole arrays," *J. Geotech. & Geoenviron. Engrg.*, ASCE, 135(6), 745-757.
- Wartman, J., Rodriguez-Marek, A., Repetto, P.C., Keefer, D.K, Rondinel, E. Zegarra-Pellane, J., and Baures, D. (2003). "Ground failure" *Earthquake Spectra*, 19(S1), 35-56.
- Wartman, J., Rodriguez-Marek, A., Macari, E. J., Deaton, S., Ramirez-Reynaga, M., Navarro-Ochoa, C, Callan, S., Keefer, D., Repetto, P., and Ovando-Shelley, E. (2005). "Geotechnical aspects of the January 2003 Tecoman earthquake," *Earthquake Spectra*, Vol. 21(2), 493-538.
- Yee, E., Stewart, J.P., and Schoenberg, F.P. (2011). "Characterization and utilization of noisy displacement signals from simple shear device using linear and kernel regression methods," *Soil Dyn. Earthquake Engrg.*, 31(1), 25-32.
- Zeghal, M., Elgamal, A.-W., Tang, H. T., and Stepp, J. C. (1995). "Lotung downhole array. II: Evaluation of soil nonlinear properties," *J. Geotech. Engrg.*, ASCE, 121 (4), 363-378.
- Zhang, J., Andrus, R.D., and Juang, C.H. (2005). "Normalized shear modulus and material damping ratio relationships," *J. Geotech. & Geoenviron. Engrg.*, ASCE, 131 (4), 453-464.



## PEER REPORTS

PEER reports are available individually or by yearly subscription. PEER reports can be ordered at [http://peer.berkeley.edu/publications/peer\\_reports.html](http://peer.berkeley.edu/publications/peer_reports.html) or by contacting the Pacific Earthquake Engineering Research Center, 325 Davis Hall mail code 1792, Berkeley, CA 94720. Tel.: (510) 642-3437; Fax: (510) 665-1655; Email: peer\_editor@berkeley.edu

- PEER 2011/09** *Calibration of Semi-Stochastic Procedure for Simulating High-Frequency Ground Motions.* Jonathan P. Stewart, Emel Seyhan, and Robert W. Graves. December 2011.
- PEER 2011/08** *Water Supply in regard to Fire Following Earthquake.* Charles Scawthorn. November 2011.
- PEER 2011/07** *Seismic Risk Management in Urban Areas. Proceedings of a U.S.-Iran-Turkey Seismic Workshop.* September 2011.
- PEER 2011/06** *The Use of Base Isolation Systems to Achieve Complex Seismic Performance Objectives.* Troy A. Morgan and Stephen A. Mahin. July 2011.
- PEER 2011/05** *Case Studies of the Seismic Performance of Tall Buildings Designed by Alternative Means.* Task 12 Report for the Tall Buildings Initiative. Jack Moehle, Yousef Bozorgnia, Nirmal Jayaram, Pierson Jones, Mohsen Rahnama, Nilesh Shome, Zeynep Tuna, John Wallace, Tony Yang, and Farzin Zareian. July 2011.
- PEER 2011/04** *Recommended Design Practice for Pile Foundations in Laterally Spreading Ground.* Scott A. Ashford, Ross W. Boulanger, and Scott J. Brandenburg. June 2011.
- PEER 2011/03** *New Ground Motion Selection Procedures and Selected Motions for the PEER Transportation Research Program.* Jack W. Baker, Ting Lin, Shrey K. Shahi, and Nirmal Jayaram. March 2011.
- PEER 2011/02** *A Bayesian Network Methodology for Infrastructure Seismic Risk Assessment and Decision Support.* Michelle T. Bensi, Armen Der Kiureghian, and Daniel Straub. March 2011.
- PEER 2011/01** *Demand Fragility Surfaces for Bridges in Liquefied and Laterally Spreading Ground.* Scott J. Brandenburg, Jian Zhang, Pirooz Kashighandi, Yili Huo, and Minxing Zhao. March 2011.
- PEER 2010/05** *Guidelines for Performance-Based Seismic Design of Tall Buildings.* Developed by the Tall Buildings Initiative. November 2010.
- PEER 2010/04** *Application Guide for the Design of Flexible and Rigid Bus Connections between Substation Equipment Subjected to Earthquakes.* Jean-Bernard Dastous and Armen Der Kiureghian. September 2010.
- PEER 2010/03** *Shear Wave Velocity as a Statistical Function of Standard Penetration Test Resistance and Vertical Effective Stress at Caltrans Bridge Sites.* Scott J. Brandenburg, Naresh Bellana, and Thomas Shantz. June 2010.
- PEER 2010/02** *Stochastic Modeling and Simulation of Ground Motions for Performance-Based Earthquake Engineering.* Sanaz Rezaeian and Armen Der Kiureghian. June 2010.
- PEER 2010/01** *Structural Response and Cost Characterization of Bridge Construction Using Seismic Performance Enhancement Strategies.* Ady Aviram, Božidar Stojadinović, Gustavo J. Parra-Montesinos, and Kevin R. Mackie. March 2010.
- PEER 2009/03** *The Integration of Experimental and Simulation Data in the Study of Reinforced Concrete Bridge Systems Including Soil-Foundation-Structure Interaction.* Matthew Dryden and Gregory L. Fenves. November 2009.
- PEER 2009/02** *Improving Earthquake Mitigation through Innovations and Applications in Seismic Science, Engineering, Communication, and Response. Proceedings of a U.S.-Iran Seismic Workshop.* October 2009.
- PEER 2009/01** *Evaluation of Ground Motion Selection and Modification Methods: Predicting Median Interstory Drift Response of Buildings.* Curt B. Haselton, Ed. June 2009.
- PEER 2008/10** *Technical Manual for Strata.* Albert R. Kottke and Ellen M. Rathje. February 2009.
- PEER 2008/09** *NGA Model for Average Horizontal Component of Peak Ground Motion and Response Spectra.* Brian S.-J. Chiou and Robert R. Youngs. November 2008.
- PEER 2008/08** *Toward Earthquake-Resistant Design of Concentrically Braced Steel Structures.* Patxi Uriz and Stephen A. Mahin. November 2008.
- PEER 2008/07** *Using OpenSees for Performance-Based Evaluation of Bridges on Liquefiable Soils.* Stephen L. Kramer, Pedro Arduino, and HyungSuk Shin. November 2008.
- PEER 2008/06** *Shaking Table Tests and Numerical Investigation of Self-Centering Reinforced Concrete Bridge Columns.* Hyung IL Jeong, Junichi Sakai, and Stephen A. Mahin. September 2008.
- PEER 2008/05** *Performance-Based Earthquake Engineering Design Evaluation Procedure for Bridge Foundations Undergoing Liquefaction-Induced Lateral Ground Displacement.* Christian A. Ledezma and Jonathan D. Bray. August 2008.

- PEER 2008/04** *Benchmarking of Nonlinear Geotechnical Ground Response Analysis Procedures.* Jonathan P. Stewart, Annie On-Lei Kwok, Youssef M. A. Hashash, Neven Matasovic, Robert Pyke, Zhiliang Wang, and Zhaohui Yang. August 2008.
- PEER 2008/03** *Guidelines for Nonlinear Analysis of Bridge Structures in California.* Ady Aviram, Kevin R. Mackie, and Božidar Stojadinović. August 2008.
- PEER 2008/02** *Treatment of Uncertainties in Seismic-Risk Analysis of Transportation Systems.* Evangelos Stergiou and Anne S. Kiremidjian. July 2008.
- PEER 2008/01** *Seismic Performance Objectives for Tall Buildings.* William T. Holmes, Charles Kircher, William Petak, and Nabih Youssef. August 2008.
- PEER 2007/12** *An Assessment to Benchmark the Seismic Performance of a Code-Conforming Reinforced Concrete Moment-Frame Building.* Curt Haselton, Christine A. Goulet, Judith Mitrani-Reiser, James L. Beck, Gregory G. Deierlein, Keith A. Porter, Jonathan P. Stewart, and Ertugrul Taciroglu. August 2008.
- PEER 2007/11** *Bar Buckling in Reinforced Concrete Bridge Columns.* Wayne A. Brown, Dawn E. Lehman, and John F. Stanton. February 2008.
- PEER 2007/10** *Computational Modeling of Progressive Collapse in Reinforced Concrete Frame Structures.* Mohamed M. Talaat and Khalid M. Mosalam. May 2008.
- PEER 2007/09** *Integrated Probabilistic Performance-Based Evaluation of Benchmark Reinforced Concrete Bridges.* Kevin R. Mackie, John-Michael Wong, and Božidar Stojadinović. January 2008.
- PEER 2007/08** *Assessing Seismic Collapse Safety of Modern Reinforced Concrete Moment-Frame Buildings.* Curt B. Haselton and Gregory G. Deierlein. February 2008.
- PEER 2007/07** *Performance Modeling Strategies for Modern Reinforced Concrete Bridge Columns.* Michael P. Berry and Marc O. Eberhard. April 2008.
- PEER 2007/06** *Development of Improved Procedures for Seismic Design of Buried and Partially Buried Structures.* Linda Al Atik and Nicholas Sitar. June 2007.
- PEER 2007/05** *Uncertainty and Correlation in Seismic Risk Assessment of Transportation Systems.* Renee G. Lee and Anne S. Kiremidjian. July 2007.
- PEER 2007/04** *Numerical Models for Analysis and Performance-Based Design of Shallow Foundations Subjected to Seismic Loading.* Sivapalan Gajan, Tara C. Hutchinson, Bruce L. Kutter, Prishati Raychowdhury, José A. Ugalde, and Jonathan P. Stewart. May 2008.
- PEER 2007/03** *Beam-Column Element Model Calibrated for Predicting Flexural Response Leading to Global Collapse of RC Frame Buildings.* Curt B. Haselton, Abbie B. Liel, Sarah Taylor Lange, and Gregory G. Deierlein. May 2008.
- PEER 2007/02** *Campbell-Bozorgnia NGA Ground Motion Relations for the Geometric Mean Horizontal Component of Peak and Spectral Ground Motion Parameters.* Kenneth W. Campbell and Yousef Bozorgnia. May 2007.
- PEER 2007/01** *Boore-Atkinson NGA Ground Motion Relations for the Geometric Mean Horizontal Component of Peak and Spectral Ground Motion Parameters.* David M. Boore and Gail M. Atkinson. May 2007.
- PEER 2006/12** *Societal Implications of Performance-Based Earthquake Engineering.* Peter J. May. May 2007.
- PEER 2006/11** *Probabilistic Seismic Demand Analysis Using Advanced Ground Motion Intensity Measures, Attenuation Relationships, and Near-Fault Effects.* Polsak Tothong and C. Allin Cornell. March 2007.
- PEER 2006/10** *Application of the PEER PBEE Methodology to the I-880 Viaduct.* Sashi Kunnath. February 2007.
- PEER 2006/09** *Quantifying Economic Losses from Travel Forgone Following a Large Metropolitan Earthquake.* James Moore, Sungbin Cho, Yue Yue Fan, and Stuart Werner. November 2006.
- PEER 2006/08** *Vector-Valued Ground Motion Intensity Measures for Probabilistic Seismic Demand Analysis.* Jack W. Baker and C. Allin Cornell. October 2006.
- PEER 2006/07** *Analytical Modeling of Reinforced Concrete Walls for Predicting Flexural and Coupled-Shear-Flexural Responses.* Kutay Orakcal, Leonardo M. Massone, and John W. Wallace. October 2006.
- PEER 2006/06** *Nonlinear Analysis of a Soil-Drilled Pier System under Static and Dynamic Axial Loading.* Gang Wang and Nicholas Sitar. November 2006.
- PEER 2006/05** *Advanced Seismic Assessment Guidelines.* Paolo Bazzurro, C. Allin Cornell, Charles Menun, Maziar Motahari, and Nicolas Luco. September 2006.
- PEER 2006/04** *Probabilistic Seismic Evaluation of Reinforced Concrete Structural Components and Systems.* Tae Hyung Lee and Khalid M. Mosalam. August 2006.

- PEER 2006/03** *Performance of Lifelines Subjected to Lateral Spreading.* Scott A. Ashford and Teerawut Juirnarongrit. July 2006.
- PEER 2006/02** *Pacific Earthquake Engineering Research Center Highway Demonstration Project.* Anne Kiremidjian, James Moore, Yue Yue Fan, Nesrin Basoz, Ozgur Yazali, and Meredith Williams. April 2006.
- PEER 2006/01** *Bracing Berkeley. A Guide to Seismic Safety on the UC Berkeley Campus.* Mary C. Comerio, Stephen Tobriner, and Ariane Fehrenkamp. January 2006.
- PEER 2005/16** *Seismic Response and Reliability of Electrical Substation Equipment and Systems.* Junho Song, Armen Der Kiureghian, and Jerome L. Sackman. April 2006.
- PEER 2005/15** *CPT-Based Probabilistic Assessment of Seismic Soil Liquefaction Initiation.* R. E. S. Moss, R. B. Seed, R. E. Kayen, J. P. Stewart, and A. Der Kiureghian. April 2006.
- PEER 2005/14** *Workshop on Modeling of Nonlinear Cyclic Load-Deformation Behavior of Shallow Foundations.* Bruce L. Kutter, Geoffrey Martin, Tara Hutchinson, Chad Harden, Sivapalan Gajan, and Justin Phalen. March 2006.
- PEER 2005/13** *Stochastic Characterization and Decision Bases under Time-Dependent Aftershock Risk in Performance-Based Earthquake Engineering.* Gee Liek Yeo and C. Allin Cornell. July 2005.
- PEER 2005/12** *PEER Testbed Study on a Laboratory Building: Exercising Seismic Performance Assessment.* Mary C. Comerio, editor. November 2005.
- PEER 2005/11** *Van Nuys Hotel Building Testbed Report: Exercising Seismic Performance Assessment.* Helmut Krawinkler, editor. October 2005.
- PEER 2005/10** *First NEES/E-Defense Workshop on Collapse Simulation of Reinforced Concrete Building Structures.* September 2005.
- PEER 2005/09** *Test Applications of Advanced Seismic Assessment Guidelines.* Joe Maffei, Karl Telleen, Danya Mohr, William Holmes, and Yuki Nakayama. August 2006.
- PEER 2005/08** *Damage Accumulation in Lightly Confined Reinforced Concrete Bridge Columns.* R. Tyler Ranf, Jared M. Nelson, Zach Price, Marc O. Eberhard, and John F. Stanton. April 2006.
- PEER 2005/07** *Experimental and Analytical Studies on the Seismic Response of Freestanding and Anchored Laboratory Equipment.* Dimitrios Konstantinidis and Nicos Makris. January 2005.
- PEER 2005/06** *Global Collapse of Frame Structures under Seismic Excitations.* Luis F. Ibarra and Helmut Krawinkler. September 2005.
- PEER 2005/05** *Performance Characterization of Bench- and Shelf-Mounted Equipment.* Samit Ray Chaudhuri and Tara C. Hutchinson. May 2006.
- PEER 2005/04** *Numerical Modeling of the Nonlinear Cyclic Response of Shallow Foundations.* Chad Harden, Tara Hutchinson, Geoffrey R. Martin, and Bruce L. Kutter. August 2005.
- PEER 2005/03** *A Taxonomy of Building Components for Performance-Based Earthquake Engineering.* Keith A. Porter. September 2005.
- PEER 2005/02** *Fragility Basis for California Highway Overpass Bridge Seismic Decision Making.* Kevin R. Mackie and Božidar Stojadinović. June 2005.
- PEER 2005/01** *Empirical Characterization of Site Conditions on Strong Ground Motion.* Jonathan P. Stewart, Yoojoong Choi, and Robert W. Graves. June 2005.
- PEER 2004/09** *Electrical Substation Equipment Interaction: Experimental Rigid Conductor Studies.* Christopher Stearns and André Filiatrault. February 2005.
- PEER 2004/08** *Seismic Qualification and Fragility Testing of Line Break 550-kV Disconnect Switches.* Shakhzod M. Takhirov, Gregory L. Fenves, and Eric Fujisaki. January 2005.
- PEER 2004/07** *Ground Motions for Earthquake Simulator Qualification of Electrical Substation Equipment.* Shakhzod M. Takhirov, Gregory L. Fenves, Eric Fujisaki, and Don Clyde. January 2005.
- PEER 2004/06** *Performance-Based Regulation and Regulatory Regimes.* Peter J. May and Chris Koski. September 2004.
- PEER 2004/05** *Performance-Based Seismic Design Concepts and Implementation: Proceedings of an International Workshop.* Peter Fajfar and Helmut Krawinkler, editors. September 2004.
- PEER 2004/04** *Seismic Performance of an Instrumented Tilt-up Wall Building.* James C. Anderson and Vitelmo V. Bertero. July 2004.
- PEER 2004/03** *Evaluation and Application of Concrete Tilt-up Assessment Methodologies.* Timothy Graf and James O. Malley. October 2004.

- PEER 2004/02** *Analytical Investigations of New Methods for Reducing Residual Displacements of Reinforced Concrete Bridge Columns.* Junichi Sakai and Stephen A. Mahin. August 2004.
- PEER 2004/01** *Seismic Performance of Masonry Buildings and Design Implications.* Kerri Anne Taeko Tokoro, James C. Anderson, and Vitelmo V. Bertero. February 2004.
- PEER 2003/18** *Performance Models for Flexural Damage in Reinforced Concrete Columns.* Michael Berry and Marc Eberhard. August 2003.
- PEER 2003/17** *Predicting Earthquake Damage in Older Reinforced Concrete Beam-Column Joints.* Catherine Pagni and Laura Lowes. October 2004.
- PEER 2003/16** *Seismic Demands for Performance-Based Design of Bridges.* Kevin Mackie and Božidar Stojadinović. August 2003.
- PEER 2003/15** *Seismic Demands for Nondeteriorating Frame Structures and Their Dependence on Ground Motions.* Ricardo Antonio Medina and Helmut Krawinkler. May 2004.
- PEER 2003/14** *Finite Element Reliability and Sensitivity Methods for Performance-Based Earthquake Engineering.* Terje Haukaas and Armen Der Kiureghian. April 2004.
- PEER 2003/13** *Effects of Connection Hysteretic Degradation on the Seismic Behavior of Steel Moment-Resisting Frames.* Janise E. Rodgers and Stephen A. Mahin. March 2004.
- PEER 2003/12** *Implementation Manual for the Seismic Protection of Laboratory Contents: Format and Case Studies.* William T. Holmes and Mary C. Comerio. October 2003.
- PEER 2003/11** *Fifth U.S.-Japan Workshop on Performance-Based Earthquake Engineering Methodology for Reinforced Concrete Building Structures.* February 2004.
- PEER 2003/10** *A Beam-Column Joint Model for Simulating the Earthquake Response of Reinforced Concrete Frames.* Laura N. Lowes, Nilanjan Mitra, and Arash Altoontash. February 2004.
- PEER 2003/09** *Sequencing Repairs after an Earthquake: An Economic Approach.* Marco Casari and Simon J. Wilkie. April 2004.
- PEER 2003/08** *A Technical Framework for Probability-Based Demand and Capacity Factor Design (DCFD) Seismic Formats.* Fatemeh Jalayer and C. Allin Cornell. November 2003.
- PEER 2003/07** *Uncertainty Specification and Propagation for Loss Estimation Using FOSM Methods.* Jack W. Baker and C. Allin Cornell. September 2003.
- PEER 2003/06** *Performance of Circular Reinforced Concrete Bridge Columns under Bidirectional Earthquake Loading.* Mahmoud M. Hachem, Stephen A. Mahin, and Jack P. Moehle. February 2003.
- PEER 2003/05** *Response Assessment for Building-Specific Loss Estimation.* Eduardo Miranda and Shahram Taghavi. September 2003.
- PEER 2003/04** *Experimental Assessment of Columns with Short Lap Splices Subjected to Cyclic Loads.* Murat Melek, John W. Wallace, and Joel Conte. April 2003.
- PEER 2003/03** *Probabilistic Response Assessment for Building-Specific Loss Estimation.* Eduardo Miranda and Hesameddin Aslani. September 2003.
- PEER 2003/02** *Software Framework for Collaborative Development of Nonlinear Dynamic Analysis Program.* Jun Peng and Kincho H. Law. September 2003.
- PEER 2003/01** *Shake Table Tests and Analytical Studies on the Gravity Load Collapse of Reinforced Concrete Frames.* Kenneth John Elwood and Jack P. Moehle. November 2003.
- PEER 2002/24** *Performance of Beam to Column Bridge Joints Subjected to a Large Velocity Pulse.* Natalie Gibson, André Filiatrault, and Scott A. Ashford. April 2002.
- PEER 2002/23** *Effects of Large Velocity Pulses on Reinforced Concrete Bridge Columns.* Greg L. Orozco and Scott A. Ashford. April 2002.
- PEER 2002/22** *Characterization of Large Velocity Pulses for Laboratory Testing.* Kenneth E. Cox and Scott A. Ashford. April 2002.
- PEER 2002/21** *Fourth U.S.-Japan Workshop on Performance-Based Earthquake Engineering Methodology for Reinforced Concrete Building Structures.* December 2002.
- PEER 2002/20** *Barriers to Adoption and Implementation of PBEE Innovations.* Peter J. May. August 2002.
- PEER 2002/19** *Economic-Engineered Integrated Models for Earthquakes: Socioeconomic Impacts.* Peter Gordon, James E. Moore II, and Harry W. Richardson. July 2002.

- PEER 2002/18** *Assessment of Reinforced Concrete Building Exterior Joints with Substandard Details.* Chris P. Pantelides, Jon Hansen, Justin Nadauld, and Lawrence D. Reaveley. May 2002.
- PEER 2002/17** *Structural Characterization and Seismic Response Analysis of a Highway Overcrossing Equipped with Elastomeric Bearings and Fluid Dampers: A Case Study.* Nicos Makris and Jian Zhang. November 2002.
- PEER 2002/16** *Estimation of Uncertainty in Geotechnical Properties for Performance-Based Earthquake Engineering.* Allen L. Jones, Steven L. Kramer, and Pedro Arduino. December 2002.
- PEER 2002/15** *Seismic Behavior of Bridge Columns Subjected to Various Loading Patterns.* Asadollah Esmaeily-Gh. and Yan Xiao. December 2002.
- PEER 2002/14** *Inelastic Seismic Response of Extended Pile Shaft Supported Bridge Structures.* T.C. Hutchinson, R.W. Boulanger, Y.H. Chai, and I.M. Idriss. December 2002.
- PEER 2002/13** *Probabilistic Models and Fragility Estimates for Bridge Components and Systems.* Paolo Gardoni, Armen Der Kiureghian, and Khalid M. Mosalam. June 2002.
- PEER 2002/12** *Effects of Fault Dip and Slip Rake on Near-Source Ground Motions: Why Chi-Chi Was a Relatively Mild M7.6 Earthquake.* Brad T. Aagaard, John F. Hall, and Thomas H. Heaton. December 2002.
- PEER 2002/11** *Analytical and Experimental Study of Fiber-Reinforced Strip Isolators.* James M. Kelly and Shakhzod M. Takhirov. September 2002.
- PEER 2002/10** *Centrifuge Modeling of Settlement and Lateral Spreading with Comparisons to Numerical Analyses.* Sivapalan Gajan and Bruce L. Kutter. January 2003.
- PEER 2002/09** *Documentation and Analysis of Field Case Histories of Seismic Compression during the 1994 Northridge, California, Earthquake.* Jonathan P. Stewart, Patrick M. Smith, Daniel H. Whang, and Jonathan D. Bray. October 2002.
- PEER 2002/08** *Component Testing, Stability Analysis and Characterization of Buckling-Restrained Unbonded Braces™.* Cameron Black, Nicos Makris, and Ian Aiken. September 2002.
- PEER 2002/07** *Seismic Performance of Pile-Wharf Connections.* Charles W. Roeder, Robert Graff, Jennifer Soderstrom, and Jun Han Yoo. December 2001.
- PEER 2002/06** *The Use of Benefit-Cost Analysis for Evaluation of Performance-Based Earthquake Engineering Decisions.* Richard O. Zerbe and Anthony Falit-Baiamonte. September 2001.
- PEER 2002/05** *Guidelines, Specifications, and Seismic Performance Characterization of Nonstructural Building Components and Equipment.* André Filiatrault, Constantin Christopoulos, and Christopher Stearns. September 2001.
- PEER 2002/04** *Consortium of Organizations for Strong-Motion Observation Systems and the Pacific Earthquake Engineering Research Center Lifelines Program: Invited Workshop on Archiving and Web Dissemination of Geotechnical Data, 4–5 October 2001.* September 2002.
- PEER 2002/03** *Investigation of Sensitivity of Building Loss Estimates to Major Uncertain Variables for the Van Nuys Testbed.* Keith A. Porter, James L. Beck, and Rustem V. Shaikhutdinov. August 2002.
- PEER 2002/02** *The Third U.S.-Japan Workshop on Performance-Based Earthquake Engineering Methodology for Reinforced Concrete Building Structures.* July 2002.
- PEER 2002/01** *Nonstructural Loss Estimation: The UC Berkeley Case Study.* Mary C. Comerio and John C. Stallmeyer. December 2001.
- PEER 2001/16** *Statistics of SDF-System Estimate of Roof Displacement for Pushover Analysis of Buildings.* Anil K. Chopra, Rakesh K. Goel, and Chatpan Chintanapakdee. December 2001.
- PEER 2001/15** *Damage to Bridges during the 2001 Nisqually Earthquake.* R. Tyler Ranf, Marc O. Eberhard, and Michael P. Berry. November 2001.
- PEER 2001/14** *Rocking Response of Equipment Anchored to a Base Foundation.* Nicos Makris and Cameron J. Black. September 2001.
- PEER 2001/13** *Modeling Soil Liquefaction Hazards for Performance-Based Earthquake Engineering.* Steven L. Kramer and Ahmed-W. Elgamal. February 2001.
- PEER 2001/12** *Development of Geotechnical Capabilities in OpenSees.* Boris Jeremić. September 2001.
- PEER 2001/11** *Analytical and Experimental Study of Fiber-Reinforced Elastomeric Isolators.* James M. Kelly and Shakhzod M. Takhirov. September 2001.
- PEER 2001/10** *Amplification Factors for Spectral Acceleration in Active Regions.* Jonathan P. Stewart, Andrew H. Liu, Yoojoong Choi, and Mehmet B. Baturay. December 2001.

- PEER 2001/09** *Ground Motion Evaluation Procedures for Performance-Based Design.* Jonathan P. Stewart, Shyh-Jeng Chiou, Jonathan D. Bray, Robert W. Graves, Paul G. Somerville, and Norman A. Abrahamson. September 2001.
- PEER 2001/08** *Experimental and Computational Evaluation of Reinforced Concrete Bridge Beam-Column Connections for Seismic Performance.* Clay J. Naito, Jack P. Moehle, and Khalid M. Mosalam. November 2001.
- PEER 2001/07** *The Rocking Spectrum and the Shortcomings of Design Guidelines.* Nicos Makris and Dimitrios Konstantinidis. August 2001.
- PEER 2001/06** *Development of an Electrical Substation Equipment Performance Database for Evaluation of Equipment Fragilities.* Thalia Agnanos. April 1999.
- PEER 2001/05** *Stiffness Analysis of Fiber-Reinforced Elastomeric Isolators.* Hsiang-Chuan Tsai and James M. Kelly. May 2001.
- PEER 2001/04** *Organizational and Societal Considerations for Performance-Based Earthquake Engineering.* Peter J. May. April 2001.
- PEER 2001/03** *A Modal Pushover Analysis Procedure to Estimate Seismic Demands for Buildings: Theory and Preliminary Evaluation.* Anil K. Chopra and Rakesh K. Goel. January 2001.
- PEER 2001/02** *Seismic Response Analysis of Highway Overcrossings Including Soil-Structure Interaction.* Jian Zhang and Nicos Makris. March 2001.
- PEER 2001/01** *Experimental Study of Large Seismic Steel Beam-to-Column Connections.* Egor P. Popov and Shakhzod M. Takhirov. November 2000.
- PEER 2000/10** *The Second U.S.-Japan Workshop on Performance-Based Earthquake Engineering Methodology for Reinforced Concrete Building Structures.* March 2000.
- PEER 2000/09** *Structural Engineering Reconnaissance of the August 17, 1999 Earthquake: Kocaeli (Izmit), Turkey.* Halil Sezen, Kenneth J. Elwood, Andrew S. Whittaker, Khalid Mosalam, John J. Wallace, and John F. Stanton. December 2000.
- PEER 2000/08** *Behavior of Reinforced Concrete Bridge Columns Having Varying Aspect Ratios and Varying Lengths of Confinement.* Anthony J. Calderone, Dawn E. Lehman, and Jack P. Moehle. January 2001.
- PEER 2000/07** *Cover-Plate and Flange-Plate Reinforced Steel Moment-Resisting Connections.* Taejin Kim, Andrew S. Whittaker, Amir S. Gilani, Vitelmo V. Bertero, and Shakhzod M. Takhirov. September 2000.
- PEER 2000/06** *Seismic Evaluation and Analysis of 230-kV Disconnect Switches.* Amir S. J. Gilani, Andrew S. Whittaker, Gregory L. Fenves, Chun-Hao Chen, Henry Ho, and Eric Fujisaki. July 2000.
- PEER 2000/05** *Performance-Based Evaluation of Exterior Reinforced Concrete Building Joints for Seismic Excitation.* Chandra Clyde, Chris P. Pantelides, and Lawrence D. Reaveley. July 2000.
- PEER 2000/04** *An Evaluation of Seismic Energy Demand: An Attenuation Approach.* Chung-Che Chou and Chia-Ming Uang. July 1999.
- PEER 2000/03** *Framing Earthquake Retrofitting Decisions: The Case of Hillside Homes in Los Angeles.* Detlof von Winterfeldt, Nels Roselund, and Alicia Kitsuse. March 2000.
- PEER 2000/02** *U.S.-Japan Workshop on the Effects of Near-Field Earthquake Shaking.* Andrew Whittaker, ed. July 2000.
- PEER 2000/01** *Further Studies on Seismic Interaction in Interconnected Electrical Substation Equipment.* Armen Der Kiureghian, Kee-Jeung Hong, and Jerome L. Sackman. November 1999.
- PEER 1999/14** *Seismic Evaluation and Retrofit of 230-kV Porcelain Transformer Bushings.* Amir S. Gilani, Andrew S. Whittaker, Gregory L. Fenves, and Eric Fujisaki. December 1999.
- PEER 1999/13** *Building Vulnerability Studies: Modeling and Evaluation of Tilt-up and Steel Reinforced Concrete Buildings.* John W. Wallace, Jonathan P. Stewart, and Andrew S. Whittaker, editors. December 1999.
- PEER 1999/12** *Rehabilitation of Nonductile RC Frame Building Using Encasement Plates and Energy-Dissipating Devices.* Mehrdad Sasani, Vitelmo V. Bertero, James C. Anderson. December 1999.
- PEER 1999/11** *Performance Evaluation Database for Concrete Bridge Components and Systems under Simulated Seismic Loads.* Yael D. Hose and Frieder Seible. November 1999.
- PEER 1999/10** *U.S.-Japan Workshop on Performance-Based Earthquake Engineering Methodology for Reinforced Concrete Building Structures.* December 1999.
- PEER 1999/09** *Performance Improvement of Long Period Building Structures Subjected to Severe Pulse-Type Ground Motions.* James C. Anderson, Vitelmo V. Bertero, and Raul Bertero. October 1999.
- PEER 1999/08** *Envelopes for Seismic Response Vectors.* Charles Menun and Armen Der Kiureghian. July 1999.

- PEER 1999/07** *Documentation of Strengths and Weaknesses of Current Computer Analysis Methods for Seismic Performance of Reinforced Concrete Members.* William F. Cofer. November 1999.
- PEER 1999/06** *Rocking Response and Overturning of Anchored Equipment under Seismic Excitations.* Nicos Makris and Jian Zhang. November 1999.
- PEER 1999/05** *Seismic Evaluation of 550 kV Porcelain Transformer Bushings.* Amir S. Gilani, Andrew S. Whittaker, Gregory L. Fenves, and Eric Fujisaki. October 1999.
- PEER 1999/04** *Adoption and Enforcement of Earthquake Risk-Reduction Measures.* Peter J. May, Raymond J. Burby, T. Jens Feeley, and Robert Wood.
- PEER 1999/03** *Task 3 Characterization of Site Response General Site Categories.* Adrian Rodriguez-Marek, Jonathan D. Bray, and Norman Abrahamson. February 1999.
- PEER 1999/02** *Capacity-Demand-Diagram Methods for Estimating Seismic Deformation of Inelastic Structures: SDF Systems.* Anil K. Chopra and Rakesh Goel. April 1999.
- PEER 1999/01** *Interaction in Interconnected Electrical Substation Equipment Subjected to Earthquake Ground Motions.* Armen Der Kiureghian, Jerome L. Sackman, and Kee-Jeung Hong. February 1999.
- PEER 1998/08** *Behavior and Failure Analysis of a Multiple-Frame Highway Bridge in the 1994 Northridge Earthquake.* Gregory L. Fenves and Michael Ellery. December 1998.
- PEER 1998/07** *Empirical Evaluation of Inertial Soil-Structure Interaction Effects.* Jonathan P. Stewart, Raymond B. Seed, and Gregory L. Fenves. November 1998.
- PEER 1998/06** *Effect of Damping Mechanisms on the Response of Seismic Isolated Structures.* Nicos Makris and Shih-Po Chang. November 1998.
- PEER 1998/05** *Rocking Response and Overturning of Equipment under Horizontal Pulse-Type Motions.* Nicos Makris and Yiannis Roussos. October 1998.
- PEER 1998/04** *Pacific Earthquake Engineering Research Invitational Workshop Proceedings, May 14–15, 1998: Defining the Links between Planning, Policy Analysis, Economics and Earthquake Engineering.* Mary Comerio and Peter Gordon. September 1998.
- PEER 1998/03** *Repair/Upgrade Procedures for Welded Beam to Column Connections.* James C. Anderson and Xiaojing Duan. May 1998.
- PEER 1998/02** *Seismic Evaluation of 196 kV Porcelain Transformer Bushings.* Amir S. Gilani, Juan W. Chavez, Gregory L. Fenves, and Andrew S. Whittaker. May 1998.
- PEER 1998/01** *Seismic Performance of Well-Confined Concrete Bridge Columns.* Dawn E. Lehman and Jack P. Moehle. December 2000.

## ONLINE REPORTS

The following PEER reports are available by Internet only at [http://peer.berkeley.edu/publications/peer\\_reports.html](http://peer.berkeley.edu/publications/peer_reports.html)

- PEER 2011/107** *Nonlinear Site Response and Seismic Compression at Vertical Array Strongly Shaken by 2007 Niigata-ken Chuetsu-oki Earthquake.* Eric Yee, Jonathan P. Stewart, and Kohji Tokimatsu. December 2011.
- PEER 2011/106** *Self Compacting Hybrid Fiber Reinforced Concrete Composites for Bridge Columns.* Pardeep Kumar, Gabriel Jen, William Trono, Marios Panagiotou, and Claudia Ostertag. September 2011.
- PEER 2011/105** *Stochastic Dynamic Analysis of Bridges Subjected to Spatially Varying Ground Motions.* Katerina Konakli and Armen Der Kiureghian. August 2011.
- PEER 2011/104** *Design and Instrumentation of the 2010 E-Defense Four-Story Reinforced Concrete and Post-Tensioned Concrete Buildings.* Takuya Nagae, Kenichi Tahara, Taizo Matsumori, Hitoshi Shiohara, Toshimi Kabeyasawa, Susumu Kono, Minehiro Nishiyama (Japanese Research Team) and John Wallace, Wassim Ghannoum, Jack Moehle, Richard Sause, Wesley Keller, Zeynep Tuna (U.S. Research Team). June 2011.
- PEER 2011/103** *In-Situ Monitoring of the Force Output of Fluid Dampers: Experimental Investigation.* Dimitrios Konstantinidis, James M. Kelly, and Nicos Makris. April 2011.
- PEER 2011/102** *Ground-motion prediction equations 1964 - 2010.* John Douglas. April 2011.
- PEER 2011/101** *Report of the Eighth Planning Meeting of NEES/E-Defense Collaborative Research on Earthquake Engineering.* Convened by the Hyogo Earthquake Engineering Research Center (NIED), NEES Consortium, Inc. February 2011.
- PEER 2010/111** *Modeling and Acceptance Criteria for Seismic Design and Analysis of Tall Buildings.* Task 7 Report for the Tall Buildings Initiative - Published jointly by the Applied Technology Council. October 2010.
- PEER 2010/110** *Seismic Performance Assessment and Probabilistic Repair Cost Analysis of Precast Concrete Cladding Systems for Multistory Buildings.* Jeffrey P. Hunt and Božidar Stojadinovic. November 2010.
- PEER 2010/109** *Report of the Seventh Joint Planning Meeting of NEES/E-Defense Collaboration on Earthquake Engineering. Held at the E-Defense, Miki, and Shin-Kobe, Japan, September 18–19, 2009.* August 2010.
- PEER 2010/108** *Probabilistic Tsunami Hazard in California.* Hong Kie Thio, Paul Somerville, and Jascha Polet, preparers. October 2010.
- PEER 2010/107** *Performance and Reliability of Exposed Column Base Plate Connections for Steel Moment-Resisting Frames.* Ady Aviram, Božidar Stojadinovic, and Armen Der Kiureghian. August 2010.
- PEER 2010/106** *Verification of Probabilistic Seismic Hazard Analysis Computer Programs.* Patricia Thomas, Ivan Wong, and Norman Abrahamson. May 2010.
- PEER 2010/105** *Structural Engineering Reconnaissance of the April 6, 2009, Abruzzo, Italy, Earthquake, and Lessons Learned.* M. Selim Günay and Khalid M. Mosalam. April 2010.
- PEER 2010/104** *Simulating the Inelastic Seismic Behavior of Steel Braced Frames, Including the Effects of Low-Cycle Fatigue.* Yuli Huang and Stephen A. Mahin. April 2010.
- PEER 2010/103** *Post-Earthquake Traffic Capacity of Modern Bridges in California.* Vesna Terzic and Božidar Stojadinović. March 2010.
- PEER 2010/102** *Analysis of Cumulative Absolute Velocity (CAV) and JMA Instrumental Seismic Intensity ( $I_{JMA}$ ) Using the PEER–NGA Strong Motion Database.* Kenneth W. Campbell and Yousef Bozorgnia. February 2010.
- PEER 2010/101** *Rocking Response of Bridges on Shallow Foundations.* Jose A. Ugalde, Bruce L. Kutter, and Boris Jeremic. April 2010.
- PEER 2009/109** *Simulation and Performance-Based Earthquake Engineering Assessment of Self-Centering Post-Tensioned Concrete Bridge Systems.* Won K. Lee and Sarah L. Billington. December 2009.
- PEER 2009/108** *PEER Lifelines Geotechnical Virtual Data Center.* J. Carl Stepp, Daniel J. Ponti, Loren L. Turner, Jennifer N. Swift, Sean Devlin, Yang Zhu, Jean Benoit, and John Bobbitt. September 2009.
- PEER 2009/107** *Experimental and Computational Evaluation of Current and Innovative In-Span Hinge Details in Reinforced Concrete Box-Girder Bridges: Part 2: Post-Test Analysis and Design Recommendations.* Matias A. Hube and Khalid M. Mosalam. December 2009.
- PEER 2009/106** *Shear Strength Models of Exterior Beam-Column Joints without Transverse Reinforcement.* Sangjoon Park and Khalid M. Mosalam. November 2009.

- PEER 2009/105** *Reduced Uncertainty of Ground Motion Prediction Equations through Bayesian Variance Analysis.* Robb Eric S. Moss. November 2009.
- PEER 2009/104** *Advanced Implementation of Hybrid Simulation.* Andreas H. Schellenberg, Stephen A. Mahin, Gregory L. Fenves. November 2009.
- PEER 2009/103** *Performance Evaluation of Innovative Steel Braced Frames.* T. Y. Yang, Jack P. Moehle, and Božidar Stojadinovic. August 2009.
- PEER 2009/102** *Reinvestigation of Liquefaction and Nonliquefaction Case Histories from the 1976 Tangshan Earthquake.* Robb Eric Moss, Robert E. Kayen, Liyuan Tong, Songyu Liu, Guojun Cai, and Jiaer Wu. August 2009.
- PEER 2009/101** *Report of the First Joint Planning Meeting for the Second Phase of NEES/E-Defense Collaborative Research on Earthquake Engineering.* Stephen A. Mahin et al. July 2009.
- PEER 2008/104** *Experimental and Analytical Study of the Seismic Performance of Retaining Structures.* Linda Al Atik and Nicholas Sitar. January 2009.
- PEER 2008/103** *Experimental and Computational Evaluation of Current and Innovative In-Span Hinge Details in Reinforced Concrete Box-Girder Bridges. Part 1: Experimental Findings and Pre-Test Analysis.* Matias A. Hube and Khalid M. Mosalam. January 2009.
- PEER 2008/102** *Modeling of Unreinforced Masonry Infill Walls Considering In-Plane and Out-of-Plane Interaction.* Stephen Kadsiewicz and Khalid M. Mosalam. January 2009.
- PEER 2008/101** *Seismic Performance Objectives for Tall Buildings.* William T. Holmes, Charles Kircher, William Petak, and Nabih Youssef. August 2008.
- PEER 2007/101** *Generalized Hybrid Simulation Framework for Structural Systems Subjected to Seismic Loading.* Tarek Elkhoraibi and Khalid M. Mosalam. July 2007.
- PEER 2007/100** *Seismic Evaluation of Reinforced Concrete Buildings Including Effects of Masonry Infill Walls.* Alidad Hashemi and Khalid M. Mosalam. July 2007.

The Pacific Earthquake Engineering Research Center (PEER) is a multi-institutional research and education center with headquarters at the University of California, Berkeley. Investigators from over 20 universities, several consulting companies, and researchers at various state and federal government agencies contribute to research programs focused on performance-based earthquake engineering.

These research programs aim to identify and reduce the risks from major earthquakes to life safety and to the economy by including research in a wide variety of disciplines including structural and geotechnical engineering, geology/seismology, lifelines, transportation, architecture, economics, risk management, and public policy.

PEER is supported by federal, state, local, and regional agencies, together with industry partners.



PEER reports can be ordered at [http://peer.berkeley.edu/publications/peer\\_reports.html](http://peer.berkeley.edu/publications/peer_reports.html) or by contacting

Pacific Earthquake Engineering Research Center  
University of California, Berkeley  
325 Davis Hall, mail code 1792  
Berkeley, CA 94720-1792  
Tel: 510-642-3437  
Fax: 510-642-1655  
Email: [peer\\_editor@berkeley.edu](mailto:peer_editor@berkeley.edu)

ISSN 1547-0587X